

2
2000

LIBRARY
Michigan State
University

This is to certify that the


dissertation entitled

P(d1)A/PGA/FE and P(d1)A/PCA/SmCo₅ Composites for
use as a Delivery Mechanism for Magnetically
Directed Chondrogenesis
presented by

Dean Alan Oppermann

has been accepted towards fulfillment
of the requirements for

Ph.D. degree in Materials Science


Major professor

Date January 12, 2000

PLACE IN RETURN BOX to remove this checkout from your record.
TO AVOID FINES return on or before date due.
MAY BE RECALLED with earlier due date if requested.

DATE DUE	DATE DUE	DATE DUE

**P(dl)A/PGA/FE AND P(dl)A/PGA/SmCo₅ COMPOSITES FOR USE AS A DELIVERY
MECHANISM FOR MAGNETICALLY DIRECTED CHONDROGENESIS**

By

Dean Alan Oppermann

A DISSERTATION

**Submitted to
Michigan State University
In partial fulfillment of the requirements
for the degree of**

DOCTOR OF PHILOSOPHY

Department of Materials Science and Mechanics

2000

ABSTRACT

P(dl)A/PGA/FE AND P(dl)A/PGA/SmCo₅ COMPOSITES FOR USE AS A DELIVERY MECHANISM FOR MAGNETICALLY DIRECTED CHONDROGENESIS

By

Dean Alan Oppermann

Magnetically directed chondrogenesis (MDC) is a fundamental approach to articular cartilage repair. In MDC a magnet is implanted into the subchondral trabecular bone underlying a cartilage defect and used to attract chondrocytes, magnetically tagged with Fe nanoparticles, to the defect site. Pilot studies by Halpern, Crimp and Grande, using solid neodymium (Nd) magnets, indicated optimistic results by producing a hyaline-like articular cartilage after 8 weeks implantation. Since solid Nd magnets introduce long-term biocompatibility issues, the focus of this dissertation was to develop P(dl)A/PGA/Fe and P(dl)A/PGA/SmCo₅ implants for use in MDC.

The effect of implant porosity, implant composition and magnetic material (Fe or SmCo₅) on the initial and degraded magnetic properties were evaluated. The biocompatibility of P(dl)A/PGA/Fe implants were investigated by implantation into New Zealand white rabbits for 8 weeks. The effect of hydrogen peroxide (H₂O₂) and ethylene oxide (EO) sterilization techniques on the molecular weight and chemical structure of P(dl)A/PGA polymers were evaluated using gel permeation chromatography and Fourier transform infrared spectroscopy. The effect of implant morphology, size and number on the von Mises stress in the trabecular bone surrounding the implant was evaluated using a finite element model.

In general, SmCo₅ implants resulted in higher magnetic fields initially and after 8 weeks of degradation than comparable Fe implants. Increases in magnetic field strength

were achieved by increasing the volume fraction of magnetic material and by increasing the PGA concentration. The magnetic field strength degradation rate decreased with increases in volume fraction of magnetic material and increases in PLA concentration. Implantation studies indicated that 50/50 P(dl)A/PGA were more bioactive than 75/25 P(dl)A/PGA with an increased cellular response that is specific to bone growth. The compressive strength and elastic modulus of porous implants were comparable to trabecular bone, and the compressive strength and elastic modulus of solid implants was higher than trabecular bone but less than cortical bone. Finite element modeling showed that the implantation of solid and porous P(dl)A/PGA/Fe implants did not significantly increase the von Mises stress concentration adjacent to the implant. The von Mises stress surrounding porous implants was higher than the solid implants which predicts faster bone remodeling. Comparing single implants to multiple implants indicated a significant decrease in von Mises stress between the implants. This would predict bone resorption in that area. H_2O_2 sterilization resulted in a gradual decrease in the molecular weight of P(dl)A/PGA polymers that was a result of hydrolytic scission of the ester bonds present between the individual monomers. The polymers were less affected by EO sterilization with only the 75/25 P(dl)A/PGA, indicating a decrease in molecular weight.

From these results, it was concluded that solid 50/50 P(dl)A/PGA/SmCo₅ implants that span the entire width of the cartilage defect should be used to optimize the attraction potential and bioactivity of the implant. Also ethylene oxide, which caused less premature implant degradation, should be used for sterilization.

To my parents, Jim and Denise,
who funded my dreams
so I could focus on the tasks at hand.

ACKNOWLEDGEMENTS

I would like to thank Dr. Melissa J. Crimp for her knowledge, direction and friendship during this investigation. I would also like to show my appreciation to the rest of the Materials Science and Mechanics department faculty and staff for their exceptional teaching and continuous help. Special thanks to Dr. Alan A. Halpern and Dr. Dan Grande for their time and support with surgeries and chondrocyte cells utilized in this thesis. Thanks, also, to all the students I have worked with, studied with, and collaborated with, their friendship will always mean a lot to me. Finally, and most importantly, I would like to thank God for giving me a loving, supporting and protecting family and for giving me strength and knowledge to succeed in this endeavor.

TABLE OF CONTENTS

LIST OF TABLES	ix
LIST OF FIGURES	xi
INTRODUCTION	1
CHAPTER 1: FABRICATION AND INITIAL MAGNETIC AND COMPRESSIVE STRENGTH OF P(dL)A/PGA/FE AND P(dL)A/PGA/SmCo₅ IMPLANTS FOR USE AS A DELIVERY DEVICE FOR MAGNETICALLY DIRECTED CHONDROGENESIS	6
Abstract	6
Introduction	7
Experimental Procedure	8
Materials	8
Methods	9
Porous Implant Fabrication	9
Solid Implant Fabrication	11
Implant Morphology	11
Magnetic Field Strength	11
Magnetic Particle Orientation	12
Compression Testing	12
In Vitro Attraction	13
Results	14
Morphology	14
Magnetic properties	16
Mechanical Properties	19
In Vitro Attraction Study	20
Discussion	21
Conclusion	24
References	25

CHAPTER 2: IN VITRO MAGNETIC DEGRADATION OF P(dl)A/PGA/FE AND P(dl)A/PGA/SmCo₅ IMPLANTS FOR USE AS A DELIVERY DEVICE IN MAGNETICALLY DIRECTED CHONDROGENESIS	30
Abstract	30
Introduction	31
Experimental Procedure	37
Materials	37
Methods	38
Porous Implant Fabrication	38
Solid Implant Fabrication	38
Aging/Degradation	39
Chondrocyte Field Strength	40
Magnetic Particle Orientation	40
Results	40
Implant Morphology	40
Chondrocyte Field Strength	41
Magnetic Field Strength	42
Porous Implants	42
Solid Implants	47
Separation Distance	50
Discussion	56
Conclusion	60
References	61
 CHAPTER 3-EFFECT OF ETHYLENE OXIDE AND HYDROGEN PERIOXIDE STERILIZATION ON THE MOLECULAR WEIGHT AND CHEMICAL STRUCTURE OF P(DL)A AND P(DL)A/PGA POLYMERS	 65
Abstract	65
Introduction	66
Experimental Procedure	70
Materials	70

Methods	70
Fourier Transform Infrared Spectroscopy (FTIR)	70
Gel Permeation Chromatography (GPC)	71
EtO Sterilization	72
H ₂ O ₂ Sterilization	72
Results	72
GPC	72
FTIR	74
Discussion	81
Conclusion	88
References	89
 CHAPTER 4-FINITE ELEMENT MODELING OF THE VON MISES STRESS OF A FEMORAL CONDYLE SUBJECT TO FULL THICKNESS CARTILAGE DEFECTS AND MAGNETICALLY DIRECTED CHONDROGENESIS IMPLANTS OF VARYING SIZE AND MORPHOLOGY	 92
Abstract	92
Introduction	93
Experimental Procedure	94
Results	99
Discussion	110
Conclusions	114
References	115
CONCLUSIONS	117
APPENDIX 1-PILOT BIOCOMPATIBILITY STUDY	121
APPENDIX 2-MAGNETIC AND MORPHOLOGICAL DATA	137

LIST OF TABLES

<u>Table</u>		<u>Page</u>
	<u>Chapter 1</u>	
1	Polymer Molecular Weights.	9
2	Calculation of the orientation F-factor for 50/50 and 85/15 P(dl)A/PGA implants containing 25 vol% Fe.	19
3	Volume Susceptibilities of solid and porous implants with SmCo ₅ .	19
4	Mechanical properties of selective implant compositions and porosity.	19
	<u>Chapter 3</u>	
1	Volume % degradation of PLA/PGA copolymers as a function of degradation time	33
2	Strength remaining and Volume % degradation of PLA/PGA Copolymers as a function of implantation time	33
3	Polymer Molecular Weights	37
4	Magnetic pole strengths of 65/35 P(dl)A/PGA implants fabricated with 10, 20, 30 or 40 vol% Fe as a function of degradation time	44
5	Magnetic pole strengths of 50/50, 65/35, 75/25 and 85/15 P(dl)A/PGA implants fabricated with 25 vol% Fe as a function of degradation time	46
6	Calculation of the orientation F-factor for 50/50 and 85/15 P(dl)A/PGA implants containing 25 vol% Fe	46
7	Pole strength data and standard deviations for porous 65/35 and 85/15 P(dl)A/PGA implants containing 25 vol% SmCo ₅	47
8	Pole strength data and standard deviations for solid 65/35 P(dl)A/PGA implants containing 12.5, 25, 30, 35, 40 and 45 vol% Fe vs. <i>in vitro</i> degradation time	49
9	Pole strength data and standard deviations for solid 65/35 and 85/15 P(dl)A/PGA implants containing 50 vol% SmCo ₅	50

10	Maximum chondrocyte/implant separation distance for 65/35 P(dl)A/PGA implants fabricated with 10, 20, 30 or 40 vol% Fe as a function of degradation time	52
11	Maximum chondrocyte/implant separation distance between 50/50, 65/35, 75/25 and 85/15 P(dl)A/PGA implants fabricated with 25 vol% Fe as a function of degradation time	53
12	Maximum chondrocyte/implant separation distance and standard deviations for solid 65/35 P(dl)A/PGA implants containing 12.5, 25, 30,35,40 and 45 vol% Fe vs. <i>in vitro</i> degradation time	54
13	Maximum separation distance and standard deviations for porous 65/35 and 85/15 P(dl)A/PGA implants containing 25 vol% SmCo ₅	55
14	Maximum separation distance and standard deviations for porous 65/35 and 85/15 P(dl)A/PGA implants containing 25 vol% SmCo ₅	56

Chapter 3

1	Material properties for the as-received 100 P(dl)A, 75/25 and 50/50 P(dl)A/PGA polymers reported by Alkermes Inc. of Wilmington, OH	70
2	Integrated peak areas for 100 P(dl)A sterilized using EtO	80
3	Integrated peak areas for 75/25 P(dl)A/PGA sterilized using EtO	80
4	Integrated peak areas for 50/50 P(dl)A/PGA sterilized using EtO	80
5	Integrated peak areas for 100 P(dl)A sterilized using H ₂ O ₂	85
6	Integrated peak areas for 75/25 P(dl)A/PGA sterilized using H ₂ O ₂	85
7	Integrated peak areas for 50/50 P(dl)A/PGA sterilized using H ₂ O ₂	85

Chapter 4

1	Material Properties used in the femoral condyle FEM model	97
---	---	----

LIST OF FIGURES

<u>Figure</u>		<u>Page</u>
	<u>Chapter 1</u>	
1	Schematic of processing strategy.	10
2	Schematic diagram of the <i>MPMS SQUID</i> magnetometer showing the implant mounted in the silicon mold and filled with PBS (left) as well as the squid magnetometer which was used to measure the magnetic susceptibility of the implant at 37°C.	13
3	A stereo-micrograph (12.5X) of a representative a) cross section and b) outer surface of a representative 85/15 P(dl)A/PGA/Fe compression sample.	14
4	SEM micrograph of the cross-section of a 65/35 P(dl)A/PGA/Fe implant, 50x.	15
5	SEM micrograph of the outer surface of 65/35 P(dl)A/PGA/Fe implant containing 25 vol% Fe, 50x.	15
6	Volume susceptibility vs. Fe content of porous 65/35 P(dl)A/PGA implants.	17
7	Volume susceptibility vs. Fe content of solid 65/35 P(dl)A/PGA implants.	17
8	Volume susceptibility vs. polymer composition of porous implants containing 25 vol.% Fe.	18
9	Optical photomicrograph of magnetically tagged chondrocytes in DEM growth medium exposed to a 50/50 P(dl)A/PGA/Fe implant. The picture was taken 5 min. after addition of chondrocytes, tagged with Fe nanoparticles.	20
	<u>Chapter 2</u>	
1	Force profile of a single chondrocyte cell subject to MDC <i>in vivo</i>	35
2	Schematic of parameters involved with the calculation of magnetic field away from implant site	36
3	Diagram of <i>in vitro</i> sample holder for use with the <i>MPMS SQUID</i>	39

Magnetometer (*Quantum Design Inc.*)

4	Scanning electron micrograph of the A) cross section and B) surface of A representative 65/35 P(dl)A/PGA implant containing 25 vol% Fe	42
5	Pole strength vs. degradation time of 50% porous composite implants fabricated with 65/35 P(dl)A/PGA and 10, 20, 30 or 40 vol% Fe	43
6	Pole strength vs. <i>in vitro</i> degradation time and polymer composition of 50% porous composite implants with 25% Fe	45
7	Pole strength vs. <i>in vitro</i> degradation time and polymer composition of 50% porous composite implants with 25 vol % SmCo ₅	47
8	Magnetic pole strength vs. <i>in vitro</i> degradation and Fe loading of 65/35 P(dl)A/PGA implants	48
9	Magnetic pole strength of solid 65/35 P(dl)A/PGA implants and 85/15 P(dl)A/PGA implants containing 50 vol% SmCo ₅ as a function of <i>in vitro</i> degradation	50
10	Maximum chondrocyte/implant separation distance as a function of degradation time and Fe concentration for 50% porous implants composed of 65/35 P(dl)A/PGA	51
11	Maximum chondrocyte/implant separation distance as a function of degradation time and polymer concentration for 50% porous implants containing 25 vol% Fe	53
12	Maximum chondrocyte/implant separation distance as a function of degradation time and Fe concentration for solid implants composed of 65/35 P(dl)A/PGA	54
13	Maximum Chondrocyte/Implant Separation Distance as a Function of Degradation Time and Polymer Concentration for solid implants containing 50 vol % SmCo ₅	55
14	Maximum chondrocyte/implant separation distance as a function of degradation time and polymer concentration for 50% porous implants containing 25 vol % SmCo ₅	56
15	Particle-particle interaction within a P(dl)A/PGA/Fe or P(dl)A/PGA/SmCo ₅ implant. The magnetic poles (B) of the individual particles are oriented in the same direction creating a magnetic field (H). As can be seen in the schematic as the particles approach each other the magnetic field of one the top particle is oriented in the opposite direction of the lower particle.	58

Chapter 3

1	Normalized molecular weight as a function of time after sterilization for: A)50/50 P(dl)A/PGA, B) 75/25 P(dl)A/PGA, and C)100 P(dl)A	75
2	FTIR spectrums of 50/50 P(dl)A/PGA polymers: A) As Received, B) 1 Day after EO Sterilization, C) 14 Days after EO Sterilization, D) Residual after 1 Day, E) Residual after 14 Days	77
3	FTIR spectrums of 75/25 P(dl)A/PGA polymers: A) As Received, B) 1 Day after EO Sterilization, C) 14 Days after EO Sterilization, D) Residual after 1 Day, E) Residual after 14 Days	78
4	FTIR spectrums of 100 P(dl)A polymers: A) As Received, B) 1 Day after EO Sterilization, C) 14 Days after EO Sterilization, D) Residual after 1 Day, E) Residual after 14 Days	79
5	FTIR spectrums of 50/50 P(dl)A/PGA polymers: A) As Received, B) 1 Day after Sterrad Sterilization, C) 14 Days after Sterrad Sterilization, D) Residual after 1 Day, E) Residual after 14 Days	82
6	FTIR spectrums of 75/25 P(dl)A/PGA polymers: A) As Received, B) 1 Day after Sterrad Sterilization, C) 14 Days after Sterrad Sterilization, D) Residual after 1 Day, E) Residual after 14 Days	83
7	FTIR spectrums of 100 P(dl)A polymers: A) As Received, B) 1 Day after Sterrad Sterilization, C) 14 Days after Sterrad Sterilization, D) Residual after 1 Day, E) Residual after 14 Days	84
8	Chemical Structure of A)PLA and B) PGA	87
9	Degradation of polylactic/polyglycolic acid a) polyester degradation via nonspecific hydrolytic scission, b) ester bond cleavage and terminal group formation	87

Chapter 4

1	X-ray of a 44-year-old male knee	96
2	Cross section diagram of the human knee	96
3	Pressure profile across the tibial plateau with application of 1500kN load	97

4	Area map of the finite element model with the loading conditions on the articular surfaces and the boundary conditions on the proximal surface (femoral shaft)	98
5	Area map of the finite element model with the loading conditions on the articular surfaces and the boundary conditions on the proximal surface (femoral shaft)	99
6	Von Mises stress distribution in the Femoral Condyle using the loading conditions on the articular cartilage and the boundary conditions on the femoral shaft	101
7	Von Mises stress distribution in the femoral condyle using the loading Profile bone surface and 0 displacement boundary conditions on the articular surface. The model indicated elevated von Mises stress concentrations underlying the articular cartilage (A) with lower von Mises stresses on the medial and lateral surfaces of the femoral condyle as well as in the femoral groove	101
8	FEA of femoral condyle with 2 full thickness defects on the articular surface. The model indicated a decrease in von Mises stress in the trabecular bone subchondral to the defect sites (A and B) and elevated von Mises stress and deformation in the lateral articular cartilage (C)	102
9	FEM model of the lateral condyle defect. The model indicated a significant amount of cartilage deformation along the surfaces of the defect (A) with increased von Mises stress at the cartilage/trabecular bone interface (B). A reduction in the von Mises stress in the trabecular bone subchondral to the defect site was also apparent (C)	103
10	FEM model of the medial condyle defect. The model indicated a Significant amount of cartilage deformation along the surfaces of the defect (A) with increased von Mises stress at the cartilage/trabecular bone interface (B). A reduction in the von Mises stress in the trabecular bone subchondral to the defect site was also apparent (C)	104
11	Area map of the femoral condyle model with cartilage defects and 2 magnetic implants	105
12	Area map of the femoral condyle model with cartilage defects and 1 magnetic implant	105
13	Von Mises stress profile of the lateral condyle femur with 2 porous implants implanted into the base of the cartilage defect. The FEM model predicted a decrease in the von Mises stress between the implants (A) and a slight increase in von Mises stress surrounding the implant (B).	107

Again stress concentration points were present at the cartilage/trabecular bone interface (C)

- | | | |
|----|--|-----|
| 14 | Von Mises stress profile of the lateral condyle with 2 solid implants implanted into the base of the defect. The FEM model predicted a decrease in the von Mises stress between the implants (A) and a slight increase in von Mises stress surrounding the implant (B). Once again stress concentration points were present at the cartilage/trabecular bone interface (C) | 107 |
| 15 | Von Mises stress profile of the femoral lateral condyle with 1 porous Magnet implanted at the base of the defect. The FEM model predicts minimal elevated von Mises stresses in the corners of the implant (A) and along the sides of implant (C). The von Mises stress was minimized on the proximal end of the implant (B) and gradually increased with distance away from the implant | 109 |
| 16 | Von Mises stress profile of the femoral lateral condyle with 1 solid Magnet implanted at the base of the defect. The FEM model predicted higher stresses in the corners of the implant (A). The stress surrounding the implant was more uniform and ranged between 0.42 and 1.10 MPa over most of the implant/trabecular bone interface (B) | 109 |

INTRODUCTION

Osteoarthritis is considered the most prevalent rheumatic disease¹ and results in a deterioration and/or loss of cartilage on articulating surfaces leading to pain and joint dysfunction in 75% of the elderly population.² For this reason, substantial effort and research has been devoted to the restoration of the structure and mechanical properties of damaged articular cartilage.

Until recently, cartilage defects, have been repaired using autografts (ex. mosaic plasty) or prosthetic devices (ex. TKR). However, donor tissue is limited and prosthetic devices have a short life-span due to the inherent risk of infection from the presence of a foreign body, leading to a loosening of the implant at the interface over time.³⁻⁵ To avoid total joint reconstruction, a number of alternative techniques for repairing articular cartilage have been attempted. The most notable of these techniques: tissue allografting/autografting (mosaic plasty)^{6,7} and chondrocyte seeding⁸⁻¹⁰, have shown limited long-term success. With tissue allografting, cartilage is excised from a donor system, or grown *in vitro* and used to fill cartilage defect sites. However, availability, biocompatibility and transplant adhesions are critical factors that limit this technique. In mosaic plasty, the donor tissue is taken from an undamaged source of the recipient's body. Even though this alleviates the biocompatibility and donor issues of tissue allografting, this technique often leaves the donor site susceptible to further cartilage degeneration and long term success is very low. Cartilage-like tissue regeneration has been shown to occur *in vivo* and *in vitro* by seeding chondrocytes on to a biodegradable polymer scaffold and implanting this scaffold into the defect site. However, these

techniques have not produced cartilage that is comparable to native hyaline cartilage and such tissue is not integrated with the surrounding cartilage.

Recently, research has shown that autologous chondrocyte transplantation can regenerate hyaline-like cartilage with tissue morphology similar to native cartilage.¹¹⁻¹³ In this technique autologous chondrocytes are harvested from the joint, expanded in tissue culture, and introduced under an implanted periosteal flap over the joint defect. This technique, although successful in producing type II collagen, utilizes multiple invasive surgeries which increases both the chance of infection and recovery time. Since a periosteal flap is inserted into the joint margin, this technique also requires an unloaded period of up to eight weeks during healing. Thus, this technique is labor intensive, expensive, and requires a long healing time at which the joint must be unloaded leaving the patient immobilized.

Halpern, Crimp, and Grande^{14,15} have also shown cartilage regeneration through chondrocyte delivery by magnetically directed chondrogenesis (MDC). MDC is a technique in which chondrocytes are tagged with iron nanoparticles leaving them susceptible to magnetic manipulation. A magnetic plug is then implanted into the subchondral bone underlying the cartilage defect to direct growth to that area. MDC resulted in a tissue with characteristics that are morphologically similar to native hyaline cartilage with chondrocytes located in well-defined lacunae and a matrix that stained positively for aggrecan. However, initial studies used a solid neodymium magnet, which is not biocompatible for long term implantation. The focus of this dissertation was to develop a porous, biodegradable, and biocompatible magnet for use in MDC.

In Chapter 1, implant fabrication and the initial magnetic and physical properties of P(dl)A/PGA/Fe and P(dl)A/PGA/SmCo₅ implants were investigated. The magnetic susceptibility of solid and porous implants were evaluated as a function magnetic material (Fe or SmCo₅) and volume of magnetic material. The mechanical strength and elastic modulus of P(dl)A/PGA/Fe implants were evaluated by compression testing and compared to the mechanical strength of trabecular and cortical bone. A preliminary *in vitro* evaluation of the attraction between P(dl)A/PGA/Fe magnetically tagged chondrocytes was performed.

In Chapter 2, the magnetic strength of P(dl)A/PGA/Fe and P(dl)A/PGA/SmCo₅ implants was investigated as a function of *in vitro* degradation time. The magnetic field strengths were then used to estimate the maximum separation distances at which the MDC implants could attract magnetically tagged chondrocytes. With this data, an implant morphology and composition that optimizes the chondrocyte/implant attraction during the first 8 weeks of implantation was determined.

In Chapter 3, the effect of ethylene oxide (EO) and hydrogen peroxide (H₂O₂) sterilization on the molecular weight and chemical structure of 50/50 P(dl)A/PGA, 75/25 P(dl)A/PGA, and P(dl)A were evaluated. The polymer molecular weight was determined by gel permeation chromatography (GPC) and the polymer structure evaluated by Fourier transform spectroscopy (FTIR). The results of this study were used to determine the most appropriate (results in the least amount of polymer destruction) for P(dl)A/PGA/Fe or P(dl)A/PGA/SmCo₅ implants used in MDC.

In Chapter 4, a finite element model was used to evaluate the von Mises stress in the femoral condyle trabecular bone surrounding a MDC implant. The effect of implant size,

stiffness and morphology on the surrounding stress was evaluated. This investigation was used to determine whether or not the addition of a MDC implant into the subchondral bone would develop stresses high enough to fracture the femur under normal loading conditions. This information was then used to determine the implant parameters, size and porosity, which would result in the least amount of alteration of the von Mises stress in the bone surrounding the implant.

In the conclusions, the data from these five studies was used to determine the optimum implant parameters for use in MDC. These parameters include the morphology of the implant (porous or solid), the magnetic material of the implant (Fe or SmCo5), the volume of magnetic material, the polymer composition, sterilization technique, and the implant size and number.

REFERENCES

1. D.S. Howell, R.D. Altman, "Cartilage Repair and Conservation in Osteoarthritis", *Osteoarthritis*, **19**, 3, 1993, 713-724.
2. H.J. Mankin, "Chondrocyte Transplantation One Answer to an Old Question", *The New Eng. J. Med.*, **331**, 14, 1994, 940-941.
3. Landon G.C., Galante, J.O., Casini, J., "Essay on Total Knee Replacement". *Clin. Ortho.*, **192**, 1985, 69-74.
4. Amstutz H.C., Dorey F., O'Carroll P.F., "Resurfacing Arthroplasty: Evolution and Long Term Results", *Clin. Ortho.*, **213**, 1986, 92-114.
5. Praemer A., Furner S., Rice D.P., "Musculoskeletal Conditions in the United States: Medical Implants and Major Joint Procedures", American Academy of Orthopaedic Surgeons, 1992: 125-141.
6. Buckwalter J.A., Mow V.C., "Cartilage Repair in Osteoarthritis", Osteoarthritis: Diagnosis and Medical/Surgical Management, WB Saunders, 1992, p71-107.
7. Buckwalter J.A., Rosenberg L.C., Hunziker E.B., "Articular Cartilage: Composition structure, response to injury and methods of facilitating repair, Articular Cartilage and

Knee Joint Function”, Basic Science and Arthroscopy, Raven Press, New York, 1990, p19-56.

- 8. Vacanti C.A., Langer R., Schloo R., Vacanti J.P., “Synthetic Polymers Seeded with Chondrocytes Provide Template for New Cartilage Formation”, *Plas. Recon. Surg.*, **88**:5, 1991, p753-759.**
- 9. Wald H.L., Sarakinos G., Lyman M.D., Mikos A.G., Vacanti J.P., Langer R., “Cell Seeding in Porous Transplantation Devices”, *Biomaterials.*, **14**, 4, 1993, 270-278.**
- 10. Freed L.E., Marquis J.C., Nohria A., Emmanuel J., Mikos A.G., Langer R., “Neocartilage Formation In Vitro and In Vivo Using Cells Cultured On Synthetic Biodegradable Polymers”. *J. Biomed. Mat. Res.*, **27**:11-23, 1993.**
- 11. M. Brittberg, A. Lindahl, A. Nilsson, C. Ohlsson, O. Isaksson, L. Peterson, “Treatment of Deep Cartilage Defects in the Knee with Autologous Chondrocyte Transplantation”, *The New Eng. J. Med.*, **331**, 14, 1994,889-895.**
- 12. L. Peterson, D. Menche, D. Grande, “Chondrocyte Transplantation-An experimental model in the rabbit”, *Transactions of the 30th Annual Orthopaedic Research Society*, 1984, p218.**
- 13. Grande D.A., Pittman M.I., Peterson L., Menche D., Klein M. “The Repair of Experimentally Produced Defects in Rabbit Articular Cartilage by Autologous Chondrocyte Transplantation”, *J Ortho. Res.*, 1989, 7, 208-218.**
- 14 A.A. Halpern, M.J. Crimp, D. Grande, “The Use of Magnetically Tagged Chondrocytes for Repair of Cartilage Defects”, *Trans. Ortho. Res. Soc.*, **22**, 1997, 541.**
- 15. A.A. Halpern, M.J.Crimp, M.G. Blowers, L.A. Lowsein, L.H. Huisepos, W.R. McPherson, “Determination of Cellular Response to Intraarticular Placement of Neodymium and Samarium Cobalt Magnetic Implants in a Canine Model”, 3rd Combined Meeting of Orthopaedic Research Society of USA, Canada, Europe, & Japan, Hamamatsu, Japan, Sept. 1998.**

CHAPTER 1

FABRICATION AND INITIAL MAGNETIC AND COMPRESSIVE STRENGTHS OF P(dl)A/PGA/FE AND P(dl)A/PGA/SmCo₅ IMPLANTS FOR USE AS A DELIVERY DEVICE FOR MAGNETICALLY DIRECTED CHONDROGENESIS

DEAN A. OPPERMAN AND MELISSA J. CRIMP

Department of Materials Science and Mechanics

Michigan State University

East Lansing, MI 48823

ALAN A. HALPERN

College of Human Medicine

Michigan State University

East Lansing, MI 48823

ABSTRACT

This study investigated the fabrication of a biocompatible, bioresorbable, magnetic implant for use in magnetically directed chondrogenesis (MDC). A solvent leaching technique was utilized to create implants using 85/15 P(dl)A/PGA, 75-25 P(dl)A/PGA, 65/35 P(dl)A/PGA and 50-50 P(dl)A/PGA copolymers. Anisotropic magnetic implants were fabricated by then adding Fe or SmCo₅ particles, which were later magnetized. Magnetic susceptibilities as high as 8.73×10^{-4} H/m were measured for implants containing SmCo₅ and 4.12×10^{-6} H/m for implants containing Fe. Compressive strengths of porous implants containing 25% Fe by volume and solid implants containing 40% Fe by volume were 8.2 ± 1.2 MPa and 48 ± 3.0 MPa respectively. The compressive strength of porous implants was comparable to trabecular bone (2-35 MPa) and the compressive strength of solid samples was significantly less than cortical bone (193 MPa). Porous

implants containing 25% Fe by volume attracted magnetically tagged chondrocytes *in vitro*, indicating that these implants may be suitable for MDC.

INTRODUCTION

Articular cartilage possesses a limited capacity for permanent defect repair¹⁻⁶. Partial articular cartilage defects show no meaningful repair. Full thickness cartilage defects have been shown to vascularize at the defect site. This vascularization leads to a healing response capable of generating new hyaline-like articular cartilage¹⁻⁵. However, this repair is short lived because this neocartilage does not incorporated into the surrounding native cartilage tissue⁶. Despite the poor outcome of cartilage repair by vascularization of the defect site, the application of chondrogenetic cells remains the rationale behind many of the current regeneration studies⁷⁻²⁰.

Perichondral grafting⁷⁻¹¹, osteochondral grafting¹²⁻¹⁶ and synthetic scaffold seeding¹⁷⁻²⁰ are all successful in limited initial repair of articular cartilage. However, results are short-lived because of either a lack of neocartilage incorporation, reduced cellular viability, or infection⁴⁻⁶. To date, the most successful cartilage regeneration technique is autologous chondrocyte transplantation where autologous chondrocytes are injected into the defect site and covered with periosteal tissue²¹⁻²⁴. This technique has limited long-term success in 1-2 year studies, involving multiple surgeries and immobilization of the joint for up to 8 weeks during healing. However, this research shows that delivering and holding chondrocytes at a defect site prompts chondrogenesis, resulting in hyaline-like articular cartilage.

Magnetically directed chondrogenesis (MDC) is similar to autologous chondrocyte transplantation in that autologous chondrocytes are used to effect a repair of the damaged tissue. However in MDC, the chondrocytes are held at the defect site by magnetic forces between the chondrocytes (which have ingested magnetic nanoparticles) and a magnet implanted into the subchondral bone beneath the defect site^{25,26}. Pilot studies by Halpern, Grande, and Crimp, using solid neodymium(Nd) magnets, produced cartilage that was morphologically and histologically similar to native hyaline cartilage^{25,26}. However, the use of solid Nd magnets introduces long-term biocompatibility issues such as bone necrosis and implant loosening due to motion between implant and the surrounding trabecular bone²⁸.

The fabrication protocols will be described for biocompatible, biodegradable, magnetic implants that will eventually be used to replace Nd. In addition, the magnetic and physical properties of both porous and solid implants will be reported as well as the results from an *in vitro* assessment of their ability to attract tagged chondrocytes.

EXPERIMENTAL PROCEEDURE

MATERIALS

High inherent viscosity (HIV) polymers of 85/15, 75/25, 65/35, and 50/50 poly(dl)lactic/glycolic acid (P(dl)A/PGA) were purchased from Alkermes of Blue Ash, OH. The manufacturers reported molecular weights for each of the four polymer compositions are given in Table 1.

Fe and SmCo₅ particles were supplied by Tengam Engineering Inc. of Otsego, MI. The particle size was measured using a Horiba, laser scattering, particle size distribution

analyzer. The average diameters of the Fe and SmCo₅ particles were 1.9 and 2.5 μm respectively.

Table 1 Polymer Molecular Weights

<u>Polymer Composition</u>	<u>Molecular Weight</u>
50/50 P(dl)A/PGA (HIV)	88,000 Daltons
65/35 P(dl)A/PGA (HIV)	141,000 Daltons
75/25 P(dl)A/PGA (HIV)	136,000 Daltons
85/15 P(dl)A/PGA (HIV)	149,000 Daltons

METHODS

Porous Implant Fabrication

Porous biodegradable, magnetic polymer implants were prepared by a salt leaching technique²⁸⁻³⁰. One gram of each polymer was dissolved in 3ml of acetone in 5cc disposable syringes over 12-24 hours. Once dissolved, the appropriate volume fractions (10, 20, 25, 30, 40 vol. %) of magnetic material (Fe or SmCo₅) and 50 vol. % sieved NaCl particles (212-300 μm) were added. The suspension was shaken for 5 min. to generate a uniform dispersion and then injected into 1cc disposable syringes. These syringes were placed into a vacuum oven at 80°C and 83 MPa for 24 hours to evaporate the solvent and dry the implant. Once dried, the temperature was increased to between 120°C and 140°C to soften the polymer in preparation for injection into the molds for magnetization.

Magnetization began by extruding the softened polymer composite into cylindrical silicon molds with a cavity of approximately 1.5mm in diameter (Figure 1). The molds were then heated to 127°C, under an external magnetic field of 55,000 Gauss, using a *MPMS SQUID* magnetometer (Quantum Design Inc.) for 10 min. followed by slow

cooling to room temperature. The magnetic field was returned to 0 and the samples removed and cut into implants, 5-8mm in length.

Compression samples were fabricated by compacting the softened P(dl)A/PGA/Fe composite material into capped 1cc syringes using the syringe plunger. The syringe acted as a cylindrical mold having a 4.5 mm diameter. After compaction, the samples were cooled to room temperature. The cast molds were then machined to lengths between 12 and 16 mm in accordance with ASTM standers for compression testing of brittle polymers using an EMCO Compact 5 high-speed lathe³¹. The polymers were then ejected from the syringe cylinder.

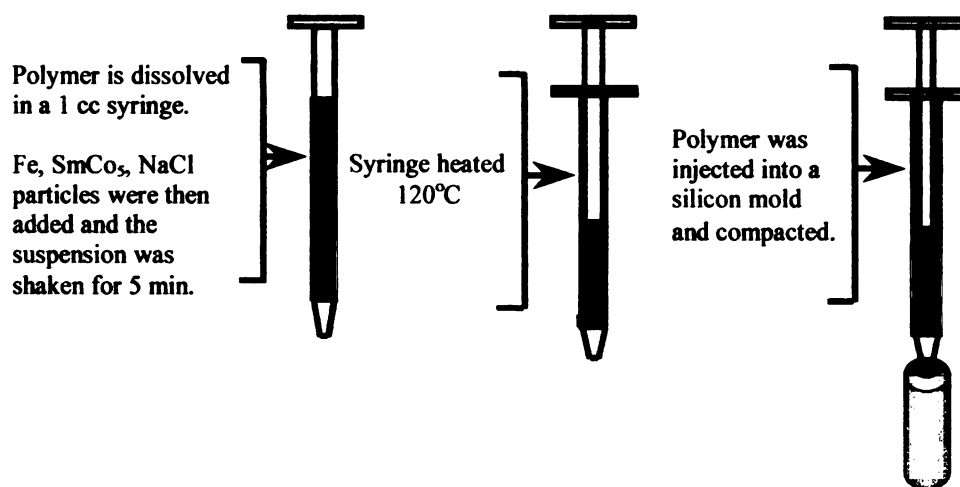


Figure 1 Schematic of processing strategy

Porous samples processed with salt particles were next leached at 37°C, in 1-dram specimen vials filled with reverse-osmosis (RO) water. The RO water was changed every 12 hours, for a period of 48 hours. After leaching, the implants were dried, weighed, and dimensions recorded for density calculations.

Solid Implant Fabrication

Solid implants were fabricated by the same processes as porous implants except implants were made without salt particles and thus the implant was not leached in water after fabrication.

Implant Morphology

The implant porosity was measured using 2 techniques. First, the implant dimensions and weight were used to calculate the implant density. The implant porosity was then determined by comparing the theoretical density of the solid implant with the measured density of the porous implant. These values were then verified using Archimede's technique. Implants were weighed dry (D), wet (M) and suspended in water (S) and the apparent porosity calculated by Equation 1:

$$\text{Apparent Porosity} = \frac{M - D}{M - S} \times 100. \quad (1)$$

The average pore size was determined by physical measurement of pores from optical micrographs. The individual pore sizes were taken from micrographs (5 cross sectional and 5 surface) from 10 different samples. The total number of pores measured was 500 with 50 pores taken from each micrograph.

Magnetic Field Strength

The magnetic field strengths of 5 samples of each implant composition were measured using the *MPMS SQUID* magnetometer. Samples were oriented in the direction of magnetization (along the long axis of the implant) by mounting the implant in a silicon

mold (Figure 2). The silicon mold was sealed in the base of a straw filled with Phosphate Buffered Saline (PBS) at 37° to simulate time zero, *in vivo* conditions.

Magnetic Particle Orientation

The degree to which the magnetic particles were oriented after initial magnetization and after 8 weeks degradation were determined for implants composed of 50/50 and 85/15 P(dl)A/PGA and 25 vol. % Fe following a technique developed by as Sakai et al³². The magnetic field strength was measured in the preferred direction of magnetization ($B_{r\bullet a}$) and the perpendicular direction ($B_{r\bullet b}$). The particle orientation factor (F) was calculated using Equation 2:

$$F = \frac{B_{r\bullet a}}{B_{r\bullet a} + B_{r\bullet b}} \quad (2)$$

For the situations where magnetization is maximized and all the particles are oriented in the same direction, the F-factor equals 1. If the particles were randomly oriented, the F-factor equals 0.5.

Compression Testing

The ultimate compression strength of 5 implants per implant composition were measured using a *Polymer Laboratories Miniature Materials*, screw driven, testing apparatus operated at a cross head speed of 1 mm/min. with a maximum compression of 5mm.

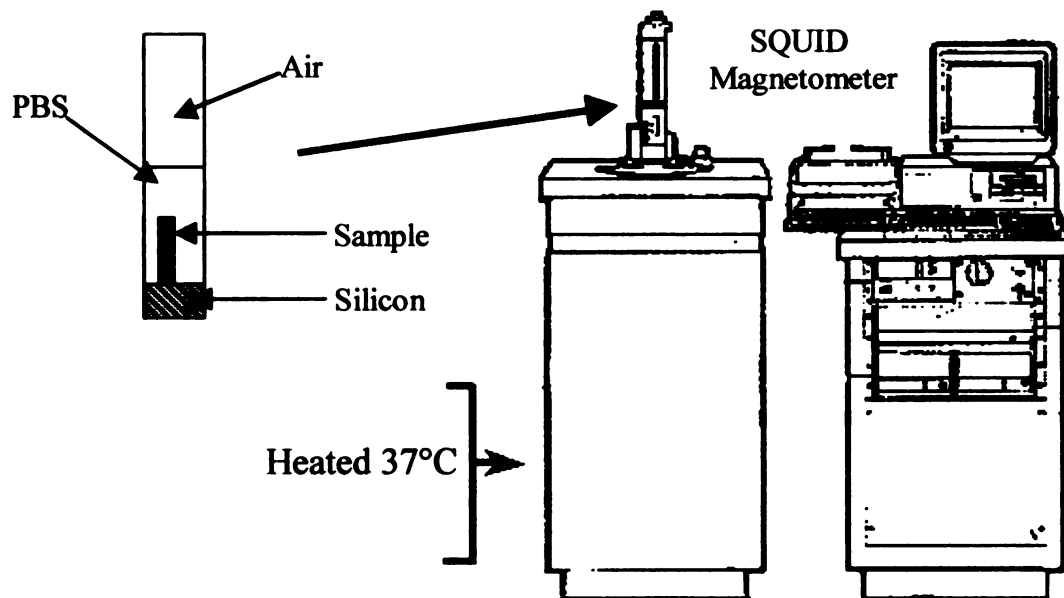


Figure 2 Schematic diagram of the *MPMS SQUID* magnetometer showing the implant mounted in the silicon mold and filled with PBS (left) as well as the squid magnetometer which was used to measure the magnetic susceptibility of the implant at 37°C

In Vitro Attraction

To evaluate the ability of this implant to serve as a delivery device for MDC, the attraction of magnetically tagged chondrocytes to the implants was evaluated. A 50/50 P(dl)A/PGA implant, having 25 vol. % Fe, 50 vol. % porosity and 1.234×10^{-6} H/m magnetic susceptibility, was placed in a petri dish filled with DMEM-F12 growth medium. A 5 ml suspension containing approximately 2.5×10^5 chondrocytes was added and the system imaged using a ZEISS Microsystems laser-scanning microscope, manufactured by Microcosm Inc. of Columbia, MD.

RESULTS

Morphology

The total porosity was 55 vol. % by both density comparison and Archimedes technique. Figures 3-5 are micrographs of the porous P(dl)A/PGA/Fe implants processed by the particulate salt leaching techniques previously described. Figure 3 shows the cross-section (Figure 3a) and the surface (Figure 3b) of a representative 85/15 P(dl)A/PGA/Fe compression sample. The porosity on the outer surface of the implants was found to be slightly smaller ($179.69 \pm 45 \mu\text{m}$) and more disperse when compared to the pores in the cross-section ($224.23 \pm 59 \mu\text{m}$). Combining these resulted in an average pore size of $200.75 \pm 57 \mu\text{m}$.

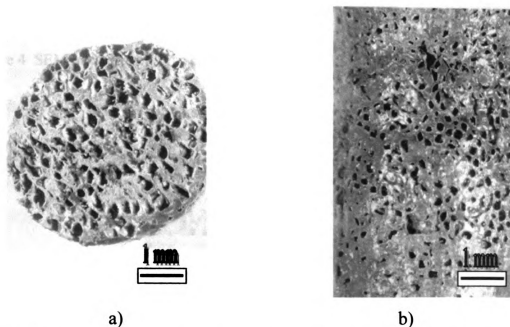


Figure 3 A stereo-micrograph (12.5X) of a representative a) cross section and b) outer surface of a representative 85/15 P(dl)A/PGA/Fe compression sample

Higher magnification photomicrographs of the implant cross section and surface porosity are shown in Figures 4 and 5 respectively. Figure 4 shows the cubic shape of the pores in the cross section of the implants, while Figure 5 shows a more irregular pore shape with only a few cubic pores. In all cases, the porosity is uniformly distributed with no evidence of residual salt.

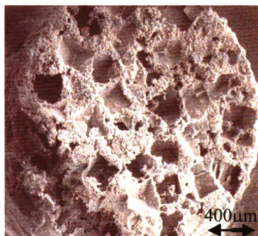


Figure 4 SEM micrograph of the cross-section of a 65/35 P(dl)A/PGA/Fe implant, 50x



Figure 5 SEM micrograph of the outer surface of 65/35 P(dl)A/PGA/Fe implant containing 25 vol. % Fe, 50x

MAGNETIC PROPERTIES

Figures 6 and 7 are plots of the magnetic susceptibility vs. Fe content of porous and solid 65/35 P(dl)A/PGA/Fe implants respectively. The volume fraction Fe is the volume fraction of the solid component that is composed of the magnetic material. As expected, in both the porous and solid 65/35 P(dl)A/PGA implants, the magnetic volume susceptibility increased linearly with the addition of Fe. The maximum volume susceptibility, $2.02 \times 10^{-6} \text{H/m}$, of the porous implants occurred at 40 vol. % Fe, while the maximum volume susceptibility, $4.12 \times 10^{-6} \text{H/m}$, of solid implants occurred at 45 vol. % Fe. This difference is attributed to the 2-fold increase in material volume of the solid implants compared to the 50% porous implants. Thus, the vol. % Fe also doubles resulting in the significant increase in magnetic susceptibility. In the case of the porous samples, the highest achievable volume fraction Fe was 40% while 45vol. % Fe was achieved in the solid implants. When implants were fabricated with volume fractions of Fe greater than 40%(porous) and 45%(solid) the implants broke during de-molding after magnetization.

Figure 8 is a graph of the implant susceptibility as a function of the polymer composition where all samples were 50% porous with 25 vol. % Fe. The magnetic susceptibility decreased with increasing PLA polymer compositions. The 50/50 copolymer resulted in an average magnetic susceptibility that doubled that of the 85/15 copolymer, 1.06×10^{-6} and $5.06 \times 10^{-7} \text{H/m}$ respectively.

The magnetic field strengths along the axis and perpendicular to the implant along with the calculated F-factors for 50/50 and 85/15 P(dl)A/PGA implants with 25 vol. % Fe are listed in Table 2. The magnetic field strengths in the direction of implant

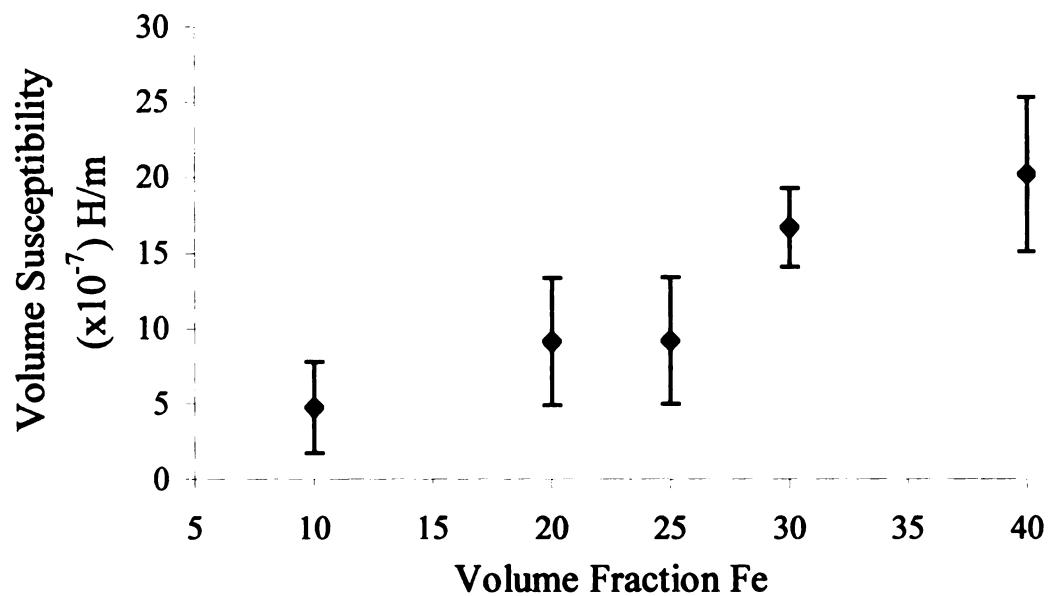


Figure 6 Volume susceptibility vs. Fe content of porous 65/35 P(dl)A/PGA implants

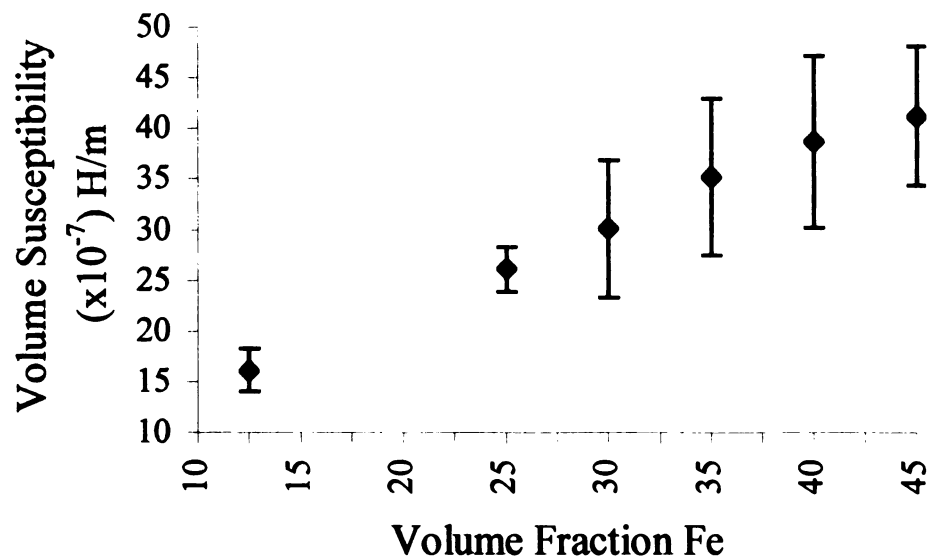


Figure 7 Volume susceptibility vs. Fe content of solid 65/35 P(dl)A/PGA implants

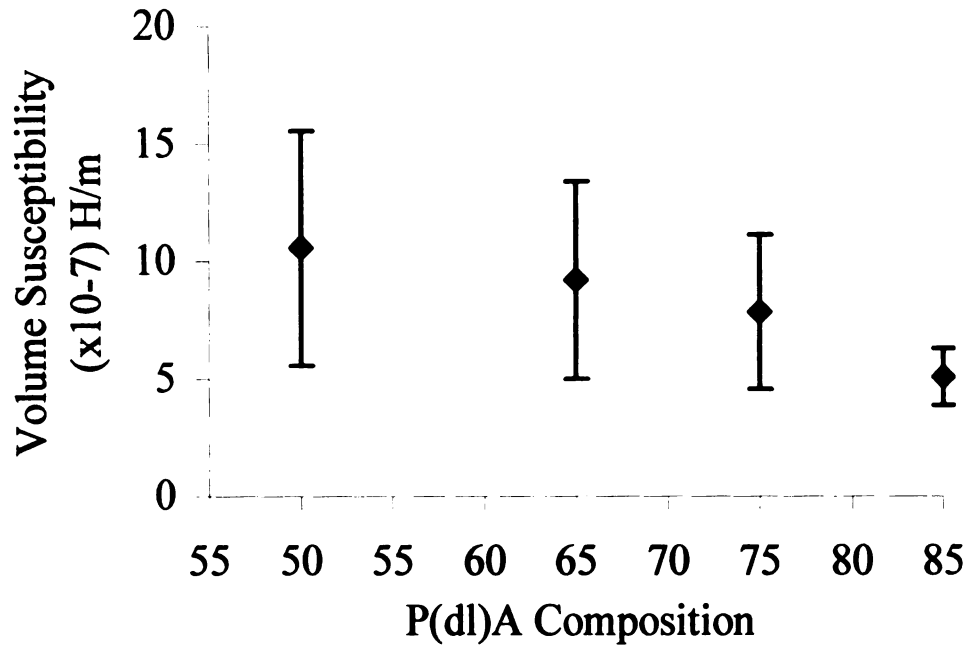


Figure 8 Volume susceptibility vs. polymer composition of porous implants containing 25 vol. % Fe

magnetization (B_{rea}) for the 50/50 P(dl)A/PGA implants were statistically higher than the 85/15 P(dl)A/PGA implants, $2.75 \pm 0.3 \times 10^{-3}$ emu and $1.23 \pm 0.8 \times 10^{-3}$ emu respectively. In each case, the magnetic field strengths were significantly less in the direction perpendicular to implant magnetization (B_{reb}) than in the direction of magnetization (B_{rea}). However, the B_{reb} of the 50/50 P(dl)A/PGA implants were not statistically different from the 85/15 P(dl)A/PGA implants, $6.32 \pm 5.7 \times 10^{-4}$ emu and $4.39 \pm 2.5 \times 10^{-4}$ emu respectively. The calculated F-Factor for the 50/50 P(dl)A/PGA implants was 0.802 ± 0.05 and for the 85/15 P(dl)A/PGA implants was 0.731 ± 0.04 .

The magnetic susceptibility of solid and porous samples made with SmCo_5 is shown in Table 3. SmCo_5 implants have a significantly higher magnetic volume susceptibility as compared to Fe implants. The highest magnetic susceptibility was $8.73 \times 10^{-4} \text{H/m}$ in 65/35/ SmCo_5 implants, containing 0% porosity and 50 vol. % SmCo_5 . The average

Table 2 Calculation of the orientation F-factor for 50/50 and 85/15 P(dl)A/PGA implants containing 25 vol. % Fe

Polymer	Fe Content	B_{ra} (emu)	B_{rb} (emu)	F-Factor
50/50 P(dl)A/PGA	25 Vol. %	$2.75 \pm 0.3 \times 10^{-3}$	$6.32 \pm 5.7 \times 10^{-4}$	0.802 ± 0.05
85/15 P(dl)A/PGA	25 Vol. %	$1.23 \pm 0.8 \times 10^{-3}$	$4.39 \pm 2.5 \times 10^{-4}$	0.731 ± 0.04

Table 3 Volume Susceptibilities of solid and porous implants with SmCo_5

Polymer Composition	Implant Porosity	SmCo_5 Content	Volume Susceptibility
65/35	0	50 vol. %	$8.73 \times 10^{-4} \pm 8.47 \times 10^{-5}$
85/15	0	50 vol. %	$7.79 \times 10^{-4} \pm 1.60 \times 10^{-4}$
65/35	50 vol. %	25 vol. %	$1.61 \times 10^{-4} \pm 3.14 \times 10^{-5}$
85/15	50 vol. %	25 vol. %	$1.06 \times 10^{-4} \pm 3.11 \times 10^{-5}$

magnetic susceptibility of SmCo_5 implants also increased with increases in PGA composition.

MECHANICAL PROPERTIES

Compressive strengths and compressive moduli for both porous and solid 50/50 P(dl)A/PGA samples are listed in Table 4 as a function of Fe content and implant porosity. The porous 50/50 P(dl)A/PGA implants have an ultimate compressive strength of 8.2 ± 1.2 MPa and a compressive modulus of 104 ± 25.0 MPa. Solid implants have significantly higher compressive strengths and compressive moduli, 48 ± 3.0 MPa and 3.4 ± 0.4 GPa respectively.

Table 4 Mechanical properties of selective implant compositions and porosity

Polymer Composition	Fe Content (Vol. %)	Porosity (Vol. %)	Compressive Strength (MPa)	Compressive Modulus (MPa)
50/50	25	50	8.2 ± 1.2	104 ± 25.0
50/50	45	0	48.0 ± 3.0	3394 ± 404.4

IN VITRO ATTRACTION STUDY

Figure 9 is an optical micrograph showing the response of chondrocytes, tagged with Fe-nanoparticles, to a 50/50 P(dl)A/PGA/Fe implant. The implant was placed in a petri dish containing approximately 2.55×10^5 chondrocytes in DEM growth medium. The implant is almost completely surrounded by chondrocytes with a large number of chondrocytes clustered along the surfaces from the center to the outer edge of the implant.

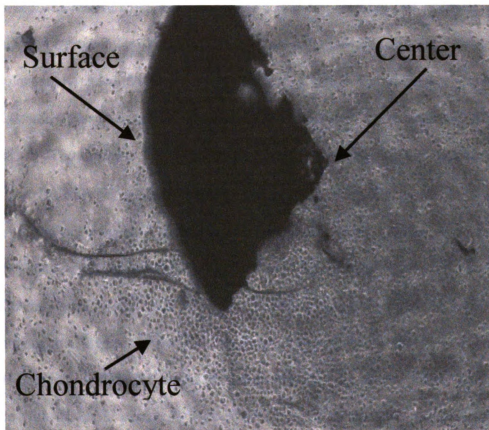


Figure 9 Optical photomicrograph of magnetically tagged chondrocytes in DEM growth medium exposed to a 50/50 P(dl)A/PGA/Fe implant. The picture was taken 5 min. after addition of chondrocytes, tagged with Fe nanoparticles

DISCUSSION

Porous implants were investigated as possible implants for use in MDC for 2 reasons. First, porous samples allow for bone in-growth along the implant/bone interface. Secondly, porous implants may be seeded with chondrogenic cells prior to implantation. This seeding could involve chondrocytes, growth factors or mesenchymal cells¹⁷⁻²⁰. This, in theory, would further increase the healing rate of the cartilage and bone defects.

Any artificial matrix used for cell seeding and tissue scaffolding must promote cell adhesion, cell growth, and maintain cell viability³³. To result in a natural tissue replacement the matrix must also provide space for cell seeding, cell multiplication and production of extracellular matrix (ECM)³⁴. Thus, an organized network of tissue cells in an implant must have an interconnected pore structure of adequate pore size³⁵⁻³⁷. Experimentally, tissue in-growth is optimized with pore sizes in the range of 100 to 400 μm ^{38,39}. The implants fabricated in this study had greater than 50% porosity with evenly distributed pores and an average pore diameter of $\approx 200.75 \pm 57 \mu\text{m}$.

The cubic pore morphology, across the cross-section of the implant, is an artifact of the cubic shape of NaCl particles and is similar to other porous implants that utilize this salt leaching technique²⁸⁻³⁰. The irregularly shaped pores on the outer surface of the implants are attributed to the fact that the samples were injected into a mold that was at room temperature. During injection, the softened polymer hardens quickly when contact is made with the mold surfaces. However, the NaCl particles are not effected by the temperature differential since they are not in a softened state. Thus, they are free to move with the softer polymer away from the outer implant surface. From this it is apparent that

surface porosity is more difficult to achieve with injection molding processing techniques.

Implants with porous surfaces and interconnected porosity were optimum for tissue engineering applications³⁵⁻³⁷. This interconnected porosity optimizes the interaction between the transplanted cells and the cells of the host tissue. Implants with a higher total porosity and improved surface porosity have been produced by non-woven fiber matting⁴⁰, gas saturation⁴¹ and phase separation^{42,43}. The NaCl particle leaching technique was used out of necessity. To optimize the anisotropic properties of the implant, the magnetic particles must be oriented under an applied magnetic field at an elevated temperature where the matrix is appreciably softened. Therefore, the only way a porous sample could be fabricated is to have a material hold the space for the pore during this stage of the implant processing. The NaCl particles used in this study serve that purpose.

The increasing magnetic pole strength associated with increasing PGA compositions measured in this study are attributed to the lower softening temperature of implants containing higher PGA concentrations. The magnetic field strengths of the anisotropic implants are highly dependent on the orientation of the individual magnetic particles^{28,44}. These individual particles are oriented by first softening the polymer matrix and then applying an external magnetic field to rotate the particle and orient the maximum number of particle domains in the direction of magnetization. The maximum temperature that can be applied by the SQUID magnetometer during magnetization is 127°C and the manufactures reported processing temperature of the polymers tested in this study range between 120°C for 50/50 P(dl)A/PGA and 150°C for 85/15 P(dl)A/PGA. Thus, the

50/50 P(dl)A/PGA polymer will be softer than the 85/15 P(dl)A/PGA polymer at 127°C and will have more particle rotation and alignment during implant magnetization. This was also shown by the F-factor calculations. For the 50/50 implants, the initial F-factor was 0.802 ± 0.05 and for the 85/15 implants, the initial F-factor was 0.731 ± 0.04 . This indicated there was a higher degree of particle orientation in the 50/50 polymer implants when compared to the 85/15 polymer implants.

Solid samples of equivalent Fe content had higher magnetic field strengths than porous implants (65/35 P(dl)A/PGA with 25 vol. % Fe in Figure 7 and the 65/35 P(dl)A/PGA with 12.5 vol. % Fe samples of Figure 6). This higher magnetic field was attributed to the improved spacing of the Fe particles within the implant. By increasing the distance between individual particles, the interaction between adjacent particles is minimized resulting in optimum overall particle magnetization.

Implants containing SmCo₅ possessed a much higher magnetic field strength in comparison to Fe containing implants. This increase was more than twice that of equivalent samples containing the same amount of Fe. This increased magnetic field arises from the high material anisotropy and critical particle size of SmCo₅ as compared to Fe. SmCo₅ has a hexagonal crystal structure having a magnetic anisotropy of 17.5×10^7 erg/cm³ at 300 K⁴⁵, which is higher than the Fe particles, which are ferromagnetic. This anisotropy focuses the magnetic field in the desired magnetization direction as compared to Fe whose magnetic field is more random and more easily manipulated. SmCo₅ also has a larger critical diameter, below which the particle can exist as a single domain particle, of $\approx 2 \mu\text{m}$ ^{46,47} compared to the critical diameter of Fe which is approximately 200nm. Since the SmCo₅ used in this study has a particle size diameter of $\approx 2.3 \mu\text{m}$ it can

be assumed that most of the particles are single domain, making them magnetically hard. However, the Fe particles used in this study, which have an average particle diameter of $1.9\mu\text{m}$, are a much softer material because of their inherent multi-domain structure.

The ultimate compressive strength of the porous implants fabricated in this study is comparable to that of trabecular bone, which depending on the density, can vary between 3 and 35MPa ⁴⁸⁻⁵⁰. The compressive modulus of the porous implants at 104 MPa, is significantly less than the 413 and 1515 MPa reported by Pugh et al.⁵¹ for femoral trabecular bone but comparable to the results from Carter and Hayes who reported Young's moduli of the femoral condyle between 10 and 200MPa ⁴⁸. The solid 50/50 P(dl)A/PGA samples had compressive strength and compressive modulus, 48 and 3397MPa respectively. These properties are considerably lower when compared to cortical bone, which has a compressive strength of approximately 193 MPa, and an elastic modulus of approximately 17000MPa ⁵².

Since this is a pilot study for fabricating biodegradable, biocompatible implants capable of attracting magnetically tagged chondrocytes, no data is available to compare magnetic field strength with other implants. Therefore, the ability of these implants to attract chondrocytes was tested *in vitro*. From the results of Figure 9, it is apparent that even in implants with magnetic susceptibilities as low as $1.234 \times 10^{-6}\text{H/m}$ the implants are capable of attracting chondrocytes.

CONCLUSIONS

Implants have been fabricated for use as a delivery device for magnetically directed chondrogenesis. Using P(dl)A/PGA copolymers, magnetic implants have been fabricated

with magnetic susceptibilities as high as 4.12×10^{-6} H/m using Fe and 8.73×10^{-4} H/m using SmCo₅. Implants containing higher concentrations of PGA resulted in higher magnetic susceptibilities because of their lower melting and softening temperatures, while solid implants produced higher magnetic susceptibilities due to improved particle distribution. Therefore, to optimize the initial magnetic contributions to magnetically directed chondrogenesis, the implants should be solid and fabricated with 50/50 P(dl)A/PGA copolymer. Porous implants containing 25 vol. % Fe were capable of attracting chondrocytes to the implant under *in vitro* conditions.

REFERENCES

1. Calandruccio, R.A. and Gilmer, W.S., "Proliferation Regeneration and Repair of Articular Cartilage of Immature Animals", *J. Bone Jt. Surg.*, **44-A**, 1962, 431-455.
2. Kim, H.K.W., Moran, M.E., and Salter, R.B., "The Potential for Regeneration of Articular Cartilage in Defects Created by Chondral Shaving and Subchondral Abrasion. An Experimental Investigation in Rabbits", *J. Bone Jt. Surg.*, **73-A**, 1991, 1301-1315.
3. Mankin, H.J., "The Reaction of Articular Cartilage to Injury and Osteoarthritis", *New England J. Med.*, **291**, 1974, 1285-1292.
4. Hunziker, E.B., "Articular Cartilage Repair: Are The intrinsic Biological Constraints Undermining this Process Insuperable", *Osteoarthritis and Cartilage*, **7**, 1999, 15-28.
5. Buckwalter, J.A. and Mankin, H.J., "Articular Cartilage", *J. Bone Jt. Surg.*, **79-A**, 1997, 612-629.
6. Shapiro, F., Koide, S., and Glimcher, M.J., "Cell Origin and Differentiation in the Repair of Full-Thickness Defects of Articular Cartilage", *J. Bone Jt. Surg.*, **75-A**, 1993, 532-553.
7. Hominga, G.N., van der Linden, T.J., and Terwindt Rouwenhorst, E.A., "Repair of Articular Cartilage Defects by Perichondrial Grafts. Experiments in the Rabbit", *Acta Orthop. Scand.*, **60**, 1994, 326-329.

8. Coutts, R.D., Woo, S.L.Y., Amiel, D., von Schroeder, H.P., and Kwan, M.K., "Rib Periochondrial Autografts in Full-Thickness Articular Cartilage Defects in Rabbits", *Clin. Ortho. Rel. Res.*, **275**, 1992, 263-273.
9. Kreder, H.J., Moran M., Keeley, F.W., and Salter, R.B., "Biologic Resurfacing of a Major Joint Defect with Cryopreserved Allogeneic Periosteum Under the Influence of Continuous Passive Motion in a Rabbit Model", *Clin. Orthop.*, **300**, 1994, 288-296.
10. Salter, R.B., Simmonds, D.F., Malcolm, B.W., Rumble, E.J., MacMichael, D., and Clements, N.D., "The Biological Effect of Continuous Passive Motion on the Healing of Full-Thickness Defects in Articular Cartilage. An Experimental Investigation in the Rabbit.", *J Bone Jt. Surg.*, **62-A**, 1980, 1232-1251.
11. Homminga, G.N., Bulstra, S.K., Bouwmeester, P.S., and van der Linden, A.J., "Perichondral Grafting for Cartilage Lesions of the Knee", *J. Bone Jt. Surg.*, **72-A**, 1990, 1003-1007.
12. Czitrom, A.A., Langer, F., McKee, N., and Gross, A.E., "Bone and Cartilage Allotransplantation: A Review of 14 Years of Research and Clinical Experience", *Clin. Ortho. Relat. Res.*, **208**, 1986, 141-145.
13. Oakeshott, R.D., Farine, I., Pritzker, K.P.H., Langer, F., and Gross, A.E., "A Clinical and Histologic Analysis of Failed Fresh Osteochondral Allografts", *Clin. Ortho. Relat. Res.*, **233**, 1988, 283-294.
14. McDermott, A.G.P., Langer, F., Pritzker, K.P.H., and Gross, A.E., "Fresh Small-Fragment Osteochondral Allografts: Long-term Follow-up Study First 100 Cases", *Clin. Ortho. Relat. Res.*, **197**, 1985, 96-102.
15. Meyers, M.H., Akeson, W., and Convery, F.R., "Resurfacing of the Knee with Fresh Osteochondral Allograft", *J. Bone Jt. Surg.*, **71-A**, 5, 1989, 704-713.
16. Kandel, R.A. Gross, A.E., Ganel, A., McDermott, A.G.P., Langer, F., and Pritzker, K.P.H., "Histopathology of Failed Osteoarticular Shell Allografts", *Clin. Ortho. Relat. Res.*, **197**, 1985, 103-110.
17. Vacanti, C.A., Langer, R., Schloo, B., and Vacanti, J.P., "Synthetic Polymers Seeded with Chondrocytes Provide Template for New Cartilage Formation", *Plast. Reconstr. Surg.*, **88**, 5, 1991, 753-759.
18. Wald, H.L., Sarakinos, G., Lyman, M.D., Mikos, A.G., Vacanti, J.P., and Langer, R., "Cell Seeding in Porous Transplantation Devices", *Biomaterials*, **14**, 4, 1993, 270-278.

19. Freed, L.E., Marquis, J.C., Nohria, A., Emmanuel, J., Mikos, A.G., and Langer, R., Neocartilage Formation In Vitro and In Vivo Using Cells Cultured On Synthetic Biodegradable Polymers", *J. Biomed. Mater. Res.*, **27**, 1993, 11-23.
20. Mooney, D.J., Sano, K., Kaufmann, P.M., Majahod, K., Schloo, B., Vacanti, J.P., and Langer, R., "Long-Term Engraftment of Hepatocytes Transplanted on Biodegradable Polymer Sponges", *J. Biomed. Mater. Sci.*, **37**, 1997, 413-420.
21. Grande, D.A., Pitman M.I., Peterson, L., Menche, D., and Klein, M., The Repair of Experimentally Produced Defects in Rabbit Articular Cartilage by Autologous Chondrocyte Transplantation, *J. Ortho.. Res.*, **7**, 1989, 208-218.
22. Brittberg, M., Lindahl, A., Nilsson, A., Ohlsson, C., Isaksson, O., and Peterson, L., Treatment of Deep Cartilage Defects in the Knee with Autologous Chondrocyte Transplantation, *New Eng. J. Med.*, **331**, 1994, 889-895.
23. Brittberg, M., Nilsson, A., Lindahl, A., Ohlsson, C., and Peterson, L., Rabbit Articular Cartilage Defects Treated with Autologous Cultured Chondrocytes, *Clin. Ortho. Rel. Res.*, **326**, 1996, 270-283.
24. Peterson, L., Menche, D., and Grande, D., "Chondrocyte Transplantation-An Experimental Model in the Rabbit", *Transactions of the 30th Annual Orthopedic Research Society*, 1984, 218.
25. Halpern, A.A., Crimp, M.J., and Grande, D., "The Use of Magnetically Tagged Chondrocytes for Repair of Cartilage Defects", *Trans. Ortho Res. Soc.*, **22**, 1997, 541.
26. Halpern, A.A., Crimp, M.J., Blowers, M.G., Lowsein, L.A., Huisepos, L.H., and McPherson, W.R., "Determination of Cellular Response to Intra-articular Placement of Neodymium and Samarium Cobalt Magnetic Implants in a Canine Model", *3rd Combined Meeting of Orthopedic Research Society of USA, Canada, Europe, & Japan*, Hamamatsu, Japan, Sept. 1998, 261.
27. Carlsson, A.S. and Gentz, C.F., "Mechanical Loosening of the Femoral Head Prosthesis in the Charnley Total Hip Arthroplasty", *Clin. Ortho.*, **147**, 1980, 262-270.
28. deGroot, J.H., Nijenhuis, A.J., Bruin, P., Pennings, A.J., Veth, R.P., Klompmaker, J., and Jansen, H.W., "Use of Porous Biodegradable Polymer Implants in Meniscus reconstruction. 1)Preparation of Porous Biodegradable Polyurethanes for the Reconstruction of Meniscus Lesions", *Colloid Polym. Sci.*, **268**, 1990, 1073-1081.
29. Mikos, A.G., Thorsen, A.J., Czerwonka, L.A., Bao, Y., Langer, R., Winslow, D.N., and Vacanti, J.P., "Preparation and Characterization of Poly(L-Lactic acid) Foams", *Polymer*, **35**, 5, 1994, 1068-1077.

30. Mooney, D.J., Organ, G., Vacanti, J.P., and Langer, R., "Design and Fabrication of Biodegradable Polymer Devices to Engineer Tubular Tissues", *Cell Transplantation*, **3**, 2, 1994, 203-210.
31. Annual Book of ASTM Standards, **08.01**, 1991, D695.
32. Sakai, T., Nakamura, K., and Morii, A., "Plastics Magnet Manufacturing Process: Mixing, Kneading, and Injection Molding", *Intern. Poly. Proc. VI*, **1**, 1991, 26-34.
33. Cima L.G., Ingber D.E., Vacanti J.P., and Langer R., "Hepatocyte Culture on Biodegradable Polymer Substrates", *Biotech. Bioeng.*, **38**, 1991, 145-158.
34. Wald, H.L., Sarakinos, G., Lyman, M.D., Mikos, A.G., Vacanti, J.P., and Langer, R., "Cell Seeding in Porous Transplantation Devices", *Biomaterials*, **14**, 4, 1993, 270-278.
35. Hulbert, S.F., Morrison, S.J., and Klawitter, J.J., "Tissue Reaction to Three Ceramics of Porous and Non-Porous Structures", *J. Biomed. Mat. Res.*, **6**, 5, 1972, 347-374.
36. Mikos, A.G., Sarakinos, G., Lyman, M.D., Ingber, D.E., Vacanti, J.P., and Langer, R., "Prevascularization of Porous Biodegradable Polymers", *Biotech. Bioeng.*, **42**, 716-723, 1993.
37. Mooney, D.J., Kaufmann, P.M., Sano, K., McNamara, K.M., Vacanti, J.P., and Langer, R., "Transplantation of Hepatocytes Using Porous Biodegradable Sponges", *Transplant. Proc.*, **26**, 6, 3425-3426, 1994.
38. Castro, H.J., Salyer, K.E., and Torano, I.R., "Bone Growth into Porous Carbon, Polyethylene, and Polypropylene Prosthesis", *J. Biomed. Mater. Res. Symposium*, **6**, 1978, 1-14.
39. Spector, M., Michno, M.J., Smarook, W.H., and Kwiatkowski, G.T., "A High Modulus Polymer for Porous Orthopedic Implants: Biomechanical Compatibility of Porous Implants", *J. Biomed. Mater. Res.*, **12**, 1978, 665-677.
40. Grande, D.A., Halberstadt, C., Naughton, G., Schwartz, R., and Manji, R., "Evaluation of Matrix Scaffolds for Tissue Engineering of Articular Cartilage Grafts", *J. Biomed. Mater. Res.*, **34**, 1997, 211-220.
41. Mooney, D.J., Baldwin, D.F., Suh, N.P., Vacanti, J.P., Langer, R., "Novel Approach to Fabricate Porous Sponges of Poly(dl-Lactic-Co-Glycolic Acid) Without the Use of Organic Solvents", *Biomaterials*, **17**, 14, 1996, 1417-1422.
42. Nakai, A., Shiwaku, T., Wang, W., Hasegawa, H., Hasimoto, T., "Phase-Separated Structures Formed in Polymer Mixtures Containing a Thermotropic Liquid Crystalline Copolyester as One Component", *Polymer*, **37**, 11, 1996, 2259-2272.

43. Liu, S.Q., and Kodama, M., “Porous Polyurethane Vascular Prostheses with Variable Compliance”, *J. Biomed. Mater. Res.*, **26**, 1992, 1489-1502.
44. Osawa, Z., Kawauchi, K., Iwata, M., and Harada, H., “Effect of Polymer Matrices on Magnetic Properties of Plastic Magnets”, *J. Mater. Sci.*, **57-A**, 2, 1975, 216-220.
45. Ermolenko, A.S., Magnetocrystalline Anisotropy of Rare Earth Intermetallics, *IEEE Transactions on Magnetics*, **12**, 6, 1976, 992-996.
46. McCurrie, R.A., Ferromagnetic Materials: Structure and Properties, Academic Press Ltd., San Diego, CA, 1994.
47. Majetich, S.A., Chowdary, K.M., and Kirkpatrick, E.M., “Size and Interaction Effects in the Magnetization Reversal in SmCo₅ Nanoparticles”, *IEEE Trans. Mag.*, **34**, 4, 1998, 985-987.
48. Carter, D. R. and Hayes, W.C., “Bone Compressive Strength: The Influence of Density and Strain Rate”, *Science*, **194**, 1976, 1174-1176.
49. Behrens, J.C., Walker, P.S., and Shoji, H., “Variations in Strength and Structure of Cancellous Bone at the Knee”, *J. Biomech.*, **7**, 1974, 201-207.
50. Ducheyne, P., Heymans, L., Martens, M., Aernoudt, E., Meester, P., and Mulier, J., “The Mechanical Behavior of Intracondylar Cancellous bone of the Femur at Different Loading Rates”, *J. Biomech.*, **10**, 1976, 747-762.
51. Pugh, J.W., Rose, R.M., and Radin, E.L., “Elastic and Viscoelastic Properties of Trabecular Bone: Dependence on Structure”, *J Biomech.*, **6**, 1973, 475-485.
52. Mow, V.C. and Hayes, W.C., Basic Orthopaedic Biomechanics: Second Edition, Lippincott and Raven Publishers, Philadelphia, 1997, 113-178.

CHAPTER 2

IN VITRO MAGNETIC DEGRADATION OF P(dl)A/PGA/FE AND P(dl)A/PGA/SmCo₅ IMPLANTS FOR USE AS A DELIVERY DEVICE IN MAGNETICALLY DIRECTED CHONDROGENESIS

DEAN A. OPPERMAN AND MELISSA J. CRIMP

Department of Materials Science and Mechanics
Michigan State University
East Lansing, MI 48823

ALAN A. HALPERN

College of Human Medicine
Michigan State University
East Lansing, MI 48823

ABSTRACT

Magnetically directed chondrogenesis (MDC) is a fundamental approach to articular cartilage repair.¹ Recent studies have evaluated the magnetic properties of P(dl)A/PGA/Fe and P(dl)A/PGA/SmCo₅ implants for use in MDC. The magnetic properties of these implants as a function of degradation time must be evaluated to optimize the implant/chondrocyte attraction during the repair process. In this study, porous and solid implants composed of 85/15, 75/25, 65/35, or 50/50 P(dl)A/PGA along with varying amounts of Fe or SmCo₄ particles were degraded *in vitro* in phosphate buffered saline (PBS). The *in vitro* magnetic field strength as a function of degradation time was measured for each implant composition at 0, 1, 2, 4, 6, and 8 weeks. This data was used to calculate the maximum attraction distance over which the chondrocytes are drawn to the implant. By increasing the volume fraction of magnetic particles, the initial

magnetic pole strength increased and the magnetic pole strength degradation rate decreased. Polymers with higher PGA compositions generated higher initial magnetic field strengths because of their lower softening temperatures. However, this higher magnetic field strength was quickly lost due to the faster degradation rate of 50/50 P(dl)A/PGA as compared to 65/35, 75/25, and 85/15 P(dl)A/PGA copolymers. The maximum interaction distance between the implants and the chondrocytes was estimated to be 2.24 ± 0.06 mm for solid 65/35/SmCo₅ implants and 0.38 ± 0.018 mm for solid 65/35/Fe implants. After 8 weeks of degradation, the maximum separation distance was reduced to 1.38 ± 0.04 mm for solid 85/15/SmCo₅ implants and 0.30 ± 0.06 mm for 65/35/Fe implants.

INTRODUCTION

Degradation of polylactic acid (PLA), polyglycolic acid (PGA) and their copolymers (PLA/PGA) is through bulk erosion, which is evidenced by the significant decrease in molecular weight that precedes monomer release.² More specifically, PLA and PGA degrade by hydrolytic scission (cleavage) of unstable ester bonds, incorporated into the polymer backbone. This random chain scission turns what was once a water insoluble polymer, into a water soluble, low molecular weight, polymeric material.³ Random chain scission continues until the cohesive polymer strength decreases to zero, producing low molecular weight fragments. These fragments then degrade into soluble monomers that are eliminated through the Krebs cycle.^{2,3}

Copolymer structure, implant morphology and *in vivo* implantation conditions influence PLA, PGA and PLA/PGA copolymer degradation rates. PLA/PGA implant

degradation rates decrease with increasing molecular weight^{4,5}, crystallinity^{6,7} and PLA composition.^{3,8} Porous implants have been shown to degrade faster than solid implants, and larger polymer implants degrade at a faster rate than smaller implants when subjected to the same *in vivo* conditions.⁹⁻¹¹ Subjecting polymer implants to elevated stress, acidic environments, and site specific enzymes also increases the degradation rates of polyester polymers.¹²⁻¹⁶

Degradation of P(dl)A, PLLA and PGA polymers has been extensively investigated over the last 30 years.¹⁷⁻³⁰ *In vivo* P(dl)A completely degrades in approximately 501 days while PGA completely degrades in approximately 112 days.³¹ Copolymers of PLA and PGA maintain the biocompatibility of their original components, but their physical properties are substantially altered depending on the molar ratios of their constituents.^{8,30,31} Cutright and Barrows have published detailed degradation results of PLA/PGA copolymers.^{30,31} A brief overview of their results is given in Tables 1 and 2. Table 1 lists the amount of polymer degradation as a function of *in vivo* degradation time and polymer composition. Table 2 compares the strength and absorption of PLA/PGA polymers degraded *in vivo*.

Theoretically, the ideal implant material for use in MDC (like bone-fracture fixation) should be rigid, non-inflammatory, non-allergenic, and remain until sufficient healing has occurred to withstand functional stresses. During healing, the material should be removed from the site at a rate comparable to the rate of bone in-growth resulting in a gradual transition of load bearing from the implant material to the newly formed bone. PLA, PGA, and PLA/PGA polymers have all been shown to possess strength comparable to bone and a degradation rate that, depending on composition and molecular weight, that

can range between 8 weeks and 2 years.^{30,31} The ideal implant material for MDC must also be sufficiently magnetic to attract magnetically tagged chondrocytes to the defect site. In addition, the magnetic field must be maintained for a period of time period of sufficient duration to allow the attracted chondrocytes to sustain the repair process.

Table 1 Volume % degradation of PLA/PGA copolymers as a function of degradation time³⁰

	0-4 weeks	8 weeks	12 weeks	16 weeks	16+ weeks
PLA	10%	10%	10%	20%	30%
75PLA/25PGA	20%	25%	25%	65%	80%
50PLA/50PGA	25%	55%	60%	80%	100%
25PLA/75PGA	2%	30%	55%	100%	100%

Table 2 Strength remaining and Volume % degradation of PLA/PGA copolymers as a function of implantation time³¹

PLA/PGA	3 weeks	12 weeks
75/25	28% original strength	23% absorbed
70/30	32% original strength	75% absorbed
65/35	8% original strength	82% absorbed

The implant/chondrocyte attraction distance can be determined by first evaluating the critical force (F) necessary to move a magnetically tagged chondrocyte cell through synovial fluid over some distance. This force is then compared to the actual force between the implant and chondrocyte. The force equation seen by a single particle in a transporting liquid is a function of: 1) drag force, 2) gravitational forces, 3) frictional

forces, 4) pressure differences, and 5) electrostatic forces³². The resulting differential is shown in Equation (1).

$$F = d[\text{drag}] - d[\text{gravity}]_{\text{solid}} - d[\text{friction}]_{\text{solid}} + d[\text{pressure}]_{\text{solid}} - d[\text{electrostatic}] \quad (1)$$

When the particle is moving slowly and the velocity approaches 0, the frictional and drag forces become negligible. An electrostatic force is generated with the application of an electric current which interacts with the chondrocyte surface charges.³² Since an electric field is not applied in MDC, the contribution of electrostatic forces are negligible. The pressure differential developed inside the knee is a complicated system during normal joint movement. However, one assumption during healing is that joint movement will be limited making any pressure differentials negligible. Therefore, the critical force necessary to move a particle is reduced to the force necessary to displace the synovial fluid directly in its path. This amount of synovial fluid is equivalent of the chondrocyte cell volume. A schematic of these forces is shown in Figure 1. The synovial fluid density was estimated to be 1.275gm/cc (measured from a pooled sample of Bovine calf synovial fluid). The dry mass of a chondrocyte cell (m_c) is 2.5×10^{-13} kg. Therefore, the critical force necessary to move a chondrocyte through synovial fluid can be calculated from Equation 2 and is equal to 8.9×10^{-12} N.

If the force of magnetic attraction between the implant and the chondrocyte is greater than 8.9×10^{-12} N, the chondrocyte will then be attracted to the implant. However, if the attraction force is less than this value, the chondrocytes will not be able to displace the synovial fluid and move toward the implant.

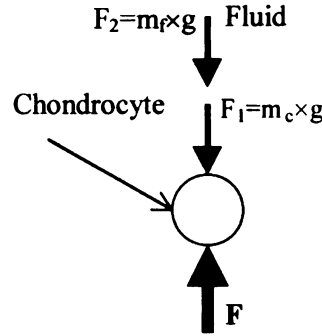


Figure 1 Force profile of a single chondrocyte cell subject to MDC *in vivo*

$$F = (m_f + m_c)g = [(1.275 \times 10^{-3} \text{ kg/cm}^3) \left(\frac{4}{3} \pi (5 \times 10^{-4} \text{ cm})^3 \right) + (2.5 \times 10^{-13} \text{ kg})] \times (9.8 \text{ m/s}^2) \quad (2)$$

$$F = 8.9 \times 10^{-12} \text{ N}$$

When a chondrocyte with a magnetic pole strength (m-Wb) is brought into a magnetic field of intensity (H-A/m), the force F(N) acting on the magnetic pole is

$$F(N) = mH \quad (3)$$

The magnetic field developed by the magnet is dependent on the distance away from the implant. This field strength, as a function of distance away from the implant, can be calculated by³³

$$H = \frac{2pl}{4\pi\mu_0 r^3} \quad (4)$$

where p = pole strength of the implant (emu/m)
 r = distance away from the implant
 l = length of the implant (5mm)
 μ_0 = permeability of vacuum ($4\pi \times 10^{-7} \text{ H/m}$)

A schematic representation of these parameters is illustrated in Figure 2.

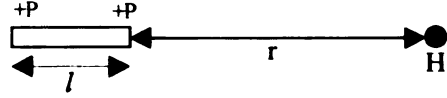


Figure 2 Schematic of parameters involved with the calculation of magnetic field away from implant site

By combining Equations (2) and (3) and solving for the separation distance, r , the maximum separation distance over which a particle is attracted to the implant can be calculated from Equation (5).

$$r \approx \sqrt[3]{\frac{(1.78 \times 10^{10})mpl}{\mu_o}} \quad (5)$$

It is apparent that r increases with increasing magnetic pole strength of the chondrocytes, m , or increasing magnetic pole strength of the implant, p .

Anisotropic polymer magnets were first developed in the early 1950s. Ever since, the physical properties of polymer magnets and the processing techniques of polymer magnet fabrication have been infrequently reported.³³⁻³⁶ Even though the magnetic properties of plastic magnets composed of a polymer matrix and magnetic particles are generally inferior to cast or sintered magnets, they are more easily fabricated than sintered magnets and can be formed into small, or complex shapes. Polymer magnets have enjoyed widespread use in electronic instruments, communication instruments, household utensils, and audio equipment. The magnetic properties of anisotropic polymer magnets

are dependent on the magnetic material³³, polymer matrix³⁴, volume of magnetic material³⁵, and orientation of the magnetic particles.^{34, 36}

In this study, the magnetic field strength of P(dl)A/PGA/Fe and P(dl)A/PGA/SmCo₅ magnetic composites as a function of *in vitro* degradation time was evaluated. This information was used to estimate the maximum chondrocyte/implant interaction distance over which magnetically tagged chondrocytes are attracted to the implant site.

EXPERIMENTAL PROCEDURE

MATERIALS

High inherent viscosity (HIV) polymers of 85/15, 75/25, 65/35, and 50/50 poly(dl-lactic/glycolic acid) were purchased from Alkermes of Blue Ash, OH. The manufacturers reported molecular weights and glass transition temperatures for each of the four polymer compositions are given in Table 3.

Table 3 Polymer Molecular Weights

Polymer Composition	Molecular Weight (Daltons)	Glass Transition Temp. (°C)
50/50 P(dL)A/PGA (HIV)	88,000	45
65/35 P(dL)A/PGA (HIV)	141,000	47
75/25 P(dL)A/PGA (HIV)	136,000	49
85/15 P(dL)A/PGA (HIV)	149,000	51

Fe and SmCo₅ particles were supplied by Tengam Engineering Inc. of Otsego, MI. The particle size was measured using a Horiba laser scattering particle size analyzer. The average diameters of the Fe and SmCo₅ particles were 1.9 and 2.5 μm respectively.

METHODS

Porous Implant Fabrication

Porous biodegradable, magnetic polymer implants approximately 1.5mm in diameter and 5-7 mm long were prepared by a salt leaching technique. Target implants contained 50% porosity with 10, 20, 25, 30, and 40 vol. % Fe or 25 vol. % SmCo₅. Porous implants were also prepared with 25 vol. % Fe and 50/50, 65/35, 75/25, or 85/15 P(dl)A/PGA copolymers. Five implants of each composition were tested.

One gram of each polymer was dissolved in 3ml of acetone in 5cc disposable syringes. Sieved NaCl particles (212-300 μ m) were then added along with the appropriate vol. % Fe or SmCo₅. The suspension was shaken for 5 min. to generate a uniform dispersion, injected into 1cc disposable syringes and placed into a drying oven at 62°C and 635mm Hg. The syringes were next heated to 120°C and injected into a silicon mold consisting of a cylindrical hole with a diameter of 1.5mm. The implants were re-heated to 127°C under an applied magnetic field of 5.5 Tesla using a MPMS SQUID magnetometer (Quantum Design Inc.). The temperature and magnetic field were held at 127°C and 5.5 Tesla for 10 minutes respectively. The implants were then slowly cooled to room temperature and the magnetic field removed. Following magnetization, the implants were leached in de-ionized H₂O for 48 hours at 37°C and dried in an oven at 62°C dried for 48 hours before morphological evaluation.

Solid Implant Fabrication

Solid samples were processed in the same way as the porous samples described above. However, no NaCl particles were added and the samples were not leached in water after

magnetization. Target implants contained 12.5, 25, 30, 35, 40, and 45 vol. % Fe or 50 vol. % SmCo₅.

Aging/Degradation

Five samples of each composite were mounted in a silicon base and placed in the bottom of a common household straw (Figure 3). The ends of the straw were then sealed with silicon sealant to prevent saline leakage. The straws were filled with PBS and placed in a water bath at 37°C for a period of 8 weeks. The PBS solution was replaced every 3 days and the magnetic field strength measured at 0, 1, 2, 4, 6, and 8 weeks. The magnetic field strength was measured using a MPMS SQUID magnetometer (Quantum Design Inc.). The magnetic fields were converted to magnetic pole strengths (normalized) by division of the measured magnetic field by the lengths of the cylindrical implants. The magnetic pole strength was then used to calculate the maximum attraction force between the implant and tagged chondrocytes. Images in this dissertation are presented in color.

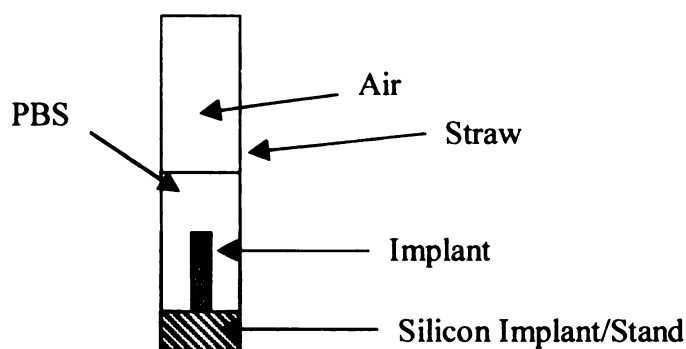


Figure 3 Diagram of *in vitro* sample holder for use with the *MPMS SQUID* Magnetometer (*Quantum Design Inc.*)

Chondrocyte Field Strength

The pole strength of the tagged chondrocytes was determined by measuring the magnetic field of 2 samples of 0.5 ml of DMEM F-12 growth media each containing approximately 2.55×10^5 chondrocytes using a *MPMS SQUID magnetometer (Quantum Design Inc.)*. The chondrocytes were counted by using a blood hemocytometer.

Magnetic Particle Orientation

The degree to which the magnetic particles were oriented after initial magnetization and after 8 weeks degradation were determined for implants composed of 50/50 and 85/15 P(dl)A/PGA and 25 vol. % Fe following a technique developed by Sakai et al.³⁶ The magnetic field strength was measured in the preferred direction of magnetization ($B_{r\bullet a}$) and the perpendicular direction ($B_{r\bullet b}$). The particle orientation factor (F) was calculated using Equation (6)

$$F = \frac{B_{r\bullet a}}{B_{r\bullet a} + B_{r\bullet b}} \quad (6)$$

For the situations where magnetization is maximized and all the particles are oriented in the same direction, the F-factor equals 1. If the particles were randomly oriented, the F-factor equals 0.5.

RESULTS

IMPLANT MORPHOLOGY EVALUATION

The average porosity was found to be 55 vol. % by both density comparison and Archimedes technique. Scanning electron micrographs (SEMs) of the porous P(dl)A/PGA/Fe implants processed by the particulate salt leaching techniques previously

described are shown in Figure 4. The cross-section and surface of a representative 65/35 P(dl)A/PGA/Fe implant are shown in SEM figures 4a and 4b respectively. The pore size on the outer surface of the implants were found to be slightly smaller, $179.69 \pm 45 \mu\text{m}$ and more disperse as compared to the pore size in the cross-section, $224.23 \pm 59 \mu\text{m}$. Therefore, the average pore size is $200.75 \pm 57 \mu\text{m}$.

CHONDROCYTE FIELD STRENGTH

The chondrocyte suspension had an average magnetic susceptibility of $1.24 \times 10^{-6} \text{ emu}/0.5\text{ml}$, which contained approximately 2.55×10^5 cells. Thus, the average cell susceptibility was

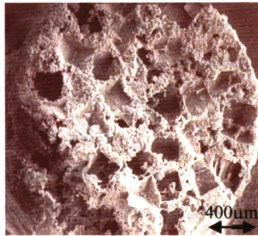
$$\chi = \frac{1.241 \times 10^{-6} \text{ emu}}{0.5 \text{ ml}} \times \frac{0.5 \text{ ml}}{2.55 \times 10^5 \text{ cells}} = 0.487 \times 10^{-11} \text{ emu/cell} \quad (7)$$

Since the average chondrocyte cell diameter is $10 \mu\text{m}$, the cell volume is estimated as $5.233 \times 10^{-16} \text{ m}^3$ (assuming a spherical cell morphology). Using this volume, the magnetic polarization of the cell is calculated by

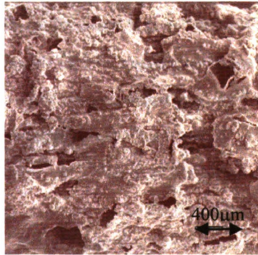
$$m = M \times A = \frac{0.487 \times 10^{-11} \text{ emu/cell}}{\frac{4}{3} \pi (5 \times 10^{-6} \text{ m})^3} \times \pi (5 \times 10^{-6} \text{ m})^2 = 7.310 \times 10^{-7} \text{ emu/m} \quad (8)$$

Conversion of this value to Webers yielded

$$m = (7.310 \times 10^{-7} \text{ emu/m}) (4\pi \times 10^{-10} \text{ Wb} \cdot \text{m}/\text{emu}) = 9.186 \times 10^{-16} \text{ Wb/cell} \quad (9)$$



A)



B)

Figure 4: Scanning electron micrograph of the A) cross section and B) surface of a representative 65/35 P(dI)A/PGA implant containing 25 vol. % Fe

MAGNETIC FIELD STRENGTH

Porous Implants

The implant magnetic field strengths as a function of degradation time are plotted in Figures 5-9. The data were analyzed by performing 2-sided t-test calculations between

adjacent curves (starting from the bottom curve) to determine significance. If the data marker is solid, it can be said with 90% certainty that the data point value is different than the corresponding value directly above it; and there is less than 90% certainty for data points with unfilled markers. Since there is nothing to compare the top line with, the top line of the graph always has solid markers.

The magnetic field strength of porous implants with 10, 20, 30, and 40 vol. % of the solid component consisting of Fe and the remaining solid component 65/25 P(dl)A/PGA were graphed in Figure 5 and listed in Table 4. The curves in Figure 5 indicate a gradual increase in the initial magnetic pole strength of the implants with increasing Fe content from $0.9518 \pm 0.6 \times 10^{-4} \text{ emu/mm}$ at 10 volume % to $4.018 \pm 1.0 \times 10^{-4} \text{ emu/mm}$ at 40 volume %. The degradation of the magnetic field was most pre dominant with the 10 vol. % samples as compared to the 40 vol. % samples, degrading to 68% and 48% of their initial magnetic field strengths respectively.

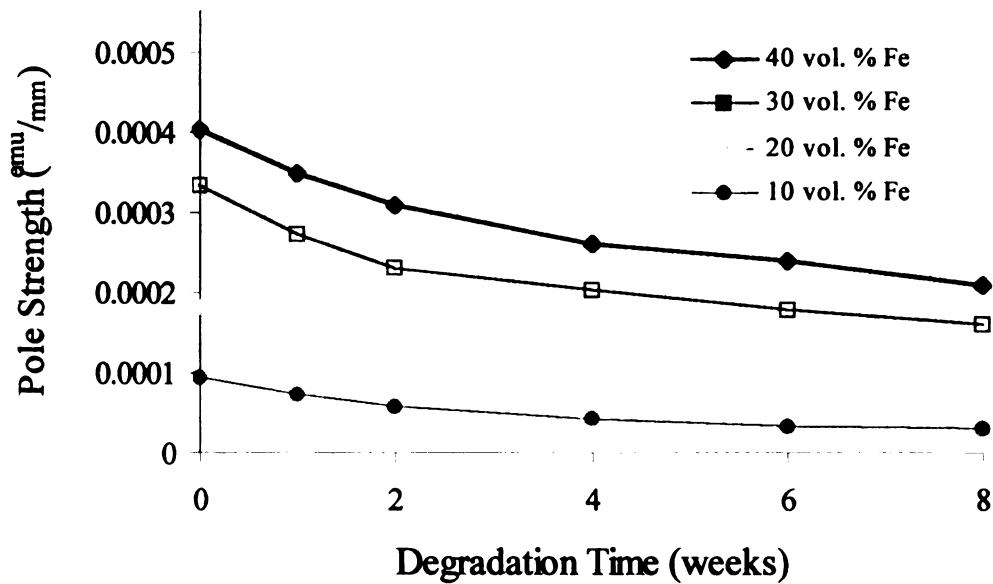


Figure 5 Pole strength vs. degradation time of 50% porous composite implants fabricated with 65/35 P(dl)A/PGA and 10, 20, 30 or 40 vol. % Fe

Table 4 Magnetic pole strengths of 65/35 P(dl)A/PGA implants fabricated with 10, 20, 30 or 40 vol. % Fe as a function of degradation time

Polymer	Fe Vol. %	t=0 (emu/mm)	t=1 week (emu/mm)	t=2 weeks (emu/mm)	t=4 weeks (emu/mm)	t=6 weeks (emu/mm)	t=8 weeks (emu/mm)
65/35	40	40.2±10.3×10 ⁻⁵	34.6±12.2×10 ⁻⁵	30.7±7.8×10 ⁻⁵	26.4±8.4×10 ⁻⁵	24.0±8.3×10 ⁻⁵	20.9±6.8×10 ⁻⁵
65/35	30	32.6±4.5×10 ⁻⁵	26.0±4.3×10 ⁻⁵	21.1±5.1×10 ⁻⁵	18.0±5.5×10 ⁻⁵	15.7±4.5×10 ⁻⁵	13.7±4.2×10 ⁻⁵
65/35	20	18.2±8.5×10 ⁻⁵	15.2±8.2×10 ⁻⁵	13.5±7.9×10 ⁻⁵	11.7±7.5×10 ⁻⁵	10.1±6.9×10 ⁻⁵	9.0±7.1×10 ⁻⁵
65/35	10	9.5±6.1×10 ⁻⁵	7.1±4.5×10 ⁻⁵	5.9±3.9×10 ⁻⁵	4.2±2.9×10 ⁻⁵	3.5±2.3×10 ⁻⁵	3.1±2.0×10 ⁻⁵

A graph of the magnetic pole strength of implants containing 50/50, 65/35, 75/25, and 85/15 P(dl)A/PGA with 25 vol. % Fe and a target porosity of 50 vol. % is shown in Figure 6 with the individual data points and standard deviations listed in Table 5. The initial implant magnetization and the rate of magnetization decay are dependent on the implant polymer composition. As the composition of the polymer shifts to higher PGA compositions, there is a gradual increase in the magnetic pole strength. However, this increased magnetic field strength in the 50/50 implants is lost during the first week of *in vitro* degradation. The shape of the 65/35, 75/25 and 85/15 curves are almost identical, showing a gradual decrease in magnetic field strength over the 8-week degradation period to 50%, 57%, and 60% of their initial strengths respectively. However, the 50/50 polymer implants degraded at a more rapid rate to approximately 80% of its initial magnetic field strength during the 8-week study.

The magnetic field strengths along the axis and perpendicular to the implant along with the calculated F-factors for 50/50 and 85/15 P(dl)A/PGA implants with 25 vol. % Fe are listed in Table 6. The magnetic field strengths in the direction of implant magnetization ($B_{r,s}$) for the 50/50 P(dl)A/PGA implants were statistically higher than the 85/15 P(dl)A/PGA implants, $2.75 \pm 0.3 \times 10^{-3}$ emu/mm and $1.23 \pm 0.8 \times 10^{-3}$ emu/mm respectively.

In the direction perpendicular to implant magnetization (B_{res}) the magnetic field strengths were significantly less than in the direction of magnetization in both cases. However, the B_{res} of the 50/50 P(dl)A/PGA implants were not statistically different from the 85/15 P(dl)A/PGA implants, $6.32 \pm 5.7 \times 10^{-4} \text{ emu/mm}$ and $4.39 \pm 2.5 \times 10^{-4} \text{ emu/mm}$ respectively. The F-Factor for the 50/50 P(dl)A/PGA implants was 0.802 ± 0.05 and for the 85/15 P(dl)A/PGA implants was 0.731 ± 0.04 . After 8 weeks of degradation, the F-factor decreased for both the 50/50 and the 85/15 P(dl)A/PGA implants. The 50/50 P(dl)A/PGA implant F-factors decreased to 0.726 ± 0.05 and the 85/15 decreased to 0.701 ± 0.03 .

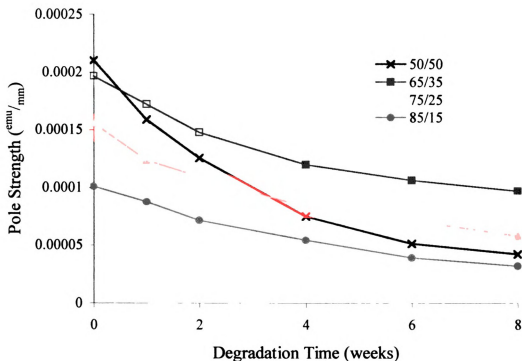


Figure 6 Pole strength vs. *in vitro* degradation time and polymer composition of 50% porous composite implants with 25% Fe

Table 5 Magnetic pole strengths of 50/50, 65/35, 75/25 and 85/15 P(dl)A/PGA implants fabricated with 25 vol. % Fe as a function of degradation time

Polymer	Fe Vol. %	t=0 (emu/mm)	t=1 week (emu/mm)	t=2 weeks (emu/mm)	t=4 weeks (emu/mm)	t=6 weeks (emu/mm)	t=8 weeks (emu/mm)
50/50	25	$21.0 \pm 10 \times 10^{-5}$	$15.9 \pm 8.5 \times 10^{-5}$	$11.2 \pm 7.6 \times 10^{-5}$	$7.5 \pm 5.3 \times 10^{-5}$	$5.1 \pm 3.3 \times 10^{-5}$	$4.2 \pm 2.8 \times 10^{-5}$
65/35	25	$19.5 \pm 5.8 \times 10^{-5}$	$17.0 \pm 4.7 \times 10^{-5}$	$14.2 \pm 3.9 \times 10^{-5}$	$11.6 \pm 3.3 \times 10^{-5}$	$10.4 \pm 3.1 \times 10^{-5}$	$9.6 \pm 2.8 \times 10^{-5}$
75/25	25	$15 \pm 6.7 \times 10^{-5}$	$12 \pm 4.3 \times 10^{-5}$	$10 \pm 4.1 \times 10^{-5}$	$8 \pm 3.5 \times 10^{-5}$	$7 \pm 2.5 \times 10^{-5}$	$6 \pm 2.2 \times 10^{-5}$
85/15	25	$10.1 \pm 2.4 \times 10^{-5}$	$8.7 \pm 2.8 \times 10^{-5}$	$7.2 \pm 2.4 \times 10^{-5}$	$5.4 \pm 1.2 \times 10^{-5}$	$4.6 \pm 1.1 \times 10^{-5}$	$4.0 \pm 1.4 \times 10^{-5}$

Table 6 Calculation of the orientation F-factor for 50/50 and 85/15 P(dl)A/PGA implants containing 25 vol. % Fe

Polymer	Time	Fe Content	B_{rea} (emu)	B_{reb} (emu)	F-Factor
50/50 P(dl)A/PGA	0	25 Vol. %	$2.75 \pm 0.3 \times 10^{-3}$	$6.32 \pm 5.7 \times 10^{-4}$	0.802 ± 0.05
85/15 P(dl)A/PGA	0	25 Vol. %	$1.23 \pm 0.8 \times 10^{-3}$	$4.39 \pm 2.5 \times 10^{-4}$	0.731 ± 0.04
50/50 P(dl)A/PGA	8 weeks	25 Vol. %	$2.742 \pm 2.38 \times 10^{-4}$	$9.34 \pm 6.67 \times 10^{-5}$	0.726 ± 0.05
85/15 P(dl)A/PGA	8 weeks	25 Vol. %	$2.26 \pm 0.70 \times 10^{-4}$	$9.68 \pm 4.05 \times 10^{-5}$	0.701 ± 0.03

The pole strengths of porous samples composed of 85/15 and 65/35 P(dl)A/PGA copolymers and 25 vol. % SmCo_5 degraded for eight weeks *in vitro* are plotted in Figure 7 and listed in Table 7. Comparing the initial magnetic pole strengths of 65/35 P(dl)A/PGA/Fe implants of Figure 6 to 63/35 P(dl)A/PGA/ SmCo_5 implants of Figure 7 shows an order of magnitude of two increase in pole strengths from $1.97 \times 10^{-4} \text{ emu/mm}$ to $3.202 \times 10^{-2} \text{ emu/mm}$ respectively. The basic shape of the degradation curves was identical, which is attributed primarily to the identical polymer compositions. The pole strength of the 85/15 implants degraded faster than the 65/35 P(dl)A/PGA/ SmCo_5 implants. More specifically, the 85/15 P(dl)A/PGA/ SmCo_5 implant magnetization decreased to 48% of the initial values while the 65/35 P(dl)A/PGA/ SmCo_5 implant magnetization decreased over 58% during the 8-week degradation period.

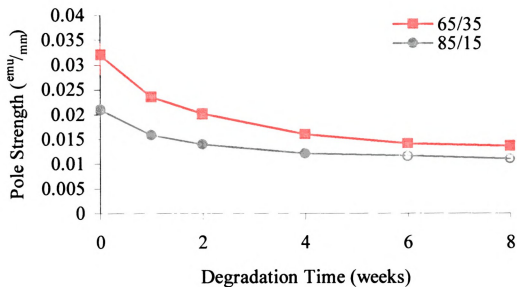


Figure 7 Pole strength vs. *in vitro* degradation time and polymer composition of 50% porous composite implants with 25 vol. % SmCo_5

Table 7 Pole strength data and standard deviations for porous 65/35 and 85/15 P(dI)A/PGA implants containing 25 vol. % SmCo_5

Polymer	Fe Vol. %	t=0 (emu/mm)	t=1 week (emu/mm)	t=2 weeks (emu/mm)	t=4 weeks (emu/mm)	t=6 weeks (emu/mm)	t=8 weeks (emu/mm)
65/35	25	$32.0 \pm 6.2 \times 10^{-3}$	$23.5 \pm 6.8 \times 10^{-3}$	$20.1 \pm 5.9 \times 10^{-3}$	$15.9 \pm 3.6 \times 10^{-3}$	$14.1 \pm 2.9 \times 10^{-3}$	$13.6 \pm 2.6 \times 10^{-3}$
85/15	25	$21.0 \pm 6.2 \times 10^{-3}$	$15.8 \pm 4.6 \times 10^{-3}$	$14.0 \pm 3.8 \times 10^{-3}$	$12.1 \pm 3.2 \times 10^{-3}$	$11.6 \pm 5.3 \times 10^{-3}$	$10.9 \pm 4.8 \times 10^{-3}$

Solid Implants

The magnetic pole strength of solid implants composed of 65/35 P(dI)A/PGA as a function of Fe content and *in vitro* degradation time are plotted in Figure 8 and listed in Table 8. As expected, the initial pole strengths increased from $3.2 \pm 0.4 \times 10^{-4}$ to $8.2 \pm 0.9 \times 10^{-4}$ emu/mm with increasing Fe additions from 12.5 vol. % to 45 vol. % respectively. After 1 week of degradation, there was a noticeable decrease in the field strength of the 45, 40, 35, and 30 vol. % Fe implants to 71%, 75%, 77%, and 80% of their

initial pole strengths respectively. The implants with 25 vol. % Fe degraded to 87% of the initial pole strength and implants with 12.5 vol. % Fe degraded to 90% of the initial pole strength after 1 week of *in vitro* degradation. After 2 weeks, the degradation rates for the remaining time for all the solid samples were essentially identical. After 8 weeks of degradation, the 12.5, 25, 30, 35, 40, and 45 vol. % Fe samples degraded to $1.86 \pm 0.4 \times 10^{-4}$ emu/mm, $2.5 \pm 0.2 \times 10^{-4}$ emu/mm, $2.83 \pm 0.6 \times 10^{-4}$ emu/mm, $3.32 \pm 1.3 \times 10^{-4}$ emu/mm, $3.35 \pm 1.0 \times 10^{-4}$ emu/mm, and $3.44 \pm 0.4 \times 10^{-4}$ emu/mm which was 58%, 48%, 47%, 47%, 43%, and 42% of their initial strengths, respectively. Even though the implants with higher Fe concentrations (>30 vol. %) degraded faster and lost more of their initial magnetic strengths than implants made with lower Fe concentrations (12.5 and 25 vol. %), they still maintained higher pole strengths throughout the entire 8-week testing period.

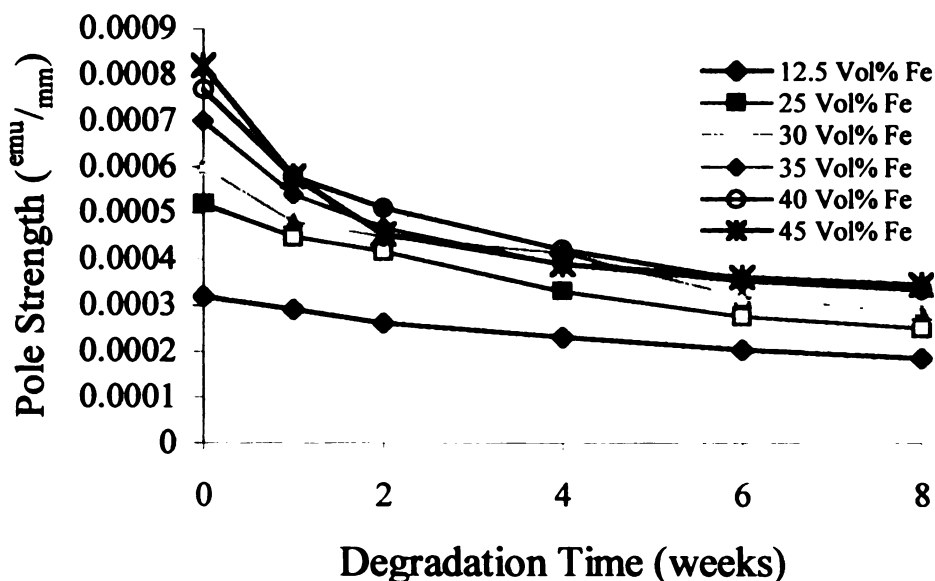


Figure 8 Magnetic pole strength vs. *in vitro* degradation and Fe loading of 65/35 P(dI)A/PGA implants

Table 8 Pole strength data and standard deviations for solid 65/35 P(dl)A/PGA implants containing 12.5, 25, 30, 35, 40 and 45 vol. % Fe vs. *in vitro* degradation time

Polymer	Fe Vol. %	t=0 (emu/mm)	t=1 week (emu/mm)	t=2 weeks (emu/mm)	t=4 weeks (emu/mm)	t=6 weeks (emu/mm)	t=8 weeks (emu/mm)
65/35	45	$81.6 \pm 9.6 \times 10^{-5}$	$57.5 \pm 7.8 \times 10^{-5}$	$45.6 \pm 5.5 \times 10^{-5}$	$39.0 \pm 6.1 \times 10^{-5}$	$36.2 \pm 4.3 \times 10^{-5}$	$34.4 \pm 4.4 \times 10^{-5}$
65/35	40	$76.8 \pm 17.0 \times 10^{-5}$	$58.1 \pm 15.1 \times 10^{-5}$	$51.1 \pm 16.5 \times 10^{-5}$	$42.2 \pm 13.8 \times 10^{-5}$	$35.6 \pm 10.2 \times 10^{-5}$	$33.5 \pm 10.0 \times 10^{-5}$
65/35	35	$69.7 \pm 15.3 \times 10^{-5}$	$53.8 \pm 13.3 \times 10^{-5}$	$46.8 \pm 12.1 \times 10^{-5}$	$38.8 \pm 13.4 \times 10^{-5}$	$35.1 \pm 13.8 \times 10^{-5}$	$33.2 \pm 12.9 \times 10^{-5}$
65/35	30	$60.4 \pm 13.5 \times 10^{-5}$	$47.6 \pm 14.5 \times 10^{-5}$	$45.4 \pm 12.8 \times 10^{-5}$	$41.3 \pm 10.6 \times 10^{-5}$	$32.0 \pm 7.8 \times 10^{-5}$	$28.3 \pm 6.4 \times 10^{-5}$
65/35	25	$52.0 \pm 4.3 \times 10^{-5}$	$44.8 \pm 4.9 \times 10^{-5}$	$41.7 \pm 5.5 \times 10^{-5}$	$33.1 \pm 7.9 \times 10^{-5}$	$27.7 \pm 2.5 \times 10^{-5}$	$24.9 \pm 1.7 \times 10^{-5}$
65/35	12.5	$32.5 \pm 4.2 \times 10^{-5}$	$29.1 \pm 4.1 \times 10^{-5}$	$26.3 \pm 3.8 \times 10^{-5}$	$22.6 \pm 4.8 \times 10^{-5}$	$20.1 \pm 3.2 \times 10^{-5}$	$18.6 \pm 3.9 \times 10^{-5}$

The magnetic pole strength of solid implants containing 50 vol. % SmCo₅ as a function of *in vitro* degradation time and polymer composition is shown in Figure 9 and Table 9. Once again, the initial magnetic field strength of the 65/35 P(dl)A/PGA implants was increased relative to the 85/15 P(dl)A/PGA implants. However, this slightly higher initial pole strength was lost during the first week of *in vitro* degradation. The shape of the two curves were very similar to that of the implants composed of Fe with a rather large decrease in magnetic strength during the first 2 weeks of degradation and a more gradual degradation rate for the remaining 6 weeks. The 65/35 implant pole strengths decreased from 0.174 ± 0.017 emu/mm to 0.059 ± 0.012 emu/mm in 2 weeks and to 0.031 ± 0.007 emu/mm in 8 weeks. The 85/15 implant pole strengths degraded from 0.155 ± 0.32 emu/mm to 0.073 ± 0.007 emu/mm in 2 weeks and to 0.040 ± 0.003 emu/mm in 8 weeks.

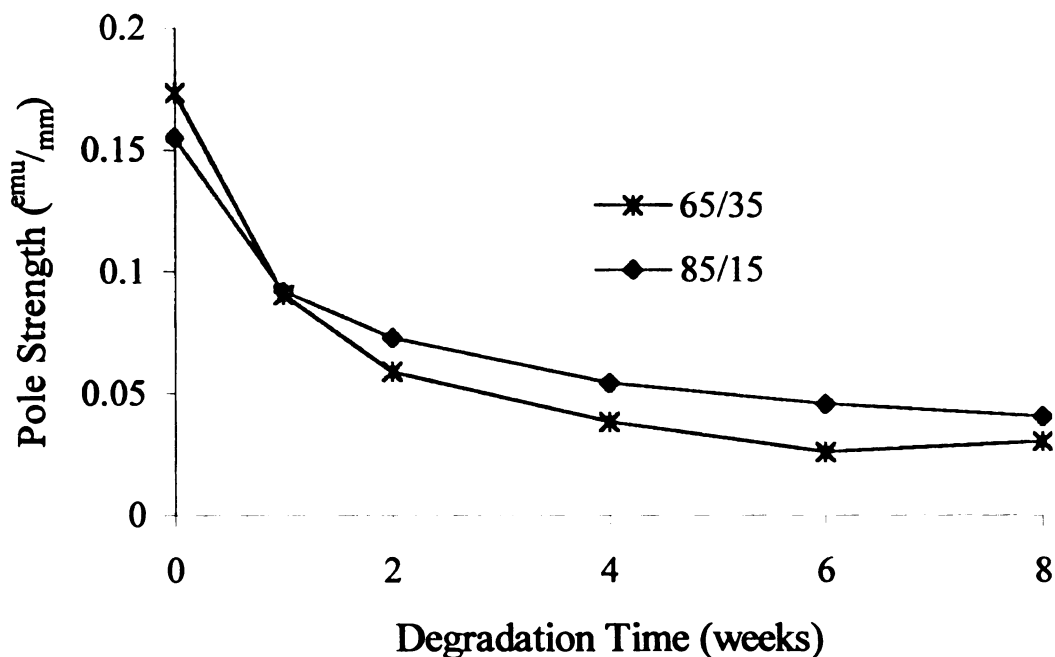


Figure 9 Magnetic pole strength of solid 65/35 P(dl)A/PGA implants and 85/15 P(dl)A/PGA implants containing 50 vol. % SmCo₅ as a function of *in vitro* degradation

Table 9 Pole strength data and standard deviations for solid 65/35 and 85/15 P(dl)A/PGA implants containing 50 vol. % SmCo₅

Polymer	SmCo ₅ Vol. %	t=0 (emu/mm)	t=1 week (emu/mm)	t=2 weeks (emu/mm)	t=4 weeks (emu/mm)	t=6 weeks (emu/mm)	t=8 weeks (emu/mm)
65/35	50	$17.4 \pm 1.6 \times 10^{-2}$	$9.1 \pm 0.7 \times 10^{-2}$	$5.8 \pm 1.1 \times 10^{-2}$	$3.8 \pm 1.1 \times 10^{-2}$	$2.6 \pm 1.5 \times 10^{-2}$	$3.1 \pm 0.7 \times 10^{-2}$
85/15	50	$15.5 \pm 3.2 \times 10^{-2}$	$9.2 \pm 4.6 \times 10^{-2}$	$7.7 \pm 0.7 \times 10^{-2}$	$5.4 \pm 0.6 \times 10^{-2}$	$4.5 \pm 0.4 \times 10^{-2}$	$4.0 \pm 0.3 \times 10^{-2}$

Separation Distance

The calculated maximum separation distances over which a chondrocyte would be attracted to implants as a function of implant composition and degradation time are plotted in Figures 10-14 and listed in Tables 10-14. From initial analysis, each of these graphs has the same shape as the previously examined pole strength graphs of Figures 5-9. Thus, Figures 10-14 were only used to quantify the magnetic strength of the individual

implants applied to MDC. Again, 2 sided t-tests were performed on adjacent curves starting at the bottom. If the data points are different, with >90% confidence, the markers are solid. Otherwise, the markers are hollow.

The maximum separation distance for porous 65/35 P(dl)A/PGA implants with 10, 20, 30, and 40 vol. % Fe are plotted in Figure 10 and listed in Table 10. The porous Fe implant separation distances decreased by 19% from 0.27 ± 0.021 mm initially to 0.22 ± 0.023 mm after 8 weeks of degradation for 40 vol. % Fe samples and from 0.16 ± 0.039 mm initially to 0.11 ± 0.024 mm at 8 weeks degradation for 10 vol. % Fe samples. The degradation curves of implants containing 10, 20, and 30 vol. % Fe were parallel with the 40 vol. % Fe implants having a slightly slower degradation rate.

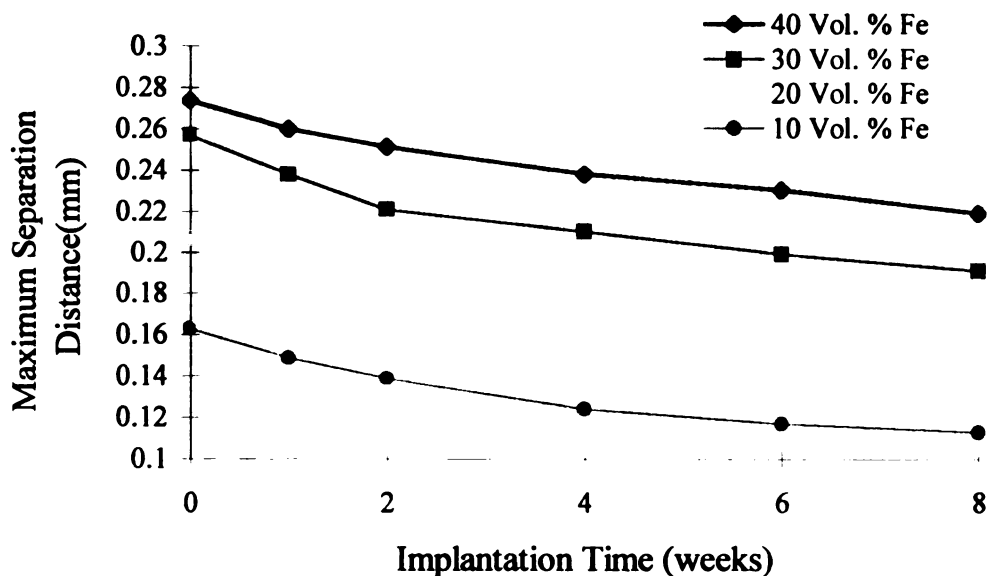


Figure 10 Maximum chondrocyte/implant separation distance as a function of degradation time and Fe concentration for 50% porous implants composed of 65/35 P(dl)A/PGA

Table 10 Maximum chondrocyte/implant separation distance for 65/35 P(dl)A/PGA implants fabricated with 10, 20, 30 or 40 vol. % Fe as a function of degradation time

Polymer	Fe Vol. %	t=0 (mm)	t=1 week (mm)	t=2 weeks (mm)	t=4 weeks (mm)	t=6 weeks (mm)	t=8 weeks (mm)
65/35	40	0.274±0.021	0.260±0.028	0.251±0.020	0.237±0.025	0.229±0.026	0.219±0.023
65/35	30	0.257±0.012	0.238±0.013	0.221±0.016	0.209±0.019	0.199±0.019	0.191±0.019
65/35	20	0.207±0.035	0.194±0.035	0.186±0.036	0.176±0.038	0.166±0.040	0.158±0.045
65/35	10	0.163±0.039	0.149±0.035	0.139±0.033	0.124±0.030	0.117±0.027	0.113±0.025

The maximum separation distance for porous 50/50, 65/35, 75/25, and 85/15 P(dl)A/PGA implants with 25 vol. % Fe are plotted in Figure 11 and listed in Table 11. The highest initial maximum separation distances were achieved by the 50/50 and 65/35 P(dl)A/PGA implants which attracted chondrocytes 0.22 ± 0.038 and 0.21 ± 0.025 mm away respectively. The 75/25 and 85/15 P(dl)A/PGA copolymers had smaller maximum attraction distances of 0.19 ± 0.030 and 0.017 ± 0.015 mm respectively. After 8 weeks of degradation the 65/35 P(dl)A/PGA polymer had the highest attraction distance of 0.17 ± 0.021 mm. The 50/50 P(dl)A/PGA polymer had an attraction distance comparable to the 85/15 P(dl)A/PGA polymer composites at 0.12 mm.

The maximum attraction distance between P(dl)A/PGA/Fe implants and tagged chondrocytes was 0.38 ± 0.18 mm for solid 65/35 samples containing 45 vol. % Fe (Figure 12). However, the attraction distance quickly decreased by 13% to 0.33 ± 0.016 mm after 1 week of degradation and by 26% to 0.28 ± 0.012 mm after 8 weeks. The maximum attraction distance of solid samples containing 25, 30, 35, and 40 vol. % all decreased rapidly and had maximum chondrocyte/implant attraction distances between

approximately 0.25-0.28 mm after 8 weeks of degradation. The 12.5 vol. % Fe implants had a slower degradation rate decreasing only 15%, from 0.27 ± 0.012 mm to 0.23 ± 0.014 mm, during the 8-week degradation study.

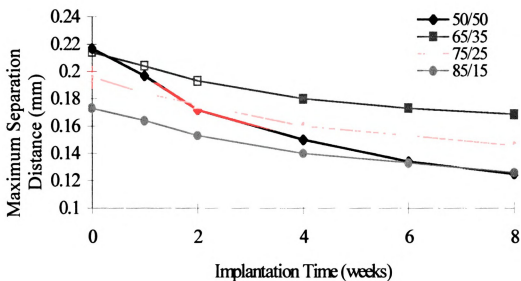


Figure 11 Maximum chondrocyte/implant separation distance as a function of degradation time and polymer concentration for 50% porous implants containing 25 vol. % Fe

Table 11 Maximum chondrocyte/implant separation distance between 50/50, 65/35, 75/25 and 85/15 P(dl)A/PGA implants fabricated with 25 vol. % Fe as a function of degradation time

Polymer	Fe Vol. %	t=0 (emu/mm)	t=1 week (emu/mm)	t=2 weeks (emu/mm)	t=4 weeks (emu/mm)	t=6 weeks (emu/mm)	t=8 weeks (emu/mm)
50/50	25	0.217±0.038	0.196±0.038	0.172±0.042	0.150±0.037	0.134±0.029	0.125±0.029
65/35	25	0.214±0.025	0.204±0.023	0.194±0.021	0.180±0.021	0.173±0.022	0.169±0.022
75/25	25	0.196±0.030	0.184±0.022	0.176±0.022	0.160±0.022	0.153±0.018	0.147±0.017
85/15	25	0.173±0.014	0.164±0.018	0.153±0.018	0.141±0.010	0.132±0.011	0.126±0.018

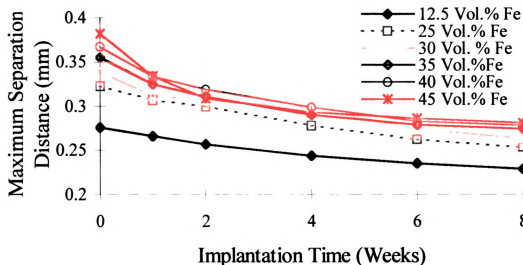


Figure 12 Maximum chondrocyte/implant separation distance as a function of degradation time and Fe concentration for solid implants composed of 65/35 P(dl)A/PGA

Table 12 Maximum chondrocyte/implant separation distance and standard deviations for solid 65/35 P(dl)A/PGA implants containing 12.5, 25, 30, 35, 40 and 45 vol. % Fe vs. *in vitro* degradation time

Polymer	Fe Vol. %	t=0 (mm)	t=1 week (mm)	t=2 weeks (mm)	t=4 weeks (mm)	t=6 weeks (mm)	t=8 weeks (mm)
65/35	45	0.382±0.018	0.334±0.016	0.309±0.013	0.293±0.016	0.286±0.012	0.281±0.012
65/35	40	0.367±0.027	0.334±0.029	0.318±0.036	0.299±0.033	0.283±0.026	0.277±0.027
65/35	35	0.355±0.029	0.325±0.029	0.310±0.026	0.290±0.033	0.280±0.039	0.274±0.038
65/35	30	0.338±0.025	0.311±0.031	0.307±0.029	0.298±0.025	0.274±0.022	0.263±0.020
65/35	25	0.323±0.008	0.307±0.011	0.300±0.012	0.278±0.012	0.262±0.008	0.253±0.006
65/35	12.5	0.276±0.012	0.266±0.013	0.257±0.012	0.244±0.017	0.235±0.012	0.230±0.014

The highest maximum interaction distances were achieved by solid implants containing SmCo₅ (Figure 13). Solid 65/35 P(dl)A/PGA implants with 50 vol. % SmCo₅ can initially attract chondrocytes that are 2.24±0.06 mm away from the implant and can

attract chondrocytes that are 1.25 ± 0.10 mm away after 8 weeks of degradation. Porous 65/35 implants composed of 25 vol. % SmCo_5 (Figure 12) can attract chondrocytes that are 1.18 ± 0.7 mm away initially and 0.88 ± 0.06 mm after 8 weeks of *in vitro* degradation. The highest maximum chondrocyte/implant attraction distance at 8 weeks were solid implants fabricated with 85/15 P(dl)A/PGA and 50 vol. % SmCo_5 , which attract chondrocytes that are 1.38 ± 0.04 mm away.

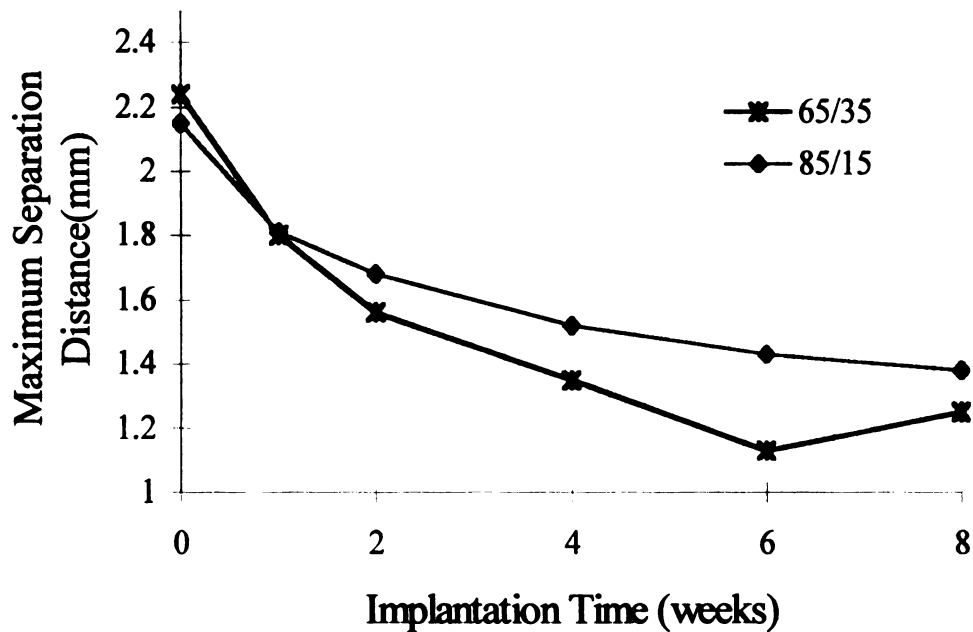


Figure 13 Maximum Chondrocyte/Implant Separation Distance as a Function of Degradation Time and Polymer Concentration for solid implants containing 50 vol. % SmCo_5

Table 13 Maximum separation distance and standard deviations for porous 65/35 and 85/15 P(dl)A/PGA implants containing 25 vol. % SmCo_5

Polymer	SmCo_5 Vol. %	t=0 (mm)	t=1 week (mm)	t=2 weeks (mm)	t=4 weeks (mm)	t=6 weeks (mm)	t=8 weeks (mm)
65/35	50	2.24 ± 0.06	1.81 ± 0.04	1.56 ± 0.09	1.35 ± 0.12	1.13 ± 0.30	1.25 ± 0.10
85/15	50	2.15 ± 0.16	1.81 ± 0.08	1.68 ± 0.05	1.52 ± 0.06	1.44 ± 0.040	1.38 ± 0.04

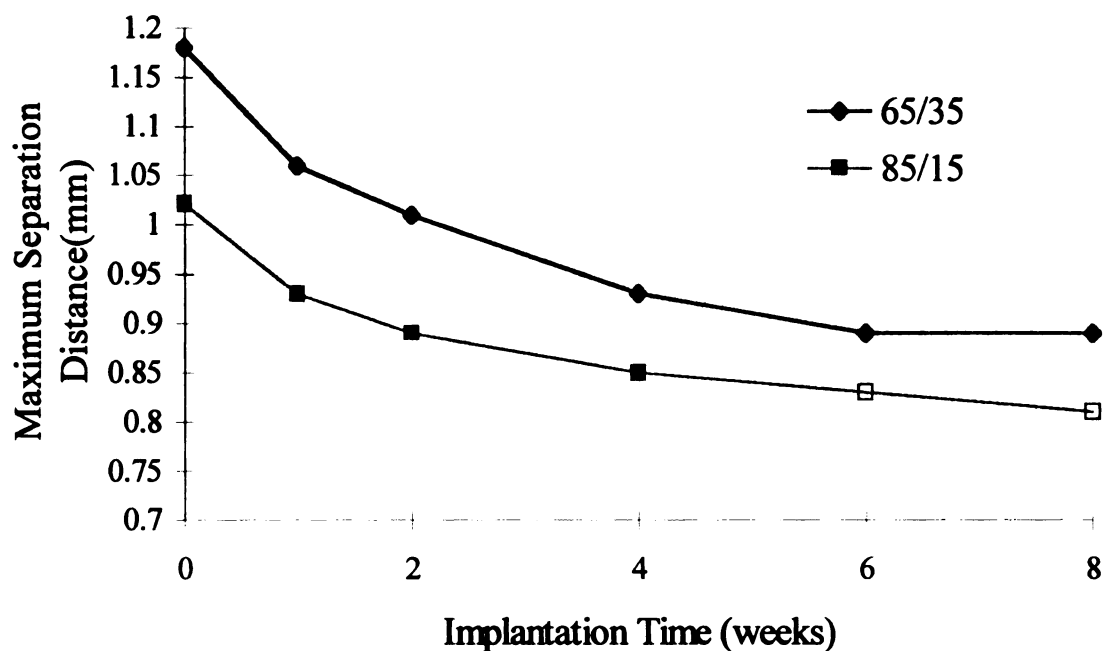


Figure 14 Maximum chondrocyte/implant separation distance as a function of degradation time and polymer concentration for 50% porous implants containing 25 vol. % SmCo_5

Table 14 Maximum separation distance and standard deviations for porous 65/35 and 85/15 P(dl)A/PGA implants containing 25 vol. % SmCo_5

Polymer	SmCo_5 Vol. %	t=0 (mm)	t=1 week (mm)	t=2 weeks (mm)	t=4 weeks (mm)	t=6 weeks (mm)	t=8 weeks (mm)
65/35	25	1.18±0.08	1.06±0.10	1.01±0.09	0.93±0.07	0.89±0.06	0.89±0.06
85/15	25	1.02±0.10	0.93±0.08	0.89±0.08	0.85±0.07	0.83±0.12	0.81±0.12

DISCUSSION

The increasing magnetic pole strengths associated with increasing PGA compositions were attributed to the lower softening temperature of implants having higher PGA concentrations. The magnetic field strengths of anisotropic polymer magnets are highly dependent on the orientation of the individual magnetic particles.^{34,36} This makes the

ability of individual particles to reorient themselves during processing under the applied external magnetic field vital to maximizing the final magnetic field strength of the implant. The maximum temperature that can be applied by the SQUID magnetometer during magnetization is 127°C, and the manufacturers reported processing temperature of the polymers tested in this study range from 120°C (50/50 P(dl)A/PGA) to 150°C (85/15 P(dl)A/PGA). Thus, the 50/50 P(dl)A/PGA polymer will be softer than the 85/15 P(dl)A/PGA polymer at 127°C and will result in more efficient particle rotation and alignment during implant magnetization. This improved orientation increases the magnetic field strength in the direction of magnetization as shown by the particle orientation and F-factor calculations of this study. In the case of the 50/50 implants the initial F-factor was 0.802 ± 0.05 , and for the 85/15 implants the initial F-factor was 0.731 ± 0.04 . This indicated a higher degree of particle orientation in the 50/50 polymer implants as compared to the 85/15 polymer implants.

Another common trend of the magnetic implants was the increase in the magnetic pole strength degradation rate for samples having higher PGA concentrations. This was attributed to the increased degradation rate of polymers containing higher concentration of PGA.^{3,8} During the initial stages of polymer degradation there is an absorption of H₂O and a decrease in the molecular weight of the polymers.^{2,3} The decrease in cohesive strength decreases the bonding strength between the magnetic particles and the polymer matrix. This frees the particles to rotate and re-align. Individual particles are then able to reorient themselves away from the magnetic axis of the implant. The particles reorient in response to the magnetic field of adjacent particles, which are in the opposite direction to their magnetic field. This situation is schematically shown in Figure 15. This particle

reorientation resulted in a decrease in the overall pole strength of the implant. This was also shown by Osawa et al.³⁴ who reported that the magnetic properties of polymer/ferromagnetic composites were dependent on the interfacial bonding between the two materials. Materials with higher compatibility or bonding strength produced harder and higher magnetic field strengths. This was confirmed in this study by the decreasing F-factor in both the 50/50 and 85/15 P(dl)A/PGA implants after 8 weeks of implant degradation. Degradation was more pronounced in the 50/50 implants whose F-factor decreased 10% as compared to the 85/15 implants that only decreased 4% after 8 weeks of degradation.

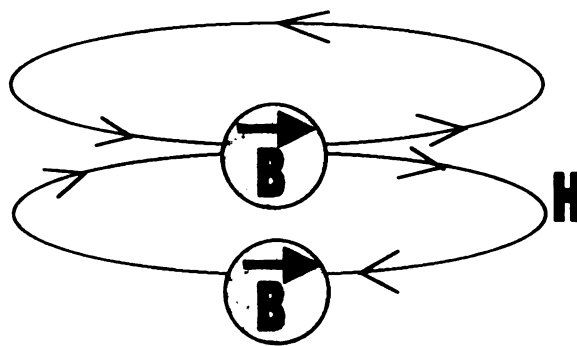


Figure 15: Particle-particle interaction within a P(dl)A/PGA/Fe or P(dl)A/PGA/SmCo₅ implant. The magnetic poles (B) of the individual particles are oriented in the same direction creating a magnetic field (H). As can be seen in the schematic as the particles approach each other the magnetic field of one the top particle is oriented in the opposite direction of the lower particle

Polymers containing SmCo₅ possess a higher initial and 8 week magnetic field strength compared to Fe. In some cases, this increase was over twice that of equivalent implants containing Fe. This increase was attributed to the large material anisotropy and critical particle size of SmCo₅ as compared to Fe. SmCo₅ has a hexagonal crystal

structure that has a magnetic anisotropy of $17.5 \times 10^7 \text{ erg/cm}^3$ at 300 K ³⁷ that is much higher than Fe, which is ferromagnetic and isotropic. This anisotropy focuses the magnetic field in the desired magnetization direction as compared to Fe, whose magnetic field is randomly oriented. SmCo_5 also has a larger critical diameter (a diameter below which the particle exists as a single domain particle) of $\approx 2 \mu\text{m}$ ^{38,39} compared to Fe, which has a single domain size of $\approx 200 \text{ nm}$. Since the SmCo_5 used in this study has a particle size diameter of $\approx 2.3 \mu\text{m}$, it was assumed that most particles were single domain, making them magnetically hard and less affected by either heat or external magnetic fields. However, the Fe particles used in this study are a magnetically softer because of their inherent multi-domain structure.

Comparing porous to solid implants having of equivalent volumes of Fe (65/35 samples of Figure 6 and the 12.5 vol. % samples of Figure 8), solid samples had higher initial magnetic field strengths and slightly slower degradation rates. The higher initial magnetic field is attributed to the improved spacing of the Fe particles in the composite. By increasing the distance between the particles, the interaction between adjacent particles, shown in Figure 15, is minimized. This in turn optimizes the individual particle magnetization. That the magnetic strength of the porous implants degraded faster than the solid implants is contrary to previously reported degradation results in other studies which show an increased degradation rate of solid polymer implants compared to porous implants.⁹⁻¹¹ The anomaly shown by these magnetic polymer implants is contributed to the presence of the second phase magnetic material that is impermeable to water. The magnetic material acts as a barrier to water absorption at the implant/fluid interface.

Thus, the higher surface area of porous samples is necessary to increase amount of water absorption and the rate of hydrolysis.

The maximum implant/chondrocyte separation distance is important to fabricate an implant that can attract enough chondrocytes to fill the entire chondrocyte thickness. Normal articular cartilage thickness for humans ranges from 1-6 mm.⁴⁰ Since the maximum separation distance achieved with P(dl)A/PGA/Fe implants was 0.382 ± 0.018 mm, the chondrocytes must be delivered to within the defect site thickness. This limited attraction potential may also lead to partial thickness healing *in vivo*. However, if SmCo₅ particles are used, this attraction distance will be increased to 2.24 ± 0.06 mm, resulting in a more complete filling of the cartilage defect with chondrocytes.

CONCLUSION

MDC may be an effective technique for soft tissue regeneration. This technique utilizes an implant that is magnetic as well as biodegradable to restore the joint to its native condition. For this reason, suitable implant materials and their magnetic properties must be investigated. The *in vitro* degradation of the magnetic pole strengths of P(dl)A/PGA/Fe and P(dl)A/PGA/SmCo₅ implants were measured as a function of polymer composition, volume of magnetic material and morphology. These results were used to assess the maximum separation distance for attraction between the implant and chondrocyte. Results of *in vitro* studies indicated that implants containing SmCo₅ had a larger initial and 8 week attraction distance. Initial magnetic pole strength increased with increasing volume of magnetic material and the magnetic pole strength degradation rate decreased. Additionally, solid implants had higher magnetic field strengths during degradation than porous implants. Implants with higher PGA compositions generated

higher initial magnetic field strengths because of their lower softening temperatures and more efficient particle alignment. Finally, for use in human models, where the cartilage thickness can range from 1-6 mm, we believe that the chondrocyte particles would have to be injected into the defect site due to the minimal maximum attraction distances of both P(dl)A/PGA/Fe and P(dl)A/PGA/SmCo₅ implants.

REFERENCE

1. Halpern, A.A., Crimp, M.J., and Grande, D., "The Use of Magnetically Tagged Chondrocytes for Repair of Cartilage Defects", *Trans. Ortho. Res. Soc.*, 1997, 541.
2. Gombotz, W.R. and Pettit, D.K., "Biodegradable Polymers for Protein and Peptide Drug Delivery", *Bioconjugate Chem.*, 6, 1995, 332-351.
3. Hollinger, J.O. and Battistone, G.C., "Biodegradable Bone Repair Materials: Synthetic Polymers and Ceramics", *Clin. Ortho. Rel. Res.*, 207, 1986, 290-305.
4. Nakamura, T., Hitomi, S., Watanabe, S., Shimizu, Y., Jamshidi, K., Hyon, S.H., and Ikada, Y., "Bioabsorption of Polylactides with Different Molecular Properties", *J. Biomed. Mater. Res.*, 23, 1989, 1115-1130.
5. Schankenraad, J.M., Nieuwenhuis, P., Molenaar, I., Helder, J., Dijkstra, P.J., and Feijen, J., "In Vivo and In Vitro Degradation of Glycine/Dl-lactic Acid Copolymers", *J. Biomed. Mater. Res.*, 23, 1989, 1271-1288.
6. Gilding, D.K. and Reed, A.M., "Biodegradable Polymers for Use in Surgery-Polyglycolic/Poly(lactic Acid) Homo-and Copolymers:1", *Polymer*, 20, 1979, 1459-1464.
7. Gilding, D.K. and Reed, A.M., "Biodegradable Polymers for Use in Surgery-Polyglycolic/Poly(lactic Acid) Homo-and Copolymers:2 In Vitro Degradation", *Polymer*, 22, 1981, 494-498.
8. Miller R.J., Brady, J.M., and Cutright, D.E., "Degradation Rates of Oral Resorbable Implants (Polylactates and Polyglycolates): Rate Modification with Changes in PLA/PGA Copolymer Ratios", *J. Biomed. Mater. Res.*, 11, 1977, 711-719.

9. Li, S.M., Garreau, H., and Vert, M., "Structure-Property Relationships in the Case of the Degradation of Massive Aliphatic Poly-(α -hydroxy acid) in Aqueous Media: Part 1 Poly(DL-Lactic Acid)", *J. Mater. Sci. Mater. Med.*, **1**, 1990, 123-130.
10. Athanasiou K.A., Agrawal, C.M., Barber, F.A., and Burkhart, S.S., "Orthopaedic Applications for PLA-PGA Biodegradable Polymers", *J. Arthro. Rel. Surg.*, **14**, 7, 1998, 726-737.
11. Lam, K.H., Nieuwenhuis, P., Molenaar, I., Esselbrugge, H., Feijen, J., Dijkstra, P.J., and Schakenraad, J.M., "Biodegradation of Porous vs. Non-porous Poly(L-lactic acid) Films", *J. Mater. Sci. Mater. Med.*, **5**, 1994, 181-189.
12. Suuronen, R., Pohjonen, T., Taurio, R., and Tormala, P., "Strength Retention of Self-Reinforced Poly-L-Lactide Screws and Plates: An *In Vivo* and *In Vitro* Study", *J. Mater. Sci. Mater. Med.*, **3**, 1992, 426-431.
13. Agrawal, C.M. and Athanasiou, K.A., "Technique to Control pH in Vicinity of Biodegrading PLA-PGA Implants", *J. Biomed. Mater. Res.*, **38**, 1997, 105-114.
14. Williams, D.F., "Mechanisms of Biodegradation of Implantable Polymers", *Clin. Mater.* **10**, 1992, 9-12.
15. Smith, R., Oliver, C., and Williams, D.F., "The Enzymatic Degradation of Polymers *In Vitro*", *J. Biomed. Mater. Res.*, **21**, 1987, 991-1003.
16. Schakenraad, J.M., Hardonk, M.J., Feijen, J., Molenaar, I., and Nieuwenhuis, P., "Enzymatic Activity Toward Poly(L-lactic acid) Implants", *J. Biomed. Mater. Res.*, **24**, 1990, 529-545.
17. Brady, J.M., Cutright, D.E., Miller, R.A., Battistone, G.C., Hunsuck, E.E., and Resorption Rate, "Route of Elimination, and Ultrastructure of the Implant Site of Polylactic Acid in the Abdominal Wall of the Rat", *J. Biomed. Mater. Res.*, **7**, 1973, 155-166.
18. Kulkarni, R.K., Pani, K.C., Neuman, C., and Leonard, F., "Polylactic Acid For Surgical Implants", *Arch. Surg.*, **93**, 1966, 839-843.
19. Tschakaloff, A., Losken, H.W., Lalikas, J., Link, J., Mooney, M.P., Von Oepen, R., Michaeli, W., and Losken, A., "Experimental Studies of DL-Polylactic Acid Biodegradable Plates and screws in Rabbits: Computed Tomography and Molecular Weight Loss", *J. Craniofac. Surg.*, **4**, 1993, 223-227.
20. Morgan, M.N., "New Synthetic Absorbable Suture Material", *Brit. Med. J.*, **2**, 1969, 308-318.

21. Postlethwait, R.W., "Polyglycolic Acid Surgical Suture", *Arch. Surg.*, **101**, 1970, 489-494.
22. Postlethwait, R.W., "Further Study of Polyglycolic Acid Suture", *Am. J. Surg.*, **127**, 1974, 617-619.
23. Katz, A.R. and Turner, R.J., "Evaluation of Tensile and Absorption Properties of Polyglycolic Acid Sutures", *Surg. Gyn. Obst.*, **121**, 1970, 701-716.
24. Herrmann, J.B., Kelly, R.J., and Higgins, G.A., "Polyglycolic Acid Sutures", *Arch. Surg.*, **100**, 1970, 486-489.
25. Scholz, K.C., Lewis, R.C., and Bateman, R.O., "Clinical Failure of Polyglycolic Acid Surgical Suture", *Surg. Gyn. Obst.*, **135**, 1972, 525-528.
26. Chu, C.C., "An *In-Vitro* Study of the Effect of Buffer on the Degradation of Poly(glycolic Acid) Sutures", *J. Biomed. Mater. Res.*, **15**, 1981, 19-27.
27. Chu C.C., "The *In-Vitro* Degradation of Poly(glycolic Acid) Suture-Effect of pH", *J. Biomed. Mater. Res.*, **15**, 1981, 795-804.
28. Chu, C.C. and Campbell, N.D., "Scanning Electron Microscopic Study of the Hydrolytic Degradation of Poly(glycolic Acid) Suture", *J. Biomed. Mater. Res.*, **16**, 1982, 117-124.
29. Browning, A. and Chu, C.C., "The Effect of Annealing Treatments on the Tensile Properties and Hydrolytic Degradative Properties of Polyglycolic Acid Sutures", *J. Biomed. Mater. Res.*, **20**, 1986, 613-632.
30. Cutright, D.E., Perez, B., Beasley, J.D., Larson, W.J., and Posey, W.R., "Degradation Rates of Polymers and Copolymers of Polylactic and Polyglycolic Acids", *Oral Surg. Oral Med. Oral Pathol.*, **37**, 1, 1974, 142-15.
31. Barrows. T.H., "Synthetic Bioabsorbable Polymers", High Performance Biomaterials: A Comprehensive Guide to Medical and Pharmaceutical Applications, ed. Szycher, M., Technomic Publ. Co., 1991, 243-255.
32. Marcus, R.D., Leung, L.S., Klinzing, G.E., and Rizk, F. Pneumatic Conveying of Solids, Chapman and Hall, London, 1990, 83-153 .
33. McCurrie, R.A., Ferromagnetic Materials: Structure and Properties, Academic Press, San Diego, 1994.
34. Osawa, Z., Kawauchi, K., Iwata, M., and Harada, H., "Effect of Polymer Matrices on Magnetic Properties of Plastic Magnets", *J. Mater. Sci.*, **57-A**, 2, 1975, 216-220.

35. Gorkturk, H.S., Fiske, T.J., and Kalyon, D.M., "Electric and Magnetic Properties of a Thermoplastic Elastomer Incorporated with Ferromagnetic Powders", *IEEE Trans. Mag.*, **29**, 6, 1993, 4170-4176.
36. Sakai, T., Nakamura, K., and Morii, A., "Plastics Magnet Manufacturing Process: Mixing, Kneading, and Injection Molding", *Intern. Poly. Proc. VI*, **1**, 1991, 26-34.
37. Ermolenko, A.S., "Magnetocrystalline Anisotropy of Rare Earth Intermetallics", *IEEE Transactions on Magnetism*, **12**, 6, 1976, 992-996.
38. McCurrie, R.A., Ferromagnetic Materials: Structure and Properties, Academic Press, New York, 1994, p251.
39. Majetich, S.A., Chowdary, K.M., and Kirkpatrick, E.M., "Size and Interaction Effects in the Magnetization Reversal in SmCo₅ Nanoparticles", *IEEE Trans. Mag.*, **34**, 4, 1998, 985-987.
40. Mow, V.C. and Hayes, W.C., Basic Orthopaedic Biomechanics: Second Edition, Lippincott and Raven Publishers, Philadelphia, 1997, pp113-178.

CHAPTER 3

EFFECT OF ETHYLENE OXIDE AND HYDROGEN PEROXIDE STERILIZATION ON THE MOLECULAR WEIGHT AND CHEMICAL STRUCTURE OF P(dl)A AND P(dl)A/PGA POLYMERS.

DEAN A. OPPERMANN, MELISSA J. CRIMP, AND SARA WOLF
Department of Materials Science and Mechanics
Michigan State University
East Lansing, MI 48823

ALAN A. HALPERN
College of Human Medicine
Michigan State University
East Lansing, MI 48823

ABSTRACT

The increased use of temperature sensitive instruments and biomaterials, such as polylactic acid (PLA), polyglycolic acid (PGA) and their copolymers, have increased the demand for low temperature sterilization processes (LTSPs). These processes must provide high level disinfection without degrading the physical properties of the material. The newest LTSPs are ethylene oxide sterilization (EtO) and hydrogen peroxide (H_2O_2) gas plasma sterilization techniques (Sterrad Sterilization). The short and long term effects of these sterilization techniques on polylactic/polyglycolic acid (PLA/PGA) have been only sparsely reported. In this study, the effects of EtO and H_2O_2 sterilization on the molecular weight and polymer structure of pure P(dl)A, 75/25 P(dl)A/PGA and 50/50 P(dl)A/PGA were measured. Molecular weight was measured using gel permeation chromatography (GPC) and the chemical structure evaluated using Fourier transform

infrared spectroscopy (FTIR). H₂O₂ sterilization resulted in a 4% decrease in the molecular weight of 100 P(dl)A and a 10% decrease in the molecular weight of 75/25 and 50/50 P(dl)A/PGA. EtO sterilization decreased the molecular weight by 10% in 75/25 P(dl)A/PGA, but was only apparent 14 days after sterilization. 100 P(dl)A and the 50/50 P(dl)A were not significantly altered by EtO sterilization. This decrease in molecular weight was accompanied by a decrease in the incidence of COC and C=O bonding, as measured by FTIR. Therefore, H₂O₂ sterilization leads to premature hydrolytic degradation of P(dl)A/PGA copolymers.

INTRODUCTION

Poly(lactic Acid (PLA, P(dl)A), polyglycolic (PGA) and their copolymers (PLA/PGA) have enjoyed substantial development as bioabsorbable sutures, bone plates, tissue scaffolds, bone screws and bone pins.¹⁻¹¹ Three degradation characteristics make PLA, PGA and PLA/PGA copolymers desirable biomaterials. First, degradation rate and mechanical properties can be controlled by changing the polymer molecular weight.^{12,13} Secondly, degradation rate and mechanical properties can be manipulated by altering the molecular concentrations of PLA/PGA copolymers.^{14,15} Finally, the degradation products of PLA, PGA and PLA/PGA are biocompatible.^{14,16}

Degradation of PLA, PGA and PLA/PGA is through bulk erosion, as evident from the significant molecular weight loss that precedes monomer release.¹⁶ More specifically, PLA and PGA degrade by hydrolytic scission (cleavage) of unstable ester bonds, that are incorporated into the polymer backbone. This random chain scission turns what was once a water insoluble polymer into a water soluble, low molecular weight, polymeric

material.¹⁴ The random chain scission continues until the cohesive polymer strength decreases to zero producing low molecular weight fragments. These fragments degrade into soluble monomers that are eliminated through the Krebs cycle.^{14,16}

Sterilization is mandatory for materials used in clinical applications. The most common of these sterilization techniques are dry heat, steam, gas and radiation sterilization.¹⁷ However, the hydrolytic degradation and inherent low softening (working) temperature of PLA/PGA copolymers (120°C-150°C) make sterilization by dry heat and steam sterilization impossible. Even though gamma radiation sterilization employs relatively low temperatures, it modifies the chemical structure of polymers leading to alterations of their mechanical properties.¹⁷⁻²² Thus, low temperature sterilization processes (LTSP) that are less destructive to the physical properties of low temperature polymers are continually being developed. EtO gas sterilization and H₂O₂ sterilization are two of these LTSPs. EtO sterilization has become the most common sterilization technique for temperature sensitive materials because of the relatively low temperatures (\approx 35°C-70°C) used, good penetration of the gas into the target material and the reputation for leaving the polymers undamaged.²³ EtO is a low molecular weight, highly water-soluble chemical that is rapidly and evenly distributed throughout most tissues upon initial exposure.²³ EtO is either used in its pure form or mixed with N₂, CO₂ or a non-ozone depleting chloro-fluorocarbon. Component sterilization results from an alkylation of sulfhydryl, amino, carboxyl, phenolic, and hydroxyl groups of nucleic acids, which cause cell injury and death.²³

Little-to-no oxidative effects on the surface were indicated and no significant decreases in fatigue strength were seen in EtO sterilized ultra high molecular weight

polyethylene (UHMWPE) when compared to non-sterilized UHMWPE.^{24,25} However, Zhang et al. found that EtO sterilization causes microcracking on the surface of polyurethane elastomers when compared to samples sterilized by other methods.²⁶ These microcracks were attributed to the hydrophobic nature of polyurethane and result from hydrolysis during sterilization. Verheyen et al. showed that the flexural strength caused by a slight decrease in molecular weight of PLA in hydroxyapatite/PLA composites after EtO sterilization.²⁷

Deaths and serious tissue reactions to EtO sterilized plastics and rubbers have been reported.²⁸⁻³⁰ Reports have shown EtO to be toxic and have classified it as a Group I carcinogen.²⁸ Exposure to EtO has been associated with lymphatic, hematopoietic cancers, lymphatic leukemia and non-Hodgkin's lymphoma.²⁸ To insure complete ethylene oxide removal, implants sterilized by EtO require aeration to reach acceptable FDA levels (<25 ppm).³¹ The amount of EtO absorbed into a polymer is dependent upon, sterilization temperature, sterilization time, concentration of EtO and the type of diluent gas used.³²

Sterrad sterilization is a newly developed LTSP that utilizes low-temperature hydrogen peroxide plasma. Sterrad sterilization rapidly destroys microorganisms in 5 phases: vacuum, injection, diffusion, plasma and vent cycles. First, an aqueous solution of H₂O₂ is injected into a sample chamber and is vaporized by an applied vacuum. The H₂O₂ vapor is then diffused into the sample for ≈40min. with the chamber temperature controlled between 40°C-45°C. A low temperature plasma is generated by decreasing the vacuum and applying an approved radio frequency to the sample chamber a low temperature plasma. In the plasma state, the hydrogen peroxide vapor breaks down into

reactive species that include free radicals. These free radicals react with and kill microorganisms²⁷.

Alfa et al. found that H₂O₂ plasma sterilization was less effective than EtO sterilization in destroying bacteria on surface carriers in the presence of serum and salt²⁷. In lumen carriers inoculated with bacteria, serum, and salt, EtO was shown to be more effective than H₂O₂, with both techniques less reliable than steam sterilization²⁷. Neither EtO nor H₂O₂ sterilization was proven to be reliable in sterilizing items contaminated with inorganic and organic debris²⁷. Even though Feldman et al. states that H₂O₂ gas plasma sterilization is effective in sterilizing a broad range of materials used in the medical industry, the materials are hydrophobic in nature, chemically stable, and resistant to oxidation and moisture are the most compatible for this technique.³³ However, polyester polymers, however, are not short-listed as one of these materials because of their hydrophilic nature and hydrolytic degradation characteristic.

Goldman et al. studied the effect of H₂O₂ gas plasma sterilization on the molecular structure, fatigue resistance and wear behavior of UHMWPE and compared this technique to other commonly used sterilization processes.¹⁸ H₂O₂ gas plasma sterilization resulted in less oxidation compared to gamma-radiation as well as an improved resistance to fatigue crack propagation and cyclic damage. In addition the bulk properties of UHMWPE, such as fatigue strength and wear behavior, remained basically unchanged compared to non-sterilized samples.

Even though the effect of EtO and H₂O₂ sterilization techniques on the mechanical and structural properties of UHMWPE have been tested, their effect on the mechanical properties and chemical structure of P(dl)A/PGA polymers have yet to be investigated.

In this study the molecular weight and chemical structure of 100 P(dl)A, 50/50 and 75/25 P(dl)A/PGA were analyzed before and after EtO and H₂O₂ sterilization. The molecular weight and the chemical structure were evaluated using gel permeation chromatography (GPC) and Fourier transform infrared spectroscopy (FTIR) respectively.

EXPERIMENTAL PROCEEDURE

MATERIALS

The Medisorb® 100 P(dl)A, 75/25 P(dl)A/PGA and 50/50 P(dl)A/PGA as-received materials were purchased from Alkermes Inc. of Wilmington, OH. The Medisorb® polymers were manufactured for medical applications and have been approved by the FDA for specific applications. The 50/50 P(dl)A/PGA, 75/25 P(dl)A/PGA, and P(dl)A polymers were manufactured in August 1997, June 1997 and September 1997 respectively. The as-received material properties for the 50/50 PLA/PGA, 75/25 PLA/PGA and 100 PLA copolymers, as reported by Alkermes, are listed in Table 1.³

Table 1 Material properties for the as-received 100 P(dl)A, 75/25 and 50/50 P(dl)A/PGA polymers reported by Alkermes Inc. of Wilmington, OH³

PLA/PGA Ratio	Inherent Viscosity (dl/g)	M _w * (daltons)	Polydispersity	T _G (°C)
50/50	0.78	69587	1.37	47.22
75/25	0.77	130132	1.676	49.6
100	0.73	128450	1.568	52.22

METHODS

Fourier Transform Infrared Spectroscopy (FTIR)

Thin films of each of the polymers were spun onto KBr disks for FTIR analysis using the following procedure. KBr disks were manufactured using *Spectrum*® crystal IR grade potassium bromide. Pressing 0.400gm of KBr with 0.656MPa of pressure generated disks 13mm in diameter and 1.3mm thick. The KBr disks were then coated with 100µl of 10 vol. % solutions of each polymer in acetone. The coated disk was placed into a centrifuge for 30 seconds at 4,000 rpm. The resulting polymer films were dried in a furnace at 60°C under a vacuum of 635 mm-Hg for 24 hours prior to FTIR measurements. Six thin films of each polymer were prepared and FTIR tested.

FTIR measurements were made using a Bio-Rad Excaliber Series spectrometer. Each sample was measured before sterilization, 1 day after sterilization and 2 weeks after sterilization. Each FTIR measurement represents the average of 64 scans. The resultant peaks were then assigned referencing Kister, et al.³⁴

Gel Permeation Chromatography (GPC)

The molecular weight of 10 as-received pellets of 100 P(dl)A, 75/25 and 50/50 P(dl)A/PGA polymers were tested using gel permeation chromatography (GPC) prior to and following EtO and H₂O₂ sterilization. The molecular weight was measured by streaming dissolved polymer solutions through a 4-column Waters Millipore Millennium 2010 GPC. The columns were calibrated every 7 days using 29,300, 44,000, and 114,200 Dalton polystyrene standards purchased from Aldrich Chemical Co. of Milwaukee, WI. 0.1 vol% polymer suspensions were made by dissolving the as-received and sterilized polymer pellets in tetrahydrofuran (THF) in 1.0 dram sample vials. To insure complete polymer dissolution the pellets were dissolved for 24 hours prior to testing.

EtO Sterilization

As-received polymer pellets and polymer/KBr thin films were EtO sterilized using a Steri-Vac 4000, manufactured by the 3M Company of St Paul, MN. Samples were placed in an uncovered petri dish and sterilized at the MSU College of Veterinary Medicine. Gas exposure occurred under warm (55°C) conditions for a period of 15 minutes. The samples were then purged using fresh air to remove residual EtO from the polymer for periods of at least 10 hours, to a maximum of 14 hours. After sterilization the polymer pellets and polymer/KBr thin films were placed in non-woven polypropylene sterilization Aspek® wraps until GPC or FTIR testing.

H₂O₂ Sterilization

The as-received polymer pellets and polymer/KBr thin films were placed in non-woven polypropylene sterilization Aspek® wraps and H₂O₂ sterilized using the Sterrad® 100-sterilization system at Borgess Medical Center in Kalamazoo, MI. After placing the sample wraps into place the sterilization the chamber was evacuated to 0.3mmHg pressure using a 59 vol. % concentration of H₂O₂ to H₂O. The H₂O₂ plasma was applied for 40 min. after which the sample chamber was purged with filtered air and the Aspek wraps sealed until GPC or FTIR testing.

RESULTS

GPC

The GPC measurements as a function of sterilization technique were done over a 6-month period. Between the EtO sterilization measurements and the H₂O₂ sterilization

measurements the pressure sensor of the Millipore GPC was replaced. Therefore, the resulting molecular weight data was normalized by the measured molecular weights before sterilization. This shifted the initial polymer molecular weights to higher molecular weights. The normalized molecular weight of the 50/50 P(dl)A/PGA, 75/25 P(dl)A/PGA, and 100 P(dl)A polymers as a function of time after H₂O₂ (Sterrad) and Ethylene Oxide (EtO) sterilization is plotted in Figure 1. Two sided t-tests were used to statistically compare the molecular weight of samples, 1 day and 14 days after sterilization, to the measured molecular weights before sterilization. If the data points are significantly different (>90% confidence) the data marker is hollow. If the data points are not significantly different (<90% confidence) the data marker is solid.

The normalized molecular weight of the 50/50 P(dl)A/PGA copolymer after EtO and H₂O₂ sterilization is plotted in Figure 1A. After EtO sterilization, the molecular weight of the 50/50 P(dl)A/PGA decreased to 95.6±5.6% of the initial molecular weight 1 day after sterilization and to 96.1±6.3% of its initial value 14 days after sterilization. However, neither of these molecular weights were statistically different than their molecular weight before sterilization. After H₂O₂ sterilization, the molecular weight of the 50/50 P(dl)A/PGA copolymer decreased to 97.2±3.5% at 1 day and to 92.9±1.3% after 14 days. The molecular weight 1 day after sterilization was not statistically different than before sterilization, but after 14 days, the molecular weight was statistically lower. Thus, the only significant difference in molecular weight was shown after H₂O₂ sterilization 14 days after sterilization.

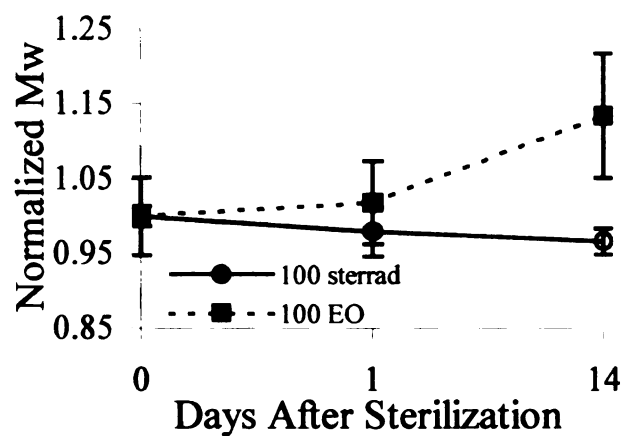
The normalized molecular weight of the 75/25 P(dl)A/PGA copolymer after EtO and H₂O₂ sterilization is plotted in Figure 1B. GPC results from the 75/25 P(dl)A/PGA

copolymer showed a gradual decrease in the molecular weight after both EtO and H₂O₂ sterilization. One day after EtO sterilization, the molecular weight increased to 102.1±11.3% and 14 days after EtO sterilization, the molecular weight decreased to 90.3±12.2% of the nonsterilized value. T-test calculations indicated the initial increase was not statistically significant while the decreased values after 14 days was significantly different. After H₂O₂ sterilization, the molecular weight of the 75/25 P(dl)A/PGA decreased gradually to 96.1±1.6% and 92.1±1.5%, after 1 and 14 days respectively. This decrease was only statistically significant at 14 days after H₂O₂ sterilization.

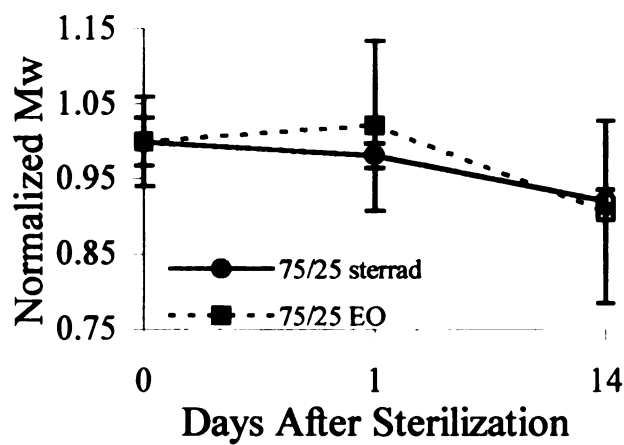
The normalized molecular weight of the 100 P(dl)A polymer after EtO and H₂O₂ sterilization is plotted in Figure 1C. One day after EtO sterilization, the molecular weight was measured to be 98.3±5.6% of the non-sterilized polymer. After 14 days, the molecular weight was measured to be 109±8.3% of the non-sterilized value. Neither measurement was statistically different than the non-sterilized 100 P(dl)A polymer. After H₂O₂ sterilization, the molecular weight gradually decreased to 97.9±3.3% after 1 day and to 96.6±1.7% after 14 days. Once again, the molecular weight at 1 day was not statistically different, but after 14 days, the molecular weight was statistically different from the non-sterilized 100 P(dl)A polymer.

FTIR

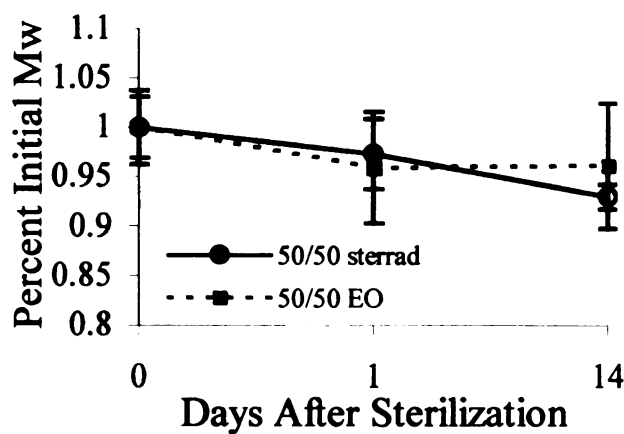
Since the 3 FTIR samples for each polymer were essentially identical with the same peak ratios, one sample was chosen as a representative sample for qualitative analysis of the effect of EtO and H₂O₂ sterilization. Representative FTIR spectrums for 100 P(dl)A,



C.



B.



A.

Figure 1 Normalized molecular weight as a function of time after sterilization for: A) 50/50 P(dl)A/PGA, B) 75/25 P(dl)A/PGA, and C) 100 P(dl)A

75/25 and 50/50 P(dl)/PGA polymers are plotted in Figures 2-7. Each spectrum is a plot of absorbance vs. wavenumber.

Figures 2-4 are the FTIR spectrums for EtO sterilized 50/50, 75/25 and 100 P(dl)A polymers respectively. Thin films were tested before sterilization (A), 24 hours after sterilization (B) and 14 days after sterilization (C). The change in the polymer structure was evaluated by subtracting the FTIR curves of the sterilized polymer from that of the as-received polymer and are shown in (D) and (E).

The polymer bonding peaks were labeled and assigned referencing Kister, et al.³⁴ The primary peaks for all experimental variables of the 100 P(dl)A, 75/25 and 50/50 P(dl)A/PGA polymers fell at: 1756 cm^{-1} (A), 1091 cm^{-1} (B), 1187 cm^{-1} (C), 1131 cm^{-1} (D) and 1270 cm^{-1} (E). The 1753 cm^{-1} peak corresponds to $\nu\text{C=O}$ bonding, the 1089 cm^{-1} peak to $\nu_s\text{COC}$ bonding, the 1186 cm^{-1} peak to $\nu_{as}\text{COC}+\nu_{as}\text{CH}_3$ bonding, the 1130 cm^{-1} peak to $\nu_{as}\text{CH}_3$ and the 1270 cm^{-1} peak to $\delta\text{CH}+\nu\text{COC}$. The subscript *s* implies symmetry and the subscript *as* implies asymmetry. The integrated areas of these peaks are shown in Tables 2-4. In these tables, the negative values represent the negative peaks shown in the subtraction curves and are indicative of the decrease in the incidence of that particular bond formation.

Only a slight effect of EO sterilization on the 100 P(dl)A, 75/25 and 50/50 P(dl)A/PGA polymer structure was found. With all three polymers, there was an increase in the polymer/KBr disk absorbance at wavelengths greater than 1700 cm^{-1} which resulted in a continuously sloped peak seen in B and C of each of the Figures 2-4. This sloping peak represents the absorption of EtO into the disks and was confirmed by measurements on uncoated KBr disks. Thus, this EtO absorption can be neglected as a

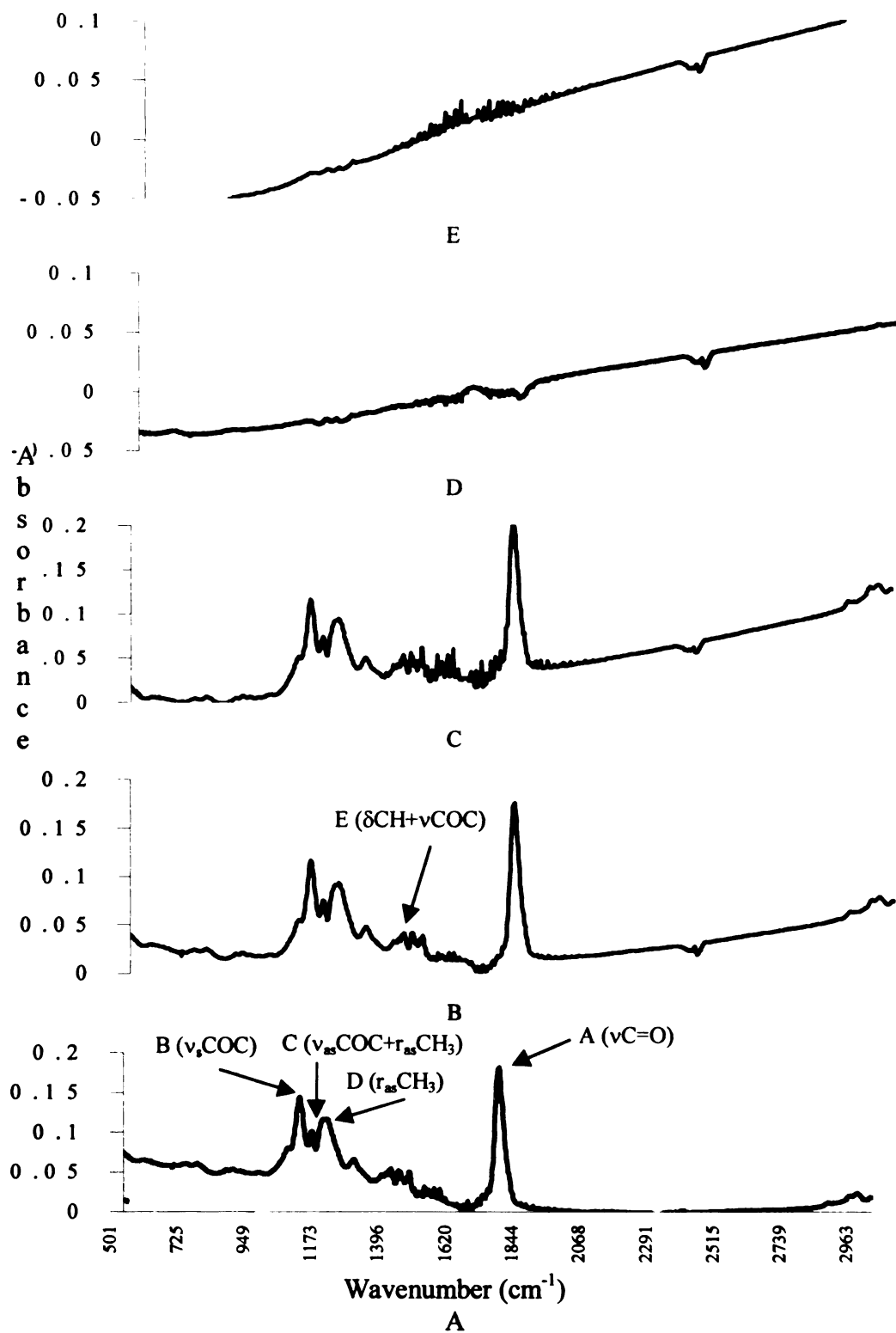


Figure 2 FTIR spectrums of 50/50 P(dl)A/PGA polymers: A) As Received, B) 1 Day after EtO Sterilization, C) 14 Days after EtO Sterilization, D) Residual after 1 Day, E) Residual after 14 Days

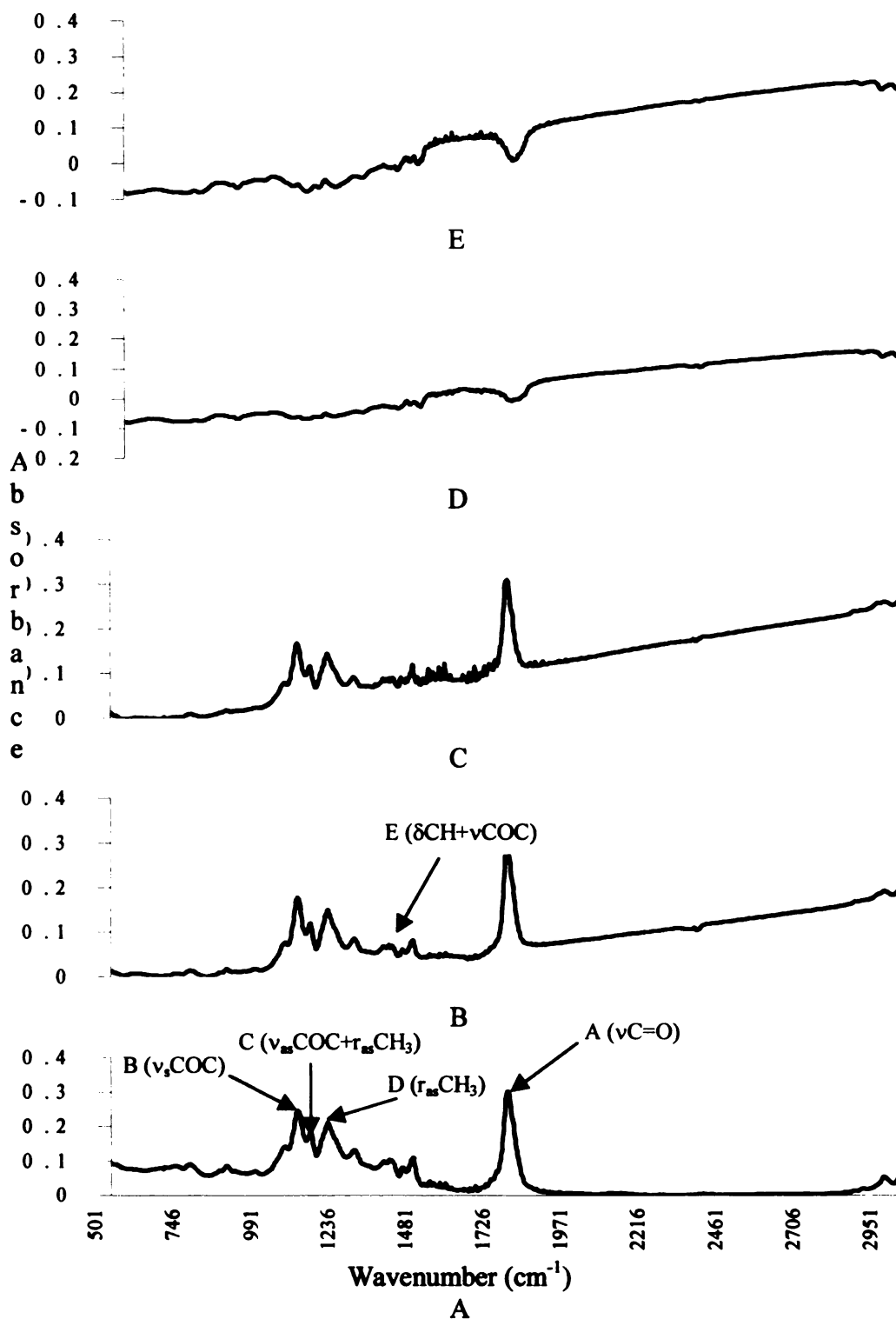


Figure 3 FTIR spectrums of 75/25 P(dl)A/PGA polymers: A) As Received, B) 1 Day after EtO Sterilization, C) 14 Days after EtO Sterilization, D) Residual after 1 Day, E) Residual after 14 Days

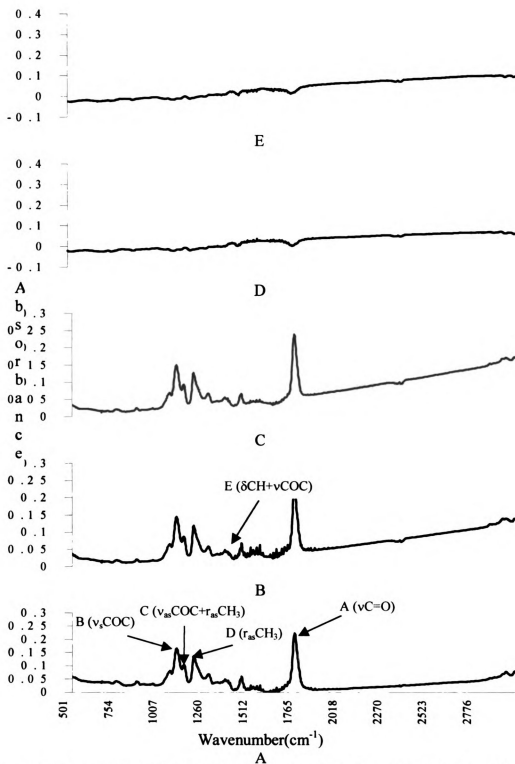


Figure 4 FTIR spectra of 100 P(dl)A polymers: A) As Received, B) 1 Day after EtO Sterilization, C) 14 Days after EtO Sterilization, D) Residual after 1 Day, E) Residual after 14 Days

Table 2 Integrated peak areas for 100 P(dl)A sterilized using EtO

Polymer\Peak	<u>1756cm⁻¹</u>	<u>1270cm⁻¹</u>	<u>1187cm⁻¹</u>	<u>1131cm⁻¹</u>	<u>1091cm⁻¹</u>
100 As Received	5.842	0.475	2.725	0.433	2.019
100 EO ster. (1 day)	5.804	0.395	2.357	0.373	1.868
100 EO ster. (14 day)	5.088	0.382	2.355	0.371	1.840
Subtraction (1 day)	-0.072	-0.094	-0.351	-0.060	-0.151
Subtraction (14 day)	-0.796	-0.096	-0.386	-0.062	-0.179

Table 3 Integrated peak areas for 75/25 P(dl)A/PGA sterilized using EtO

Polymer\Peak	<u>1756cm⁻¹</u>	<u>1270cm⁻¹</u>	<u>1187cm⁻¹</u>	<u>1131cm⁻¹</u>	<u>1091cm⁻¹</u>
75/25 As Received	11.601	0.660	3.458	0.545	2.280
75/25 EO ster. (1 day)	8.267	0.486	2.983	0.475	2.119
75/25 EO ster. (14 day)	6.073	0.382	2.492	0.391	1.855
Subtraction (1 day)	-4.117	-0.182	-0.439	-0.067	-0.161
Subtraction (14 day)	-2.905	-0.290	-0.936	-0.150	-0.425

Table 4 Integrated peak areas for 50/50 P(dl)A/PGA sterilized using EtO

Polymer\Peak	<u>1756cm⁻¹</u>	<u>1270cm⁻¹</u>	<u>1187cm⁻¹</u>	<u>1131cm⁻¹</u>	<u>1091cm⁻¹</u>
50/50 As Received	5.818	0.436	1.960	0.217	1.390
50/50 EO ster. (1 day)	5.717	0.426	1.860	0.201	1.366
50/50 EO ster. (14 day)	5.222	0.403	1.798	0.197	1.318
Subtraction (1 day)	0.064	0.009	0.010	0.016	0.024
Subtraction (14 day)	0.337	0.034	0.013	0.020	0.072

processing artifact to using self manufactured KBr disks for mounting the thin film polymer samples.

The FTIR spectrum and the peak areas indicated no differences in the subtraction scans, D and E, of the 50/50 and 100 polymers. However, the 75/25 samples did have a decrease in peak height at approximately 1753cm⁻¹. The decreasing area of the 1753cm⁻¹ peak area from 11.6 initially to 8.3 confirmed these decreasing peaks after 1 day and to 6.1 after 14 days. This decrease in the C=O peak was accompanied by decreases in the COC peaks at 1187cm⁻¹ and 1091cm⁻¹.

The FTIR spectrums for polymers sterilized by H_2O_2 sterilization methods are plotted in Figures 5-7 with the integrated peak areas listed in Tables 5-7. The 50/50 polymer and the 75/25 polymer subtraction spectrums indicated distinct decreasing peaks at approximately 1756 cm^{-1} and less defined decreasing peaks at 1187 cm^{-1} and 1091 cm^{-1} . This is verified by the decreases in the 1756 cm^{-1} peak areas from 38.5 to 24.0 for the 50/50 P(dl)A/PGA polymer and from 23.0 to 17.0 for the 75/25 P(dl)A/PGA polymer. In the 75/25 polymer these decreasing peaks were not readily apparent until 14 days after sterilization. The 100 P(dl)A polymer, however, showed no decrease in the intensity of the 1270 cm^{-1} , 1187 cm^{-1} , 1131 cm^{-1} , or 1091 cm^{-1} peaks after 1 day and only slight changes after 14 days. However, the 1760 peak did decrease in area from 23.3 to 18.8 but subtraction curves did not have a visibly different peak at this wavenumber. Thus, the decrease in peak area is likely attributed to the absorption of H_2O_2 and the sloping absorption curve that alters the integration and not an actual decrease in the occurrence of this specific bonding.

For each of the polymers tested there were no other changes in the chemical structure. There was no appreciable shifting of the peaks or addition of new peaks that would indicate absorption of EtO or H_2O_2 into the polymer.

DISCUSSION

The GPC data and FTIR spectrums indicate that the 100 P(dl)A, 75/25 and 50/50 P(dl)A/PGA polymers were most effected by H_2O_2 sterilization. Both the 75/25 and 50/50 P(dl)A/PGA polymers showed a gradual decrease in the molecular weight of

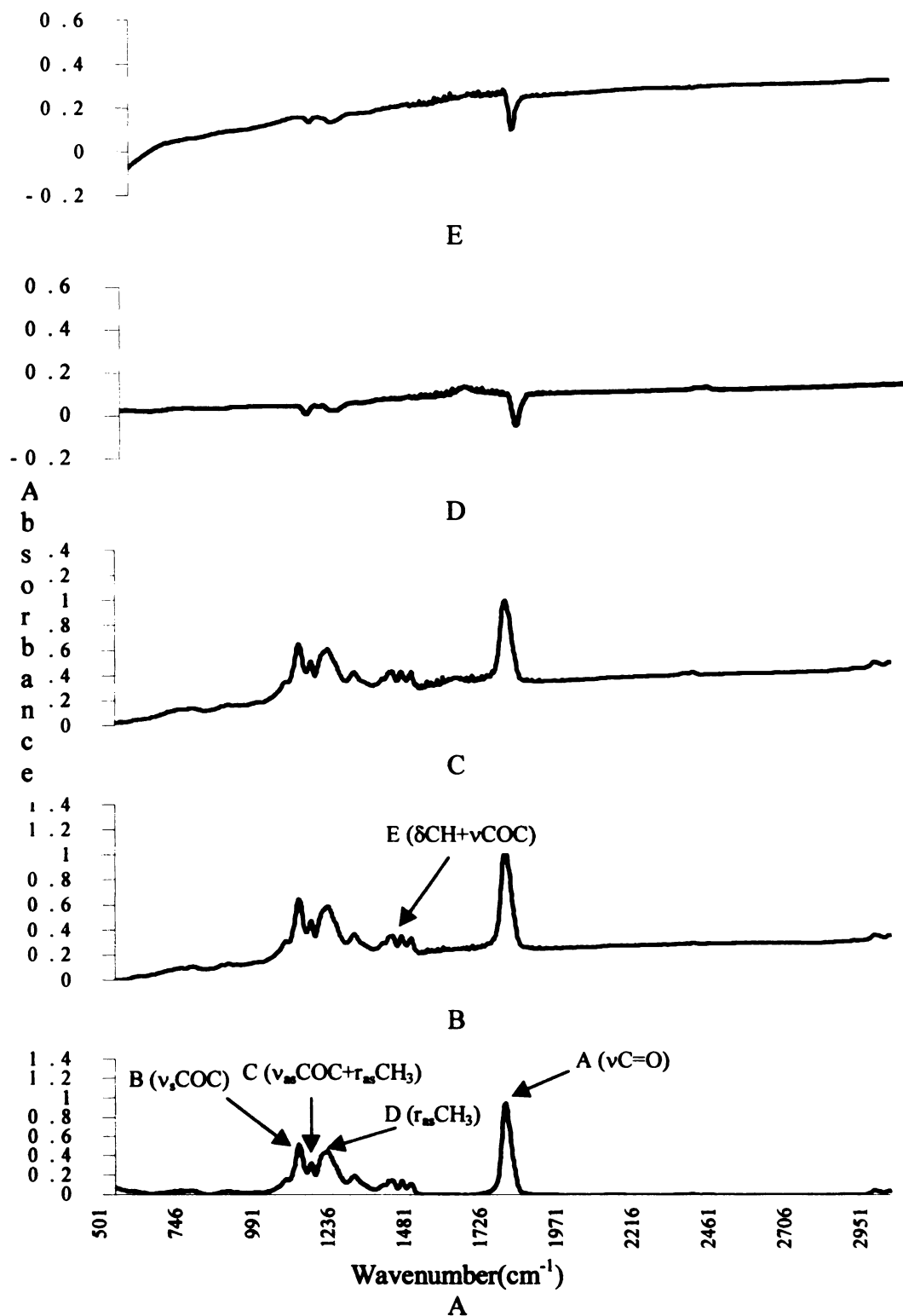


Figure 5 FTIR spectrums of 50/50 P(dl)A/PGA polymers: A) As Received, B) 1 Day after H₂O₂ Sterilization, C) 14 Days after H₂O₂, D) Residual after 1 Day, E) Residual after 14 Days

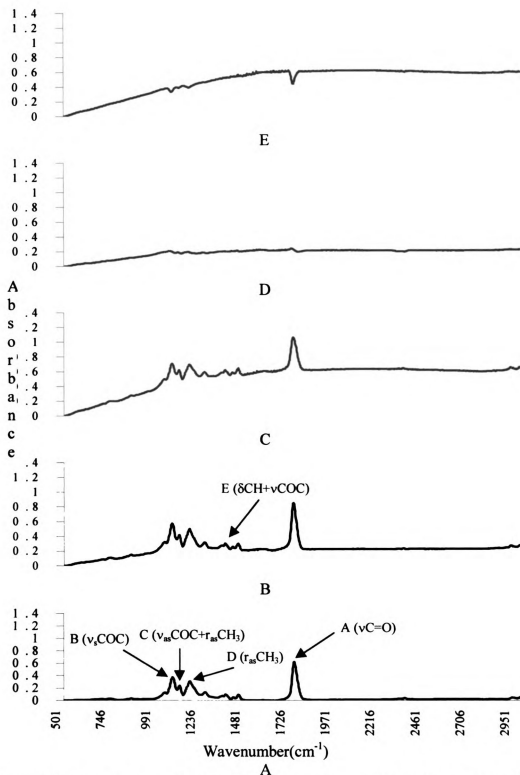


Figure 6 FTIR spectra of 75/25 P(dl)A/PGA polymers: A) As Received, B) 1 Day after H₂O₂ Sterilization, C) 14 Days after H₂O₂ Sterilization, D) Residual after 1 Day, E) Residual after 14 Days

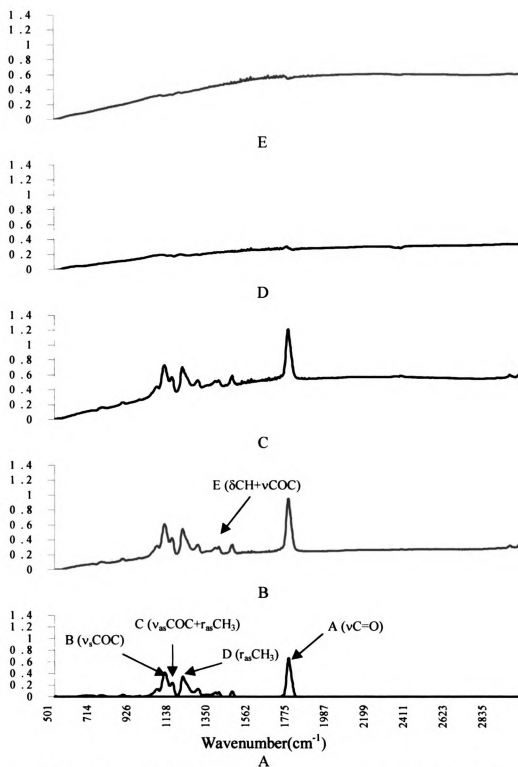


Figure 7 FTIR spectra of 100 P(dl)A polymers: A) As Received, B) 1 Day after H_2O_2 Sterilization, C) 14 Days after H_2O_2 Sterilization, D) Residual after 1 Day, E) Residual after 14 Days

Table 5 Integrated peak areas for 100 P(dl)A sterilized using H₂O₂

Polymer\Peak	1756cm⁻¹	1270cm⁻¹	1187cm⁻¹	1131cm⁻¹	1091cm⁻¹
100 As Received	23.346	1.612	8.900	1.568	6.121
100 H ₂ O ₂ ster. (1 day)	21.425	1.642	9.208	1.681	6.073
100 H ₂ O ₂ ster. (14 day)	18.755	1.629	8.684	1.619	5.779
Subtraction (1 day)	-0.536	-	-	-	-
Subtraction (14 day)	-0.815	-0.036	-0.308	-0.033	-0.134

Table 6 Integrated peak areas for 75/25 P(dl)A/PGA sterilized using H₂O₂

Polymer\Peak	1756cm⁻¹	1270cm⁻¹	1187cm⁻¹	1131cm⁻¹	1091cm⁻¹
75/25 As Received	22.943	1.195	8.115	1.351	5.249
75/25 H ₂ O ₂ ster. (1 day)	21.464	1.128	7.741	1.207	5.093
75/25 H ₂ O ₂ ster. (14 day)	17.025	1.159	6.435	1.098	3.899
Subtraction (1 day)	-0.217	-0.034	-0.424	-0.036	-0.289
Subtraction (14 day)	-4.693	-0.099	-1.574	-0.257	-1.365

Table 6 Integrated peak areas for 50/50 P(dl)A/PGA sterilized using H₂O₂

Polymer\Peak	1756cm⁻¹	1270cm⁻¹	1187cm⁻¹	1131cm⁻¹	1091cm⁻¹
50/50 As Received	38.467	2.535	11.162	1.166	7.075
50/50 H ₂ O ₂ ster. (1 day)	29.823	2.332	10.470	1.187	6.676
50/50 H ₂ O ₂ ster. (14 day)	24.011	2.161	9.298	1.101	5.893
Subtraction (1 day)	-4.586	-0.209	-0.617	-0.021	-0.399
Subtraction (14 day)	-1.0417	-0.372	-1.806	-0.065	-1.182

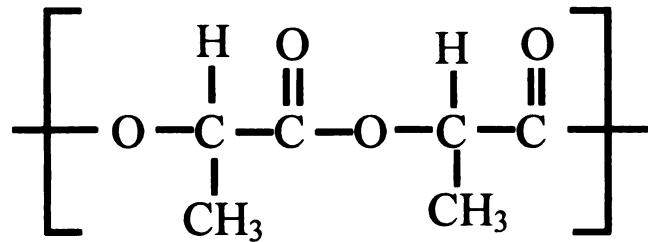
approximately 10% and decreases in the 1760 cm⁻¹ (C=O), 1270 cm⁻¹ (CH+COC), 1187 cm⁻¹ (COC+CH₃), 1131 cm⁻¹ (CH₃) and 1091 cm⁻¹ (COC) peak areas while the 100 P(dl)A gradually decreased to 4%. These decreases in molecular weight can be explained by PLA/PGA polymer degradation theory.

The chemical structure of PLA and PGA are polyester polymers are shown in Figure 8a and b. The principal bond joining the individual monomers is the COC bond. The degradation of these polymers in H₂O has been well studied and documented.^{4,8,14} PLA/PGA degradation occurs by hydrolytic scission and cleavage of the ester bonds that

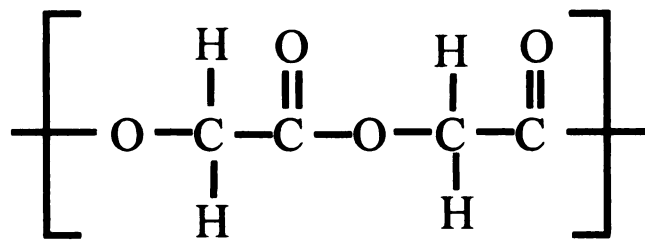
connect the individual monomers. In this process (Figure 9), the OH molecules from absorbed water bond to the carbon atom of the COC ester bonds and form a carboxyl (COH) end group that terminates the polymer sequence. Even though the amount of H₂O available during sterilization is minimal, the OH⁻ molecules are readily available during the ionization phase of H₂O₂ gas plasma sterilization. Therefore, it is apparent that hydrolytic degradation decreases the incidence of the COC bonds similar which is apparent by the decrease in the 1270 cm⁻¹, 1187 cm⁻¹ and 1091 cm⁻¹ bonds shown in this study.

It has also been well established that this degradation process occurs quicker in polymers having higher concentrations of PGA.³⁵ The methyl (CH₃) groups present on the repeating lactic acid chains protect the carbonyl carbons from tissue fluid, which reduces the hydrolysis rate of PLA as compared to PGA.¹⁴ Therefore, hydrolytic degradation occurs faster in polymers with higher concentrations of PGA. This explains the increased degradation rate of the 50/50 and 75/25 polymers when compared to the 100 P(dl)A polymers which degraded to 93, 92 and 96% respectively. The looser chemical structure of the P(dl)A/PGA copolymers allowed for easier diffusion of the H₂O₂ and H₂O chemical species into the polymer and an increased interaction between OH⁻ species and the COC bond of the polymers.

Since the polymer molecular weights continued to decrease for up to 14 days after sterilization, the polymer likely reacts with the H₂O₂/H₂O initially as well as absorb into the polymer for the reactions to continue to take place after sterilization is complete. This was confirmed by the presence of a continuous sloping peak at wavelengths greater than 1700 cm⁻¹ that represents the absorbance of H₂O₂ and H₂O groups. The extent of

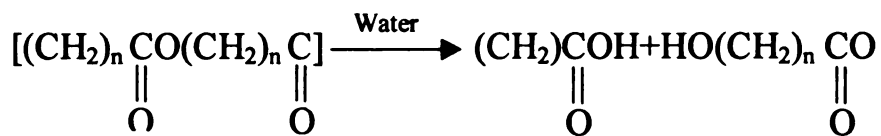


A)

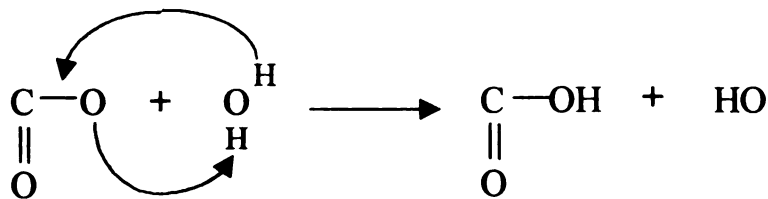


B)

Figure 8 Chemical Structure of A)PLA and B) PGA



A)



B)

Figure 9 Degradation of polylactic/polyglycolic acid a) Polyester degradation via nonspecific hydrolytic scission, b) ester bond cleavage and terminal group formation¹⁴

this degradation and the extent of how long it continues to occur should be the subject for future studies.

Saalman validated FTIR spectroscopy studies to show the absorption of EtO into polymers.³⁶ Subtraction spectrum of UHMWPE subject to EtO gave characteristic EtO peaks at 866 cm^{-1} , 1270 cm^{-1} and 3066 cm^{-1} . However, in this study these characteristic peaks were not apparent. Regardless, the absorption of EtO into the polymers cannot be ruled out because the characteristic peaks of EtO are at the same wavelengths as PLA/PGA polymers. Thus, FTIR is not a good tool for this application using these polymers.

CONCLUSIONS

EtO did effect the intensity of the peaks for the 75/25 PLA/PGA copolymer, but did not effect the molecular weight and polymer structure of the 50/50 PLA/PGA and 100 P(dl)A polymers 24-hours, and 14 days post-sterilization. However, H_2O_2 sterilization resulted in a decrease in the molecular weight of 100 P(dl)A, 75/25 and 50/50 P(dl)A/PGA polymers, as well as decreases in the absorbance of C=O and COC FTIR peaks. The molecular weight of 75/25 and 50/50 P(dl)A/PGA copolymers decreased by approximately 10%, while the molecular weight of 100 P(dl)A decreased about 4 %. This was consistent with the increased degradation rate of polymers with higher PGA. H_2O_2 sterilization of P(dl)A/PGA polymers resulted in polymer degradation through hydrolytic scission and ester bond cleavage, similar to that occurring in PLA/PGA degradation.

REFERENCES

1. Orthosorb Absorbable Pin: Setting the Standard for Absorbable Internal Fixation for Shear or Torque Forces in the Foot, Hand, and Knee, Johnson and Johnson, 1994.
2. Bioabsorbable Materials Technology (Linvale Corp. Promotional Brochure), 1994.
3. Medisorb®, Bioabsorbable Polymers, (Alkermes technical brochure), 1996.
4. Reed, J. and Gilding D.; "Biodegradable Polymers for Use in Surgery – Polyglycolic/Poly(lactic acid) Homo- and Copolymers", *Polymer*, **20**, 1979: 1459-1464.
5. Tschakaloff, A., Losken, H.W., Lalikos, J., Link, J., Mooney, M.P., Von Oepen, R., Michaeli, W., and Losken, A., "Experimental Studies of DL-Polylactic Acid Biodegradable Plates and Screws", *J. Cranio. Surg.*, **4**, 4, 1993, 223-227.
6. James, K. and Kohn, J., "New Biomaterials for Tissue Engineering", *MRS Bulletin*, **11**, 1996, 22-26.
7. Athanasiou, K., Niederauer, G., and Agrawal, C.M., "Sterilization, Toxicity, Biocompatibility and Clinical Applications of Polylactic acid/Polyglycolic Acid Copolymers", *Biomaterials*, **17**, 2, 1996, 93-102.
8. Singhal, A.R., Mullen, J.T., Singhal, M., Agrawal, C.M., and Athanasiou, K.A., "In Vitro Degradation Characteristics of a 50:50 PLGA Biodegradable Implant", *Orthopaedic Research Society, 41st Annual Meeting*, Feb. 13-16, 1995, Orlando, FL.
9. Von Schroeder, H.P., Kewan, M., Amiel, D., and Coutts, R.D., "The Use of Polylactic Acid Matrix and Periosteal Grafts for the Reconstruction of Rabbit Knee Articular Defects", *J. Biomed. Mat. Res.*, **25**, 1991, 329-339.
10. Freed, L.E. and Vunjak-Novakovic, G., "Chondrogenesis in a Cell-Polymer-Bioreactor System", *Experimental Cell Research*, **240**, 1998, 58-65.
11. Freed, L.E., Langer, R., Martin, I., Pellis, N.R., and Vunjak-Novakovic, G., "Tissue Engineering of Cartilage in Space", *Proceedings from the National Academy of Science, USA*, **94**, 13885-13890.
12. Nakamura, T., Hitomi, S., Watanabe, S., Shimizu, Y., Jamshidi, K., Hyon, S.H., and Ikada, Y., "Bioabsorption of Polylactides with Different Molecular Properties", *J. Biomed. Mater. Res.*, **23**, 1989, 1115-1130.
13. Schankenraad, J.M., Nieuwenhuis, P., Molenaar, I., Helder, J., Dijkstra, P.J., and Feijen, J., "In Vivo and In Vitro Degradation of Glycine/DL-lactic Acid Copolymers", *J. Biomed. Mater. Res.*, **23**, 1989, 1271-1288.

14. Hollinger, J.O. and Battistone, G.C., "Biodegradable Bone Repair Materials: Synthetic Polymers and Ceramics", *Clin. Ortho. Rel. Res.*, **207**, 1986, 290-305.
15. Miller R.J., Brady, J.M., and Cutright, D.E., "Degradation Rates of Oral Resorbable Implants (Polylactates and Polyglycolates): Rate Modification with Changes in PLA/PGA Copolymer Ratios", *J. Biomed. Mater. Res.*, **11**, 1977, 711-719.
16. Gombotz, W.R. and Pettit, D.K., "Biodegradable Polymers for Protein and Peptide Drug Delivery", *Biocon. Chem.*, **6**, 1995, 332-351.
17. Suwanprateeb, J., Tanner, K.E., Turner, S., and Bonfield, W., "Influence of Sterilization by Gamma Irradiation and of Thermal Annealing on Creep of Hydroxyapatite-Reinforced Polyethylene Composites", *J. Biomed. Mater. Res.*, **39**, 16-22, 1998.
18. Goldman, M. and Pruitt, L., "Comparison of the Effects of Gamma Radiation and Low Temperature Hydrogen Peroxide Gas Plasma Sterilization on the Molecular Structure, the Fatigue Resistance, and Wear Behavior of UHMWPE", *J. Biomed. Mater. Res.*, **40**, 1998, 378-384.
19. Goldman, M., Gronsky, R., and Pruitt, L., "The Influence of Sterilization Technique and Aging on the Structure and Morphology of Medical-Grade Ultrahigh Molecular Weight Polyethylene", *J. Mater. Sci. Mater. Med.*, **9**, 1998, 207-212.
20. Ries, M., Weaver, K., Rose, R., Gunther, J., Sauer, W., and Beals, N., "Fatigue Strength of Polyethylene After Sterilization by Gamma Irradiation or Ethylene Oxide", *Clin. Ortho. Rel. Res.*, **333**, Dec. 1996: 87-95.
21. Goldman, M. and Pruitt, L., "Comparison of the Effects of Gamma Radiation and Low Temperature Hydrogen Peroxide Gas Plasma Sterilization on the Molecular Structure, Fatigue Resistance, and Wear Behavior of UHMWPE", *J. Biomed. Mater. Res.*, **40**, 1998, 378-384.
22. Agrawal, C.M., Kennedy, M.E., and Micallef, D.M., "The Effect of Ultrasound Irradiation on a Biodegradable 50-50% Copolymer of Polylactic and Polyglycolic Acid", *J. Biomed. Mater. Res.*, **28**, 1994, 851-859.
23. Muscarella, L., "Are All Sterilization Processes Alike?", *AORN*, **67**, 5, 1998, 966-976.
24. Costa, L., "Oxidation in Orthopaedic UHMWPE Sterilized by Gamma-Radiation and Ethylene Oxide", *Biomaterials*, **19**, 1998, 659-668.

25. Zhang, Y.Z., Bjursten, L.M. Freij-Larsson, C., Kober, M., and Wesslen, B., "Tissue Response to Commercial Silicone and Polyurethane Elastomers after Different Sterilization Procedures", *Biomaterials*, **17**, 1996: 2265-2272.
26. Verheyen, C.C., deWijn, J.R., van Blitterswijk, C.A., and deGroot, K., "Evaluation of Hydroxyapatite/Poly(L-Lactide) Composites: Mechanical Behavior", *J. Biomed. Mater. Res.*, **26**, 1992, 1277-1296.
27. Alfa, M.J., "Comparison of Ion Plasma, Vaporized Hydrogen Peroxide, and 100% Ethylene Oxide Sterilizers to 12/88 Ethylene Oxide Sterilizer", *Infection Control and Hospital Epidemiology*, **17**, 1996, 87-91.
28. Meeting of the IARC Working Group on Some Industrial Chemicals, *Scand. J. Work Environ. Health*, **20**, 3, 1994, 227-229.
29. Muller, T.F., Seitz, M., Eckle, I., Lange, H., and Kolb, G., "Biocompatibility Differences with Respect to the Dialyzer Sterilization Method", *Nephron*, **78**, 1998, 139-142.
30. "Meeting of the IARC Working Group on Some Industrial Chemicals", *Scand. J. Work. Environ. Health*, Meeting Reports, **20**, 1994, 227-229.
31. Ferrell, M., Wolff, C., Ellenbogen, K., Wood, M., Clemo, H., and Gilligan, D., "Ethylene Oxide on Electrophysiology Catheters Following Resterilization: Implications for Catheter Reuse", *Am. J. Cardio.*, **80**, 1997, 1558-1560.
32. Vink, P. and Pleijsier, K., "Aeration of Ethylene Oxide-Sterilized Polymers", *Biomaterials*, **7**, 1986, 225-230.
33. Feldman, L.A. and Hui, H.K., "Compatibility of Medical Devices and Materials with Low Temperature Hydrogen Peroxide Gas Plasma", *Medical Devices and Diagnostic Industry*, 1997, 57-62.
34. Kister G., Cassanas, G., and Vert, M., "Effects of Morphology, Conformation and Configuration on the IR and Raman Spectra of Various Poly(lactic acid)s", *Polymer*, **39**, 2, 1998, 267-273.
35. Miller R.J., Brady, J.M., and Cutright, D.E., "Degradation Rates of Oral Resorbable Implants (Polylactates and Polyglycolates): Rate Modification with Changes in PLA/PGA Copolymer Ratios", *J. Biomed. Mater. Res.*, **11**, 1977, 711-719.
36. Saalman, E., "Infrared Spectroscopic Study of Polymers Exposed to Ethylene Oxide", *Biomaterials*, **6**, 4, 1985, 225-230.

CHAPTER 4

FINITE ELEMENT MODELING OF THE VON MISES STRESS OF A FEMORAL CONDYLE SUBJECT TO FULL THICKNESS CARTILAGE DEFECTS AND MAGNETICALLY DIRECTED CHONDROGENESIS IMPLANTS OF VARYING SIZE AND MORPHOLOGY

DEAN A. OPPERMAN AND MELISSA J. CRIMP
Department of Materials Science and Mechanics
Michigan State University
East Lansing, MI 48823

ALAN A. HALPERN
College of Human Medicine
Michigan State University
East Lansing, MI 48823

ABSTRACT

Magnetically directed chondrogenesis (MDC) has been shown to be a promising technique for cartilage repair.^{1,2} In this technique, a magnet implanted into the subchondral bone beneath a cartilage defect is used to attract magnetically tagged chondrocytes to the defect site. The effect of implant/magnet morphology, as well as the number of magnets implanted into the defect site on the stress profile of the femoral condyle has to be evaluated to insure the stability of the post-operative joint and to optimize the conditions for bone in-growth. In this study, an Ansys 5.5 finite element model was developed to determine the von Mises stress concentration in the femoral condyle with 6mm wide full thickness cartilage defects and PLA/PGA/Fe MDC implants of different size, number and porosity under standing loading conditions. The von Mises

stress concentration adjacent to the implant was not significantly increased with the inclusion of empty cartilage defects or implantation of polymer magnets at the defect site. No significant alterations in stress at the base of the implants were found when comparing smaller implants equally spaced across the defect site to implants that spanned the entire defect site. A significant decrease was found in the stress between the two smaller implants. Solid implants produced less stress in the areas adjacent to the defect site when compared to porous implants. However, in all cases the stresses in the bone remained appreciably under the reported ultimate strengths of trabecular bone. Therefore, P(dl)A/PGA/Fe implants will not significantly increase the stress in the implantation area. To optimize the rate of bone in-growth, the porous implant should span the entire defect site up to 6 mm. This implant morphology is expected to promote bone in-growth by generating elevated stress levels that are below the compressive strength of trabecular bone.

INTRODUCTION

Osteoarthritis is considered to be the most prevalent rheumatic disease.³ It results in a deterioration and/or loss of articular cartilage leading to pain and joint dysfunction in 75% of the elderly population.⁴ In 1985, Wilson et al. performed a case study of 98 patients showing symptomatic osteoarthritis of either the hip or knee.⁵ 78 of the 98 people had some level of osteoarthritis of the knee joint.⁵ The knee joint serves as a synovial hinge joint that connects the femoral and tibial condyle and the patellae and trochlear surface of the femur. Most commonly, cartilage defects occur on the mid-medial

surface of the femoral condyle. These lesions eventually develop into full thickness cartilage defects.⁶

Repair of articular cartilage has been studied for centuries⁷. As early as 1743, William Hunter, stated that “from Hippocrates to the present time, it is universally allowed that ulcerated cartilage is a troublesome thing, and that when it is once destroyed, it is not repaired”.⁷ Magnetically directed chondrogenesis (MDC) is a novel, fundamental approach to articular cartilage repair.^{1,2} Histology results from the pilot study by Halpern, Grande and Crimp, have shown optimistic results by producing a hyaline-like cartilage after 8 weeks implantation.² MDC requires the implantation of a biodegradable polymer magnet into the subchondral bone underlying the cartilage defect. This magnet is used to attract magnetically tagged chondrocytes to the defect site and hold the chondrocytes to facilitate cartilage formation. The effect of this implant on the stress concentration of the femoral condyle is unknown.

In this study, a finite element model was developed and used to investigate the effect of P(dl)A/PGA/Fe implants on the von Mises stress in the human femoral condyle. The effect of implant size, number and porosity on the von Mises stress in the trabecular bone, subchondral to a cartilage defect and surrounding MDC implants, was investigated.

EXPERIMENTAL PROCEDURE

A quasi-static, linear elastic, finite deformation model for the femoral condyle was developed (Ansys 5.5). The topography of a human femur was modeled by tracing an x-ray image of a 44-year-old male (Figure 1). The knee joint appeared healthy with equal articular space medial and lateral and a combined thickness of the articular surfaces of

approximately 5mm. The topography of the articular surface of the femoral condyles was taken from scale pen and ink drawings of Cahill et al. who drew the profile of coronal planes of the human knee from cadaver studies (Figure 2).⁸ This figure was enlarged to match the size of the x-ray and the articular surface traced onto the femoral surface. The solid model was then meshed using 8-node quad meshing with 3404 elements.

The material properties used for the bone and cartilage are given in Table 1. The elastic modulus for cartilage was taken from the tensile modulus reported by Akizuki et al.⁹ The elastic modulus for trabecular bone was taken from the data reported by Carter and Hayes.¹⁰ Poisson's ratio for both the articular cartilage and the trabecular bone were based on a study by Li et al. who modeled the patello-femoral joint of NZW rabbits.¹¹

The boundary and loading conditions for the present study were adapted from a study by Furukubayashi and Kurosawa who applied a 1500N load to human cadaver knees.¹² Furukubayashi et al. measured the contact area and pressures (Figure 3) on the tibial plateau using a pressure sensitive film.¹² A line across the middle of the tibial plateau was then drawn. The pressure distribution along the line was used as the pressure profile along the articular surface in the 2-D model. Zero displacement boundary conditions were applied to the femoral shaft surface of the model and the stress distribution calculated (Figure 4). Images in this dissertation are presented in color.

Since the goal of this research is to analyze the effect of MDC implants on the stress concentrations in the femoral condyle, full thickness defects and implant magnets were inserted into the articular cartilage and subchondral trabecular bone to simulate an arthritic joint subject to MDC implants. The addition of these defects acts to redistribute the loading across the articulating surfaces of the knee. Thus, the loading for an arthritic knee



Figure 1 X-ray of a 44-year-old male knee

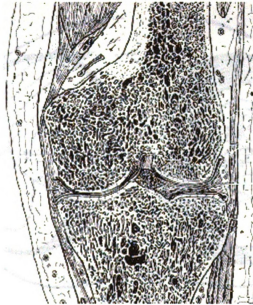


Figure 2 Cross-section diagram of the human knee²³

would be altered from that of Furkubayashi and Kurosawa. Therefore, the loads generated on the femoral surface of Figure 4 were used as the loading condition and the zero displacement boundary condition was placed on the articular cartilage surface (Figure 5).

Table 1 Material Properties used in the femoral condyle FEM model

Material	Elastic Modulus	Poisson's Ratio
Bone	200 MPa	0.3
Cartilage	13.7 MPa	0.49
Solid PLA/PGA/Fe implant	3.394 ± 4.04 GPa	0.3
Porous PLA/PGA/Fe implant	104 ± 25 MPa	0.3

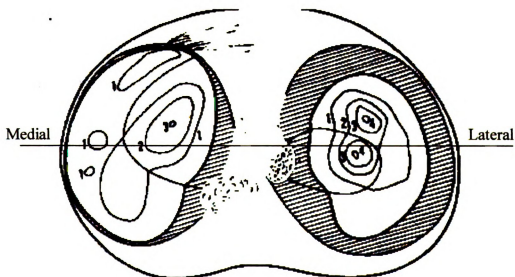


Figure 3 Pressure profile across the tibial plateau with application of 1500kN load⁸

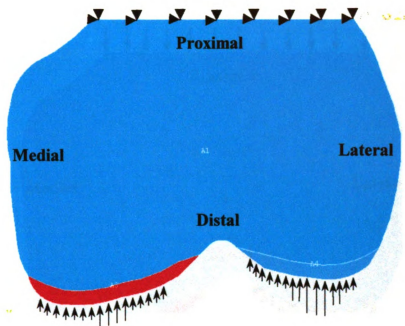


Figure 4 Area map of the finite element model with the loading conditions on the articular surfaces and the boundary conditions on the proximal surface (femoral shaft)

To determine the stress profile in the femoral condyle of joints with cartilage defects, cartilage segments were removed from the areas of highest loading on both the medial and lateral condyles. The defects extended to the subchondral bone (full thickness) and were approximately 6mm wide. Porous and solid 50/50/Fe implants with 2 different implant sizes, 6mm in diameter by 6mm long and 1.5 mm in diameter by 6mm long, were evaluated. The larger implants spanned the entire defect site while the smaller implants were located 1 mm toward the center of the defect site, separated by 1 mm. The material properties of these three implant materials, are given in Table 1. The elastic modulus was measured from compression tests of 5 cylindrical implants prepared by the previously explained methods¹³. Because of the lack of published Poisson's ratio values for PLA/PGA, the Poisson's ratio was estimated to be that of bone, 0.3.

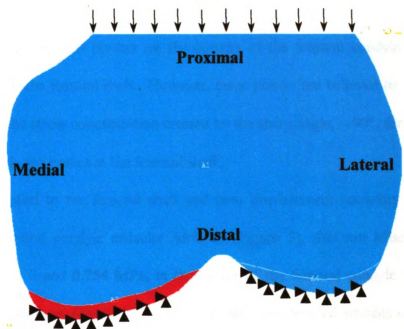


Figure 5 Area map of the finite element model with the loading conditions on the articular surfaces and the boundary conditions on the proximal surface (femoral shaft)

RESULTS

The nodal solution of the finite element model where the pressure profile is applied to the articular surface showed elevated stresses at the articular surface at the location of the applied pressures with stress concentrations apparent in the areas of highest loading (Figure 6). The von Mises stresses in the articulating surfaces were the highest, between 2.25 and 3.00 MPa, in the middle of the lateral condyle (A) and ranged between 1.50 and 2.25 MPa in the middle of the medial condyle (B). In general, the von Mises stress and the deformation in the articulating surfaces mirrored the applied loading with the maximum deformation and stress occurring in the cartilage that was subject to the highest loads. In the subchondral trabecular bone, lower von Mises stress, between 0 and 0.75 MPa, in the

middle, were predicted in the middle of the femur, the medial surface and the lateral surface (C) with elevated stresses in strips beneath the articular surfaces (D). Stress concentration points are also present on the corners of the femoral condyle where the model terminates at the femoral shaft. However, these points are believed to be artifacts of the model and the stress concentration created by the sharp angle, $\sim 90^\circ$, formed where the femoral condyle terminates at the femoral shaft.

With loads applied to the femoral shaft and zero displacement boundary conditions applied to the femoral condyle articular surfaces (Figure 5), the von Mises stress is minimized, between 0 and 0.754 MPa, in the center of the femoral condyle and on the medial and lateral surfaces (Figure 7). The model showed elevated stresses of 0.75 and 1.5 MPa in the trabecular bone underlying the cartilage contact surfaces (A). In the lateral articular cartilage, the von Mises stress and deformation were evenly distributed with the articular surface maintaining the same curvature as in the unloaded condition. However, in the medial articular cartilage, the von Mises stress distribution varied between 0 and 1.5 MPa with von Mises stress distributions between 0 and 0.75 in the middle of the condyle and between 0.75 and 1.5 at the edges of the contact surface. The maximum stress of 6.75 MPa was located where the model terminates at the medial surface of the femoral shaft.

With the application of 6 mm wide full thickness articular cartilage defects to both the medial (A) and lateral (B) articular surfaces, the von Mises stress concentration in the trabecular bone subchondral to the defect site decreased to 0 - 0.75 MPa (Figure 8). The application of full thickness defects increased the stress in the articular cartilage, apparent in the elevated von Mises stress in the medial condyle and the increased cartilage

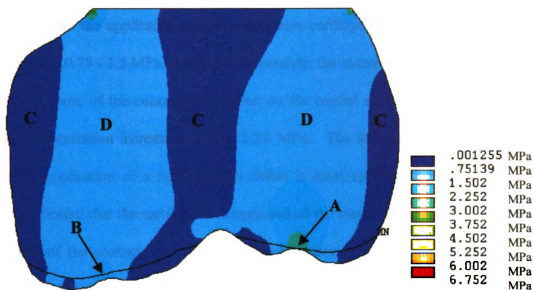


Figure 6 Von Mises stress distribution in the femoral condyle using the loading conditions on the articular cartilage and the boundary conditions on the femoral shaft

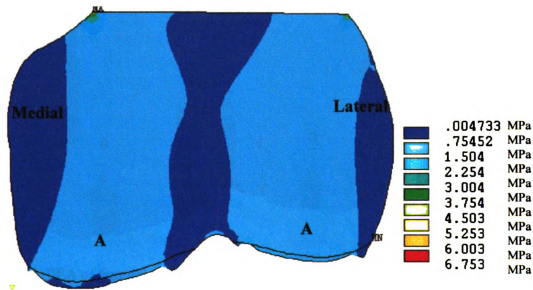


Figure 7 Von Mises stress distribution in the femoral condyle using the loading profile bone surface and 0 displacement boundary conditions on the articular surface. The model indicated elevated von Mises stress concentrations underlying the articular cartilage (A) with lower von Mises stresses on the medial and lateral surfaces of the femoral condyle as well as in the femoral groove

deformation (C). In Figure 7, the stress distribution across the medial condyle was 0 -1.5 MPa but with the application of a full thickness cartilage defect, the stress distribution increased to 0.75 - 1.5 MPa. In the lateral condyle, the stress still ranged from 0.75 to 1.5 MPa for most of the contact surface but on the medial side of the lateral condyle the stress concentration increased to over 2.25 MPa. The increased cartilage deformation with the application of a full thickness defect is most apparent in the medial condyle, which indicated that the cartilage is compressed all the way down the subchondral bone at the ends of the contact surface (C). This complete deformation was not apparent in articular surfaces not having cartilage defects (Figure 7).

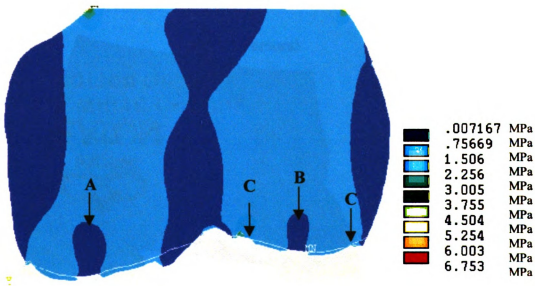


Figure 8 FEA of femoral condyle with 2 full thickness defects on the articular surface. The model indicated a decrease in von Mises stress in the trabecular bone subchondral to the defect sites (A and B) and elevated von Mises stress and deformation in the lateral articular cartilage (C)

The von Mises stress at the base of the cartilage defect in both the lateral and medial condyles was approximately 0 and gradually increased with distance away from the defect site (Figures 9 and 10). In both cases, there was a rounding of the articular cartilage on the surfaces of the defect (A). This deformation is accompanied by an increase in von Mises stress at the cartilage bone interface (B). In both the lateral and medial condyles, the von Mises stress in this region (B) increases to between 1.7 and 2.1 MPa and is the maximum stress concentration in the region of the defect site. In the trabecular bone, subchondral to the cartilage defect (C), there was a decrease in the von Mises stress to between 0 and 0.24 MPa. The von Mises stress then gradually increased as one moves toward proximal toward the femoral shaft (arrow).

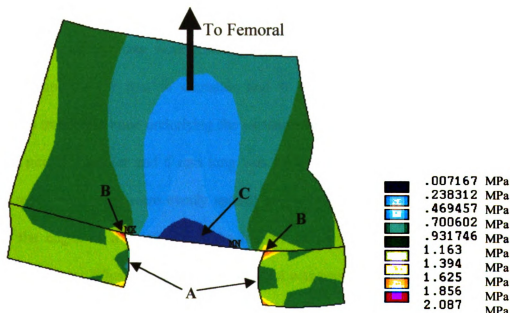


Figure 9 FEM model of the lateral condyle defect. The model indicated a significant amount of cartilage deformation along the surfaces of the defect (A) with increased von Mises stress at the cartilage/trabecular bone interface (B). A reduction in the von Mises stress in the trabecular bone subchondral to the defect site was also apparent (C)

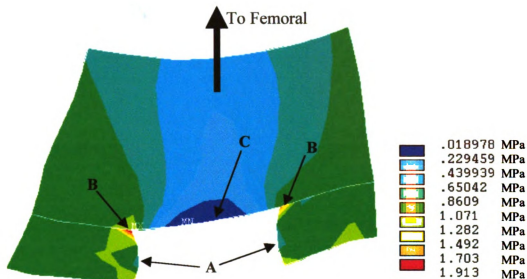


Figure 10 FEM model of the medial condyle defect. The model indicated a significant amount of cartilage deformation along the surfaces of the defect (A) with increased von Mises stress at the cartilage/trabecular bone interface (B). A reduction in the von Mises stress in the trabecular bone subchondral to the defect site was also apparent (C)

Two MDC implant sizes were tested using this finite element model. Either two cylindrical implants 1.5 mm in diameter and 6 mm long were implanted into the subchondral trabecular bone underlying the cartilage defect (Figure 11) or one cylindrical implant 6 mm in diameter and 6 mm long was implanted (Figure 12). When 2 smaller implants were used, they were evenly spaced across the defect site leaving 1-mm gaps between the edges of the defect and the implant as well as a 1mm gap between the individual implants. When the larger MDC implant was tested, the implant spanned across the entire defect site.

The insertion of two porous implants into the trabecular bone subchondral to the defect site resulted in little to no alterations of the von Mises stress in the bone and cartilage surrounding the defect site (Figure 13). The von Mises stress at the base of the cartilage

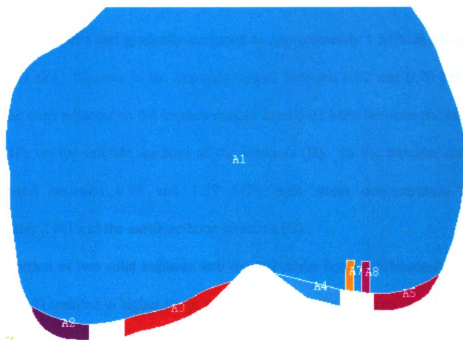


Figure 11 Area map of the femoral condyle with cartilage defects and 2 magnetic implants

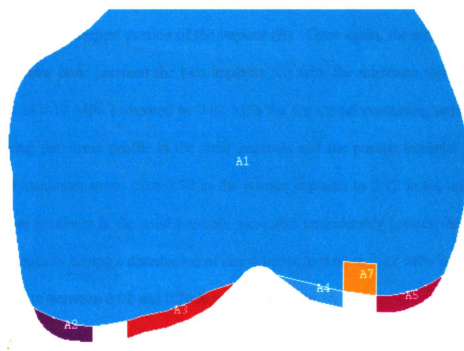


Figure 12 Area map of the femoral condyle model with cartilage defects and 1 magnetic implant

defect was 0.020 MPa and gradually increased to approximately 1 MPa at areas proximal to the defect site. Stresses in the implants ranged between 0.02 and 0.70 MPa and the stress in the bone adjacent to the implant ranged from 0.02 MPa between the implants (A) to 0.93 MPa on the outside surfaces of the implants (B). In the articular cartilage the stress ranged between 0.93 and 1.39 MPa with stress concentration points of approximately 2 MPa at the cartilage/bone interface (C).

The insertion of two solid implants into the trabecular bone subchondral to the defect site (Figure 14) resulted in higher stress concentrations in the implants and stress gradients in the trabecular bone adjacent to the implant sites as compared to porous implants. The von Mises stress in the trabecular bone adjacent to the MDC implants ranged between 1.0 and 1.25 MPa at the cartilage surface (A) and gradually decreased to between 0.39 and 0.61 MPa at the deepest portion of the implant (B). Once again, the stress was lowest in the trabecular bone between the two implants (C) with the minimum stress of the solid implants of 0.17 MPa compared to 0.02 MPa for the model containing porous implants. Comparing the stress profile in the solid implants and the porous implants indicated an elevated maximum stress from 0.70 in the porous implants to 2.12 in the solid implants. The stress gradients in the solid implants were also considerably greater than that of the porous implants having a distribution of stress between 0.60 to 2.12 MPa in solid implants compared to between 0.02 and 0.70 in porous implants.

With the implantation of one porous implant that spans the entire width of the defect site (Figure 15) the von Mises stress profile was very similar to that of Figure 14 where no implant was used. The stress concentration was at a minimum (0.04 MPa) at the base of

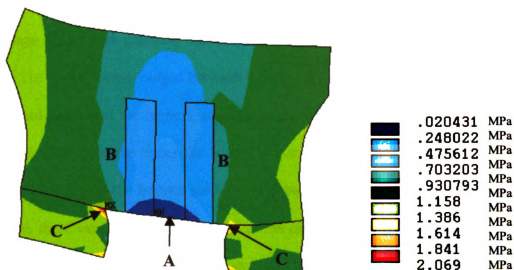


Figure 13 Von Mises stress profile of the lateral condyle femur with 2 porous implants implanted into the base of the cartilage defect. The FEM model predicted a decrease in the von Mises stress between the implants (A) and a slight increase in von Mises stress surrounding the implant (B). Once again stress concentration points were present at the cartilage/trabecular bone interface (C)

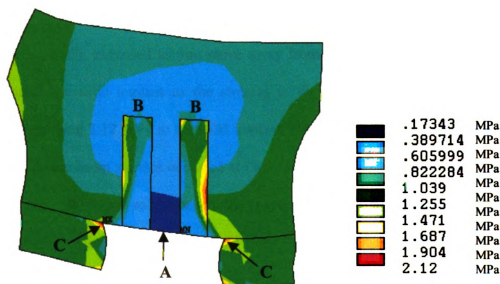


Figure 14 Von Mises stress profile of the lateral condyle with 2 solid implants implanted into the base of the defect. The FEM model predicted a decrease in the von Mises stress between the implants (A) and a slight increase in von Mises stress surrounding the implant (B). Once again stress concentration points were present at the cartilage/trabecular bone interface (C)

the cartilage defect and gradually increased radially toward the center of the femoral condyle. The implant stress ranged between 0.04 and 0.70 MPa from most of the implant with elevated stresses at the corners, adjacent to the defect site (A), of up to 1.56 MPa. The von Mises stress in the trabecular bone adjacent to the implant ranged between 0.48 and 1.346 MPa (B) on the bottom surface and between 0.91 and 1.35 on the sides (C). Once again, there were stress concentrators at the cartilage/bone interface at the edge of the defect site that resulted in a von Mises stress of 2.00 MPa. Throughout the rest of the cartilage the stress ranges between 0.91 and 1.35 MPa.

Insertion of one solid implant beneath the cartilage defect resulted in a decrease in the stress in the trabecular bone adjacent to the implant as well as increases in the stress in the implant (Figure 16). In this case the location of the minimum stress (0.08 MPa) moved from what was the implant/defect interface to the middle of the implant. The von Mises stress then gradually increased as you move away from this minimum. Comparing the stresses inside the solid implant to the stresses in the porous implant showed higher stresses approaching 3.12 MPa in the solid implant compared to 1.56 MPa in the porous implant. Both maximum stresses occurred at the top corner of the implant adjacent to the defect site (A). With the solid implant the stress gradient was much higher than the porous implant ranging between 0.08 and 3.12 MPa. The von Mises stress in the trabecular bone adjacent to the implant ranged between 0.42 and 1.10 MPa (B) on the bottom surface and between 0.42 and 1.43 on the sides (C) which was slightly less than if porous implants were used. With solid implants that span the entire defect site the stress concentrators at the cartilage/bone interface at the edge of the defect site were not

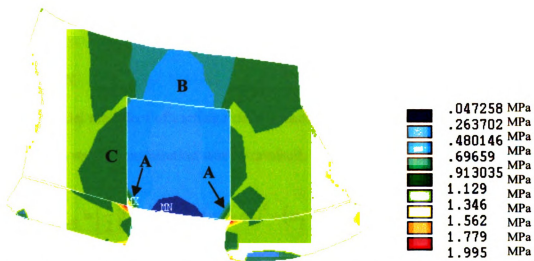


Figure 15 Von Mises stress profile of the femoral lateral condyle with 1 porous magnet implanted at the base of the defect. The FEM model predicts minimal elevated von Mises stresses in the corners of the implant (A) and along the sides of implant (C). The von Mises stress was minimized on the proximal end of the implant (B) and gradually increased with distance away from the implant

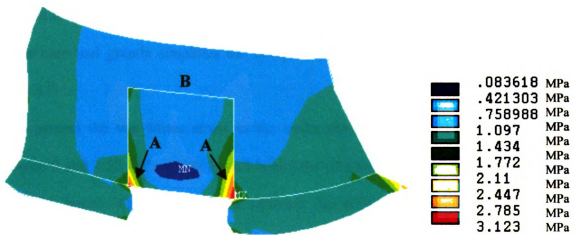


Figure 16 Von Mises stress profile of the femoral lateral condyle with 1 solid magnet implanted at the base of the defect. The FEM model predicted higher stresses in the corners of the implant (A). The stress surrounding the implant was more uniform and ranged between 0.42 and 1.10 MPa over most of the implant/trabecular bone interface (B)

apparent and the stress throughout the rest of the cartilage ranged between 0.75 and 1.43 MPa which once again was slightly lower than with porous implants.

DISCUSSION

In this model the effect of cartilage defects and the implantation of MDC implants on the von Mises stress concentration was determined. The von Mises stress is calculated by:

$$\sigma_{mi} = \left[\frac{1}{2} \left\{ (\sigma_1 - \sigma_2)^2 + (\sigma_1 - \sigma_3)^2 + (\sigma_2 - \sigma_3)^2 \right\} \right]^{\frac{1}{2}} \quad (1)$$

From Equation 1 the von Mises stress is calculated as the average difference in the principal stresses σ_1 , σ_2 and σ_3 . The von Mises stress can then be compared to stress values obtained from samples of the material tested in the laboratory in uni-axial compression to estimate the probability of failure.¹⁴ Even though this comparison is less effective for anisotropic materials such as bone and articular cartilage it is often still used in this case and greatly simplifies the interpretation and representation of FEA stress analysis.¹⁴

In general the von Mises stress in the trabecular bone in all cases studied varied between 0 and 1.52 MPa which is well below the ultimate compression strength for the trabecular bone. Carter and Hayes reported the ultimate compressive strengths of trabecular bone to range between 2 and 10 MPa for samples having apparent densities between 0.2 and 0.5 gm/cc respectively.¹⁵ Behrens et al. reported compressive strengths between 2.95 and 29 MPa for trabecular bone having apparent densities between 0.3 and 0.9 gm/cc respectively.¹⁶ Ducheyne et al. reported ultimate compression strengths of the trabecular bone in human femurs that ranged between 15.7 MPa on the lateral condyle and

34.6MPa on the medial condyle.¹⁷ The increased ultimate compression strengths of the medial condyle was attributed to the higher density of bone on the medial side due to the fact that a greater portion of the joint force during the free stance phase of walking is concentrated on the medial condyle. Thus, based on these results the introduction of articular cartilage defects or the implantation of porous or solid MDC implants would not appreciably compromise the strength of the subchondral trabecular bone and initial failure of the femoral condyle.

The two drawbacks to this study are: 1) a lack of published data on the material properties of PLA/PGA/Fe implants the Poisson's ratio of the MDC implants were estimated to be 0.3, and 2) the loading conditions for knee subject to 6mm full thickness cartilage defects are not known. Figures 6 and 7 show that the location of the applied loads and the boundary conditions play effect the von Mises stress in the articular cartilage and in the subchondral trabecular bone. With the loading forces applied to the articular cartilage surface the maximum von Mises stress in the cartilage and subchondral bone reached between 2.25 and 3.00 MPa. With the loading forces applied to the femoral shaft, the maximum stresses in the cartilage and subchondral bone ranged between 0.75 and 1.50 MPa. This reduction was attributed to the fact that when the boundary conditions are applied to the articulating surface, the stress is redistributed and averaged across the boundary condition. However, since the maximum stress for both models is significantly less than the maximum compressive stress for bone and in this study the effects of adding MDC implants to the subchondral bone on the stress are being evaluated, the magnitude is less critical.

The small von Mises stress concentrations, between 0 and 2 MPa, which dominate this study are the result of two factors. First, the stress in articular cartilage and subchondral trabecular bone is minimized in this study by the fact that the loading is placed on the femoral surface condyle and the zero displacement boundary condition is placed on the articular surface (Figures 5). This resulted in a redistribution of the stresses across the articular surface (Figure 7) as compared to models which load the femoral condyle through the articular cartilage and have the boundary condition on the femoral shaft (Figures 4 & 6). However, this model is necessary in order to evaluate the stresses in a femoral condyle where the articular surface is compromised and the contact surface is different than previous studies where the loading is analyzed.

The second reason the von Mises stresses are low in this study is that a full thickness articular cartilage defect is applied to the medial and lateral condyles. The application of this defect reduces the contact area of the boundary condition. Thus, the subchondral trabecular bone to the defect site is unconstrained. This reduces the stress in that area which was shown in Figure 8. This reduces the stress in the trabecular bone even further before the MDC implants are implanted. This is important because according to Wolff's law this reduced stress state in the trabecular bone subchondral to the defect site could result in a significant amount of bone resorption or remodeling under the cartilage defect.

In 1892 Julian Wolff published his monograph on bone remodeling.¹⁴ His main observation was that bone is reformed in response to the loading conditions that act on it. Wolff emphasized that the remodeling of cancellous bone follows mathematical rules corresponding to the principle stresses that act on it. Bone not subject to forces due to inactivity have been shown to resorb and decrease in apparent density and bone subject to

increased stress has been shown to remodel increase in apparent density in the areas of elevated stress.¹⁸⁻²⁰ Thus, not only is it important to evaluate the stress as it may contribute to bone failure, but it is also important to evaluate the stress conditions in the trabecular bone and how they will effect the bone in-growth into the implant site as the implant degrades.

Comparing the von Mises stress profiles of condyles subject to multiple implants to condyles subject to single MDC implants indicated higher stresses in the trabecular bone surrounding single implants. The von Mises stress between two smaller implants ranged between 0.2 and 0.5 MPa which is significantly lower than the von Mises stresses in the same area of a femur not subject to full thickness cartilage defects or MDC implants which was between 0.75 and 1.5 MPa (Figure 7). Thus, by placing multiple implants into the defect site the bone between the implants will most likely resorb or remodel to decreased apparent density and load bearing capacity due to the decreased stress in that area. In the regions outside of the implants the von Mises stresses are more comparable to the native condition and higher for single implants as compared to multiple implants. Thus, by Wolff's law it is also expected that the regeneration around the single implants would be accelerated as compared to the bone surrounding the smaller multiple implants.

Comparing the stress concentrations of solid implants compared to porous implants this study indicated that solid implants resulted in higher stresses in the implants as well as decreased stresses in the trabecular bone surrounding the implants. The increased stress in the solid implants would result in an increased implant degradation rate. Implants placed in anatomic sites exposed to greater degrees of stress have been shown to degrade faster than implants in low stress areas.²¹ The elevated stresses are believed to lead to cracks in

the implant, which both reduce the effective strength of the implants and increase the surface area of the implant resulting in an increase in water absorption and increased degradation kinetics. The elevated von Mises stress in the trabecular bone surrounding porous implants is also important because once again this predicts an increased bone remodeling rate in that area.

CONCLUSIONS

A finite element model was used to evaluate the stress concentration in the subchondral trabecular bone of a femoral condyle subject to articular cartilage defects and MDC implants. Results showed that the addition of full thickness cartilage defects decreased the stress concentration in the subchondral bone underlying the cartilage defect with minimal to no increases in stress to the trabecular bone surrounding the defects. Solid and porous magnetic implants, located directly beneath the cartilage defect, did not significantly increase the stress concentration in that area. Implanting two polymer magnets that are 1.5mm wide and 6mm long into the subchondral bone underlying cartilage defects shielded the subchondral bone between the implants and were predicted to result in bone resorption. However, implants that span the entire width of the defect resulted in an increase in the von Mises stress in the surrounding subchondral bone and is predicted to remodel more quickly. Solid PLA/PGA/Fe implants resulted in decreases in von Mises stress in the surrounding subchondral bone and articular cartilage as well as significant increases in the stresses developed within the implant itself as compared to porous implants. However, even with elevated stresses in the bone and the implant both are significantly lower than the ultimate compressive strengths of trabecular bone. Thus, for

cartilage defects that are 6 mm wide, porous magnets that span the entire defect site would be the most beneficial to maximizing the rate of bone in-growth during implant degradation without compromising the strength of the subchondral trabecular bone.

REFERENCES

1. Halpern, A.A., Crimp, M.J., Blowers, M.G., Lowsein, L.A., Huisepos, L.H., and McPherson, W.R., "Determination of Cellular Response to Intraarticular Placement of Neodymium and Samarium Cobalt Magnetic Implants in a Canine Model", *3rd Combined Meeting of Orthopedic Research Society of USA, Canada, Europe, & Japan*, Hamamatsu, Japan, Sept. 1998, 161.
2. Halpern, A.A., Crimp, M.J., and Grande, D., "The Use of Magnetically Tagged Chondrocytes for Repair of Cartilage Defects", *Trans, Ortho. Res. Soc.*, 1997, 541.
3. Howell, D.S. and Altman, R.D., "Cartilage Repair and Conservation in Osteoarthritis", *Osteoarthritis*, **19**, 3, 1993, 713-724.
4. Mankin, H.J., "Chondrocyte Transplantation One Answer to an Old Question", *New Eng. J. Med.*, **331**, 14, 1995, 940-941.
5. Wilson, M.G., Michet, C.J., Ilstrup, D.M., and Melton III, L.J., "Idiopathic Symptomatic Osteoarthritis of the Hip and Knee: A Population-Based Incidence Study", *Mayo. Clin. Proc.*, **65**, 1990, 1214-1221.
6. Personal communication-A. Halpern, 1999.
7. Robinson, P.D., "Histologic Study of Articular Cartilage Repair in the Marmoset Condyle", *J. Oral Maxillofac. Surg.*, **51**, 1993, 1088-1094.
8. Cahill, D.R., Orland, M.J., and Miller, G.M., Atlas of Human Cross-Sectional Anatomy, Wiley-Liss, New York, 1995, p133.
9. Akizuki, S., Mow, V.C., Muller, F., Pita, J.C., Howell, D.S., and Manicourt, D.H., "Tensile Properties of Human Knee Joint Cartilage: Influence of Ionic Concentrations, Weight Bearing, and Fibrillation on the Tensile Modulus", *J. Orthop. Res.*, **5**, 1986, 379-392.
10. Carter, D. R. and Hayes, W.C., "Bone Compressive Strength: The Influence of Density and Strain Rate", *Science*, **194**, 1976, 1174-1176.

11. Li, X., Haut, R.C., and Altiero, N.J., "An Analytical Model To Simulate Blunt Impact Response of the Rabbit Patello-Femoral Joint", *ASME J. Biomech. Eng.*, **117**, 485-491.
12. Fukubayashi, T. and Kurosawa, H., "The Contact Area and Pressure Distribution Pattern of the Knee", *Acta Orthop. Scand.*, **51**, 1980, 871-879.
13. Oppermann, D.A., Crimp, M.J., and Halpern, A.A., "Fabrication and Initial Magnetic and Compressive Strengths of P(dl)A/PGA/Fe and P(dl)A/PGA/SmCo5 Implants for Use as a Delivery Device for Magnetically Directed Chondrogenesis", to be submitted for publication.
14. Mow, V.C. and Hayes, W.C., Basic Orthopaedic Biomechanics: Second Edition, Lippincott and Raven Publishers, Philadelphia, 1997, pp113-178.
15. Carter, D.R. and Hayes, W.C., "The Compressive Behaviour of Bone as a Two-Phase porous structure", *J. Bone Jt. Surg.*, **59A**, 954-962.
16. Behrens, J.C., Walker, P.S., and Shoji, H., "Variations in Strength and Structure of Cancellous Bone at the Knee", *J. Biomech.*, **7**, 1974, 201-207.
17. Ducheyne, P., Heymans, L., Martens, M., Aernoudt, E., Meester, P., and Mulier, J., "The Mechanical Behavior of Intracondylar Cancellous Bone of the Femur at Different Loading Rates", *J. Biomech.*, **10**, 1977, 747-762.
18. Frost, H.M., "Pathomechanics of the osteoporoses", *Clin. Ortho.*, **200**, 1985, 198-225.
19. Pazzaglia, U.E., Andrini, L., and Di Nucci, A., "The Effects of Mechanical Forces on Bones and Joints", *J. Bone Jt. Surg.*, **79-B**, 6, 1997, 1024-1030.
20. Jones, H.H., Priest, J.D., Hayes, W.C., Tichenor, D.C., and Nagel, D.A., "Humeral Hypertrophy in Response to Exercise", *J. Bone Jt. Surg.*, **59-A**, 2, 1977, 204-208.
21. Suuronen, R., Pohjonen, T., Taurio, R., and Tormala, P., "Strength Retention of Self-Reinforced Poly-L-Lactide Screws and Plates: An *In Vivo* and *In Vitro* Study", *J. Mater. Sci. Mater. Med.*, **3**, 1992, 426-431.

CONCLUSIONS

This research has been successful in producing a biocompatible, biodegradable, magnetic, polymer implant. In Chapter 1 solid implants and implants with predictable porosities could be fabricated by salt leaching and extrusion molding techniques. The compressive strength and elastic modulus of porous samples equated well with those of trabecular bone, while the compressive strength of solid samples was significantly less than cortical bone. The elastic modulus of the solid samples was equivalent to that of cortical bone. Implants fabricated with SmCo_5 possessed higher magnetic field strengths as compared to equivalent samples composed of Fe particles. In both cases the initial implant magnetization increased with increases of magnetic material, PGA composition and decreases in implant porosity. In a preliminary study of the chondrocyte/implant attraction, photomicrographs indicated that magnetically tagged chondrocytes coated porous 50/50 P(dl)A/PGA implants containing 25 vol. % Fe.

In pilot biocompatibility studies, the biocompatibility of P(dl)A/PGA/Fe implants was tested by implantation into the femoral groove of NZW rabbits. Results indicated a minimal immunological response with normal fibrous encapsulation and a minimal foreign body response to both 50/50 and 75/25 P(dl)A/PGA implants. 50/50 P(dl)A/PGA composites resulted in a greater degree of bioactivity with a larger amount of bone forming cells in the vicinity of the implant as compared to equivalent implants made from 75/25 P(dl)A/PGA.

In Chapter 2, the magnetic strength of P(dl)A/PGA/Fe and P(dl)A/PGA/ SmCo_5 implants was investigated as a function of *in vitro* degradation time. This data was then used to estimate the maximum chondrocyte/implant separation distance. Results showed

that implants that contained SmCo₅ had a larger initial and 8 week attraction distance. The initial magnetic pole strength increased with increasing volume of magnetic material, and the magnetic pole strength degradation rate decreased. Additionally, solid implants had higher magnetic field strengths during degradation than porous implants. Implants with higher PGA compositions generated higher initial magnetic field strengths. However, the higher magnetic field strengths of the 50/50 P(dl)A/PGA implants degraded quicker than the 65/35, 75/25, and 85/15 P(dl)A/PGA implants. The maximum separation distance at which the implant is capable of attracting chondrocyte cells was calculated to be 2.24 mm for SmCo₅ samples and 0.38 mm for Fe samples.

In Chapter 3, the effect of H₂O₂ and EtO sterilization techniques on the molecular weight and chemical structure of 100 P(dl)A, 75/25 P(dl)A/PGA, and 50/50 P(dl)A/PGA polymers was investigated to determine the most appropriate sterilization strategy. GPC analysis showed a decrease in the molecular weight of 50/50 and 75/25 polymers subject to hydrogen peroxide sterilization, while no significant changes were found with polymers subjected to ethylene oxide sterilization. FTIR analysis supported these results and indicated a decrease in the incidence of the COC ester bonds, which is consistent with the initial stages of PLA/PGA hydrolysis.

In Chapter 4, finite element analysis of a femoral condyle subjected to articular cartilage defects and MDC implants indicated that solid and porous magnetic implants, located directly underneath the cartilage defect, did not alter the stress concentration in bone surrounding the implant. However, solid implants resulted in lower stresses in the surrounding subchondral bone as well as significant increases in the stresses developed within the implant itself as compared to porous implants. However, even with the

elevated stresses, the stress level in the implants was well below their ultimate compressive strengths.

From these results, the optimum implant for magnetically directed chondrogenesis would be solid, composed of 50/50 P(dl)A/PGA and contain 50 vol. % SmCo₅. The choice of the 50/50 P(dl)A/PGA polymer was made on the basis that 50/50 P(dl)A/PGA implants had the highest initial magnetic field and a greater level of bioactivity than implants containing higher concentrations of PLA. The only drawback to the 50/50 P(dl)A/PGA implants is their increased degradation rate, which limits the attraction distance 8 weeks after implantation.

The optimum implants are solid for two reasons. First, the magnetic field strength of solid implants was significantly higher due to the larger amount of magnetic material and improved magnetic particle spacing. Secondly, solid implants resulted in a decreased degradation rate due to the decreased surface area open to H₂O absorption. The drawback to solid implants is that it was shown that porous implants are predicted to result in higher von Mises stresses in the subchondral bone surrounding the implant. This would theoretically increase the rate of bone in-growth during implant degradation.

The optimum implant would be composed of SmCo₅ because of the higher implant chondrocyte/attraction distance, which should result in a more complete filling of a full thickness defect site with chondrocytes. The maximum separation distance for P(dl)A/PGA/Fe implants was 0.38 mm and for P(dl)A/PGA/SmCo₅ implants was 2.24 mm. However, for use in human models, where the cartilage thickness can range from 1-6 mm, it was determined that the chondrocyte particles would still have to be injected

into the defect site due to the minimal maximum attraction distances of both P(dl)A/PGA/Fe and P(dl)A/PGA/SmCo₅ implants.

The implants should be sterilized by EtO sterilization instead of H₂O₂ sterilization in order to minimize the amount of hydrolytic degradation before implantation. H₂O₂ sterilization of 50/50 P(dl)A/PGA polymers resulted in a 10% decrease in the molecular weight 14 days after sterilization, and EtO sterilization of 50/50 P(dl)A/PGA did not have a significant effect on the molecular weight. Thus, in order to optimize the properties of the implant at the time of implantation, EtO sterilization is the most appropriate sterilization method.

For cartilage defects less than 6 mm wide, the implants should span the entire defect site in order to optimize the magnetic field across the defect site. Neither single nor multiple implants resulted in a significant increase in the von Mises stress in the surrounding subchondral trabecular bone. In fact, the stress between multiple implants was decreased considerably and could possibly lead to resorption of that bone anyway. In any case implants under 6 mm in diameter and 6 mm long have been shown to only minimally increase the stress of the trabecular bone in the femoral condyle.

APPENDIX 1

AN *IN VIVO* STUDY OF THE BIOCOMPATIBILITY AND BIOREACTIVITY OF 50/50 P(dl)A/PGA/FE AND 75/25 P(dl)A/PGA/FE IMPLANTS USED AS DELIVERY DEVICES FOR MAGNETICALLY DIRECTED CHONDROGENESIS

ABSTRACT

Recent studies have evaluated the magnetic properties of P(dl)A/PGA/Fe implants as a magnetic delivery device for magnetically directed chondrogenesis (MDC). However, the biocompatibility of P(dl)A/PGA/Fe implants has not been evaluated. In this study, the biocompatibility of 75/25 and 50/50 P(dl)A/PGA/Fe implants were evaluated following implantation into the mid-portion of the trochlea in each knee of 2 New Zealand White (NZW) rabbits for 8 weeks. 50/50 and 75/25 implants showed a fibrous encapsulation that contained cellular activity. In the 75/25 implants, encapsulation was greatly reduced with less cellular response apparent in the implant region. In this pilot study, the immune response to both the 50/50 and 75/25 P(dl)A/PGA/Fe implants was minimal but before absolute biocompatibility can be determined more specific biocompatibility studies must be performed.

INTRODUCTION

The recent studies of magnetically directed chondrogenesis (MDC) as a cartilage regeneration technique capable of forming tissue with hyaline-like cartilage morphology has necessitated the development of biodegradable, biocompatible, magnets.^{1,2} Specifically, implants composed of P(dl)A/PGA copolymers combined with 1.9 μm Fe

particles have been shown to possess a sufficient magnetization to attract magnetically tagged chondrocytes *in vitro*. However, the biocompatibility of this type of implant is still not completely understood.

The biocompatibility of bioresorbable polyesters such as polylactic acid (PLA)³⁻⁹, polyglycolic acid (PGA)¹⁰⁻¹⁷ and their copolymers (PLA/PGA)¹⁸⁻²² have been studied extensively in the form of sutures, bone rods and bone screws. In general, little to no immune response was reported and bone formation adjacent to the implant occurred in as early as 3 weeks post-operative.^{3-7,11-13,18-20} However, PGA has shown a moderate foreign body reaction, in the form of bone rods that is characterized by macrophage and giant cell activity^{11,12} with numerous cases resulting in aseptic sinus formation.^{13,14} This immune response is contributed to the rapid degradation rate of the PGA polymer. PLA has also been found to produce a late foreign body reaction.⁹ In the case of PLA, this response consists primarily of giant cell, monocyte, and fibroblast cellular activity at the site of PLA implantation.

Fe is a readily available ferromagnetic material that is tolerated by the body and has a proven record of safety and biocompatibility.²³ Although, Fe is an essential mineral, at high doses it can be toxic. This has initiated biocompatibility studies of Fe particles resulting from implant wear.²⁴⁻²⁷ The biocompatibility of 55 μm steel particles was evaluated by Lucas et al.²⁴ Lucas et al. reported that 55 μm particles were too large to be transported systemically and resulted in an immune response that included a loss of ultrastructural organization of the surrounding cells that increased with particulate concentration.²⁴ In a study by Buchhorn et al., Fe particles with particle sizes ranging between 0.5 and 0.65 μm , subcutaneously injected into the back of rats. A mild

inflammatory response at the site of implantation was noted, along with a strong active absorption of the particles away from the implant site.²⁵ Thus, the size of Fe particles plays an important role in the biocompatibility and the resulting inflammatory response.

In this study, the biocompatibility of porous P(dl)A/PGA implants, containing 25 vol. % by volume of 1.9 μm Fe particles was evaluated. The MDC implants were implanted into the mid-portion of the trochlea of New Zealand White (NZW) rabbits. Biocompatibility was assessed at the implant site by histological examination of the surrounding trabecular bone, 8 weeks after implantation.

EXPERIMENTAL METHODS

MATERIALS

50/50 P(dl)A/PGA polymer and 75/25 P(dl)A/PGA polymer implants with 25 vol. % Fe and a target 50 vol. % porosity were prepared using the processing techniques described in Chapter 1. The implants were cylindrical, approximately 1.5mm in diameter and 5mm long. For each of the implants evaluated, the initial magnetic parameters and general material properties of the implants are given in Table 1.

Table 1: Physical properties of the implants used.

<i>Implant</i>	<i>Density (gm/cc)</i>	<i>Estimated Porosity</i>	<i>Field strength (emu)</i>	<i>Magnetic Susceptibility (emu/gm)</i>
50/50 Implant A	1.622	43%	9.928×10^{-3}	0.764
50/50 Implant B	1.534	46%	2.540×10^{-3}	0.110
75/25 Implant A	1.595	45%	1.608×10^{-3}	0.404
75/25 Implant B	1.242	44%	6.525×10^{-4}	0.423

Prior to implantation, the implants were placed in pouches, sterilized with ethylene oxide and aerated under a vacuum for 8 hours.

METHODS

Implantation

Under general anesthesia, the knee region was shaved, prepped and draped in a sterile fashion. A medial parapatellar incision was used to enter the knee joint and expose the distal femur and trochlea (patello/femoral joint). A drill fitted with a customized bit, sized approximately 0.01-0.05mm greater than the implant diameter, was used to create two defects in the mid-portion of the trochlea. One defect was approximately 1 cm distal to the superior joint margin and one defect was approximately 1 cm proximal to the superior joint margin. In this same fashion, a full thickness cartilage defect was generated that was approximately 3mm in diameter. The implant was then inserted using a polyethylene guide and tap. The implant was set flush with the subchondral bone/cartilage interface. The joint capsule, subcutaneous tissue and skin were then closed using 4-0 nylon sutures.

At 8 weeks post-operative, the animals were sacrificed by injection of Pentobarbital and the knees harvested for histologic evaluation.

Histological Preparation

Fixation

The knees were fixed by submerging the tissue into a buffered isotonic solution of 4% formaldehyde to avoid tissue digestion by enzymes or bacteria and to preserve the physical structure of the knee. Formaldehyde reacts with the amine groups (NH₂) in the tissue proteins which blocks the enzyme or bacteria attack. The knees were then

sectioned into cubic 2.54 cm blocks that encapsulated the implant site. The sectioned knees were stored frozen in this isotonic solution prior to subsequent tissue preparation. The tissue was then thawed and washed with tap H₂O for 3 hours prior to embedding.

Embedding

The tissue was next embedded. Embedding was broken down into 2 stages: dehydration and clearing. During dehydration, water in the tissue was replaced with an organic solvent by rinsing the tissue with increasing alcohol concentrations. Subjecting the tissue to continuously increasing alcohol concentrations then dehydrated the tissues. The joint was next rinsed with 70% ETOH for 6 hours, 95% ETOH overnight with agitation and then 3 rinses of 100% ETOH for 3-6 hours with the ETOH being replaced after each rinse. The second stage of embedding is clearing. During clearing, ethanol was replaced by a solvent miscible with the embedding medium (Paraffin). This was accomplished with 3 rinses of 100% methyl salicylate for 3-6 hours with the methyl salicylate being replaced after each rinse. The tissue was finally floated in melted paraffin at 60-65°C under an applied vacuum. The heat evaporated the solvent and the resulting vacant spaces then filled with liquid paraffin. The embedded tissues were then cooled to room temperature.

Sectioning/Staining

The embedded block containing the tissue sample was sectioned using an *Isomet* low speed bone saw. Tissue sections approximately 1-10µm in thickness were floated in warm H₂O and transferred onto glass slides for microscopic evaluation. The slides were

then stained by a combination of Hematoxylin and Eosin stains. Hematoxylin stains the cell nucleus and acidic structures blue, while eosin stains the cell cytoplasm red and stains collagen pink.

RESULTS

Figures 1 and 2 are the histological optical photomicrographs of the 50/50 P(dl)A/PGA/Fe implants after 8 weeks. Images in this dissertation are presented in color. The implant site is the hollow portion in the middle of both micrographs, marked A. The material that appears to be floating in the center of this hole (B) is believed to be what is left of the implant. Surrounding each of the implants is a thin fibrous encapsulation layer that is approximately 0.10-0.25 mm thick (C). The pores (D), surrounding the implant and outside of the implant encapsulation, is the marrow region.

A higher magnification of the marrow space and encapsulation are shown in Figures 3 and 4 respectively. The tissue in Figure 3 shows little evidence of an immune response. The marrow appears healthy with few areas, close to the implant, where marrow pores are filled with lymphocytes and lymph nodes. These lymphocytes are considered to be only a mild foreign body reaction. In Figure 4, the purple fibrous encapsulation appears to be filled with darker cells (marked A). These cells are similar to those found in the immune response of previous studies.^{6,30} Matlaga et al labeled these cells as macrophage and fibroblast cells.³⁰ Cutright et al. labeled these cells as plump fibroblasts, endothelial cells, and mononuclear phagocytes.⁶ Red blood vessels have also begun forming at the implant/bone interface (marker B).

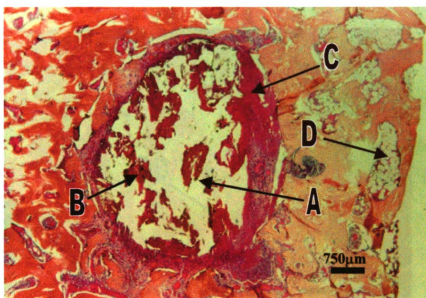


Figure 1 Cross-section of 50/50 P(dl)A/PGA/Fe Implant after 8 weeks. The implantation site (A) is filled with residual implant fragments (B) and surrounded with a fibrous encapsulation (C). The bone marrow regions (D) shows little evidence of an immune response , 25X

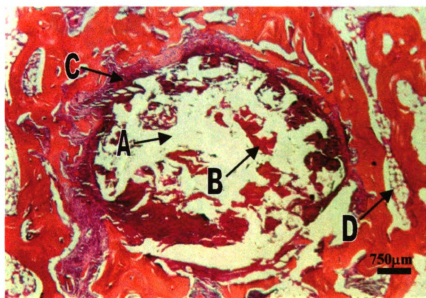


Figure 2 Cross-section of 50/50 P(dl)A/PGA/Fe Implant after 8 weeks. The implantation site (A) is filled with residual implant fragments (B) and surrounded with a fibrous encapsulation (C). The bone marrow regions (D) shows little evidence of an immune response, 25X

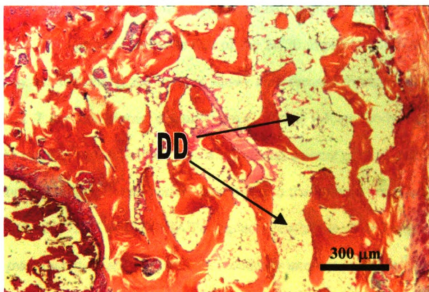


Figure 3 Histological micrograph of the marrow region (DD) surrounding the 50/50 P(dL)A/PGA/Fe implant 75X

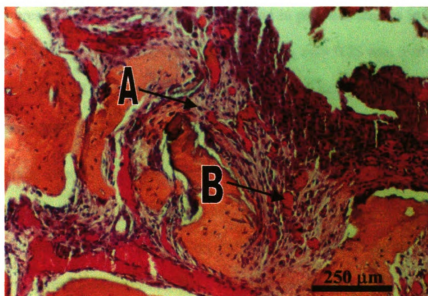


Figure 4 Histological micrograph of the fibrous encapsulation surrounding the 50/50 P(dl)A/PGA/Fe implant. The purple fibrous encapsulation is filled with osteocytes, osteoblasts and osteoclasts (A) as well as red blood vessels (B), 100X

Figure 5 is a histological photomicrograph of a 75/25 P(dl)A/PGA/Fe implant. Once again, the implant site (A) is filled with residual implant material (B). Fibrous encapsulation of the implant, similar to that of the 50/50 implant, is minimal. However, the marrow space, adjacent to the implant shows an increased foreign body activity (C). Figures 6 and 7 are the higher magnifications of this foreign body response to the implant. The marrow region is filled with a significant amount of dark cells (CC). These cells are lymphocytes and lymph nodes. Compared to the immune response of the 50/50 P(dl)A/PGA/Fe, the 75/25 P(dl)A/PGA/Fe implants resulted in more lymphocyte activity in the bone marrow region and borders on a secondary immune response.²⁹

DISCUSSION

The fibrous encapsulation or walling off of the implant to the surrounding bone, shown in Figures 1, 2 and 4, is similar to that found in previous studies involving PGA and PLA.^{6,12,19,30} However, this region is thin, extending only 0.25 mm from the implant surface. This indicated that the reaction is minimal and rated, 1 of 5 where 0 is no immune response and 5 is complete implant rejection.²⁹ Mäkelä et al. showed this type of encapsulation as early as 3 weeks after implanting pure PGA into NZW rabbits.¹¹ They found that at 4 weeks, this reaction increases considerably as pieces of PGA break away from the implant. The encapsulation is fibrous in nature as evidenced by its pink coloration of a collagen matrix, which indicated the presence of collagen fibers.²⁸ Blood vessels, scattered fibrocytes and macrophage cells were found in the fibrous encapsulation and in the areas immediately surrounding the implant. This is consistent with the findings of Mooney et al. who implanted porous PLGA and PLA sponges seeded

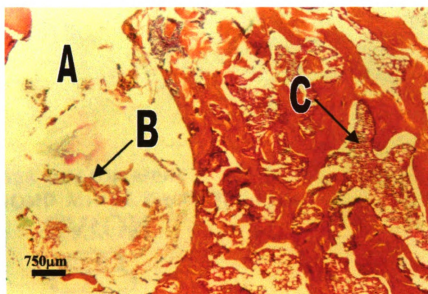


Figure 5 Cross section of 75/25 P(dl)A/PGA/Fe implant. The implantation site (A) is filled with residual implant fragments (B) The bone marrow regions (c) shows evidence of an immune response, 25X

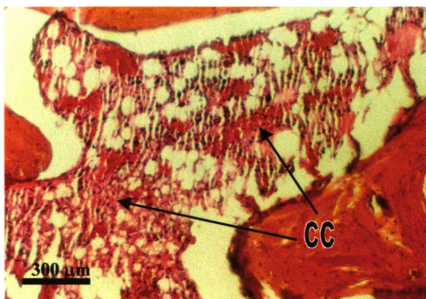


Figure 6 Histological micrograph of the marrow region surrounding the 75/25 P(dl)A/PGA/Fe implant, 75X

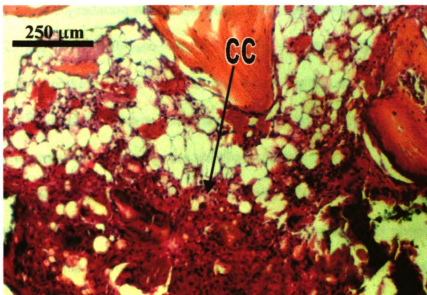


Figure 7 Histological micrograph of the marrow region surrounding the 75/25 P(dl)A/PGA/Fe implant showing lymphocyte activity (CC), 100X

with hepatocyte cells into Lewis rats.^{20,21} They reported fibrovascular tissue encapsulation and in-growth with composite tissue consisting of blood vessels and fibrous tissue. Capillaries from the host tissue grew into the newly formed tissue and resulted in the formation of an integrated tissue consisting of implanted cells and mesenchymal elements from the host tissue.²¹

In the 50/50 and 75/25 P(dl)A/PGA/Fe implants, no secondary immune response was noted since the surrounding marrow regions were not completely filled with foreign body cellular material. Some areas are partially full of lymphocytes and lymph nodes, which indicates an elevated immune response to the implants. However, the reaction is minimal near the implant site and is constrained to regions near the implant.

Comparing this slight immune response to the responses of previous studies shows an absence of macrophage and giant cell activity in both the 75/25 and 50/50 implants.¹²

The absence in macrophage and giant cell activity at 8 weeks post-operative is attributed to the more rapid degradation rate of the pure PGA used by Ruuskanen et al.¹² compared to the 75/25 and 50/50 polymers used in this study. Macrophage and giant cells are responsible for breaking down the PGA and exporting the material for disposal. The implants in this study, however, have not degraded to the point of disintegration so exporting and removal mechanisms are not apparent.

The encapsulation surrounding the implants was filled with dark spots. These spots are comparable to other studies that labeled them as fibroblast and phagocytes. Other notable artifacts of the 50/50 implants are the presence of red blood vessels supplying the area with osteocytes necessary for bone re-growth (Figure 4). In the 75/25 P(dl)A/PGA samples, shown in Figures 5, 6 and 7 there was less of a response adjacent to the implant, however the cellular response in the bone marrow region was more pronounced, bordering on a secondary foreign body reaction.

An immune response to the Fe is not apparent from these results. When 55 μm Fe particles are implanted into soft tissues, local cells have been reported to lose their ultra-structural organization.²⁴ Such cells are not readily apparent in these micrographs. The osteocytes, osteoblasts and osteoclast cells remain viable as indicated by the formation of the fibrous collagen encapsulation surrounding the implant. When smaller particles of Fe have been introduced, lymph nodes are created for storage and resorption of the particles.^{26,27} Even though lymphocytes and lymph nodes surround both the 50/50 and 75/25 P(dl)A/PGA implants, at 8 weeks the reaction is minimal. Thus, the 1.9 μm Fe particles used in this study gave the same tissue reaction as the 0.5-0.65 μm Fe used in previous studies^{26,27} and are probably are eliminated in the same fashion.

CONCLUSION

50/50 P(dl)A/PGA/Fe and 75/25 P(dl)A/PGA/Fe implants were placed into the subchondral bone of a NZW rabbit for 8 weeks. Histological analysis of both the 50/50 and 75/25 P(dl)A/PGA/Fe implants showed a fibrous encapsulation and lymph node formation at the interface between the bone and implant. However, the response was considered minor. The cellular activity in the encapsulation region of the 50/50 P(dl)A/PGA/Fe implants was significantly greater than the 75/25 implants. The 1.9 μm Fe particles indicated an immune response comparable to other studies that utilized 0.5-0.65 μm Fe particles.^{26,27} Based on this pilot study, 50/50 and 75/25 P(dl)A/PGA/Fe implants pose no obvious biocompatibility concerns. However, more specific biocompatibility studies need to be performed before an absolute biocompatibility can be determined.

REFERENCE:

1. Halpern, A.A., Crimp, M.J., and Grande, D., "The Use of Magnetically Tagged Chondrocytes for Repair of Cartilage Defects", *Trans. Ortho Res. Soc.*, **22**, 1997, 541.
2. Halpern, A.A., Crimp, M.J., Blowers, M.G., Lowsein, L.A., Huisepos, L.H., and McPherson, W.R., "Determination of Cellular Response to Intra-articular Placement of Neodymium and Samarium Cobalt Magnetic Implants in a Canine Model", *3rd Combined Meeting of Orthopedic Research Society of USA, Canada, Europe, & Japan*, Hamamatsu, Japan, Sept. 1998, 261.
3. Casteleyn, P.P., Handelberg, F., and Haentjens, P., "Biodegradable Rods Versus Kirshner Wire Fixation of Wrist Fractures. A randomized Trial", *J. Bone Jt. Surg.*, **74-B**, 1992, 858-861.
4. Barford, G. and Svendsen, R.N., "Synovitis of the Knee after Intra-articular Fracture Fixation with BioFix. Report of Two Cases", *Acta Ortho. Scand.*, **63**, 6, 1992, 680-681.

5. Frøkjaer, R.K. and Møller, B.N., "Biodegradable Fixation of Ankle Fractures. Complications in a Prospective Study of 25 Cases", *Acta Ortho. Scand.*, **63**, 4, 1992, 434-436.
6. Cutright, D.E., Beasley, J.D., and Perez, B., "Histologic Comparison of Polylactic and Polyglycolic Acid Sutures", *Oral Surg.*, **32**, 1971, 165-173.
7. Galgut, P., Pitrola, R., Waite, I., Doyle, C., and Smith, R., "Histological Evaluation of Biodegradable and Non-Degradable Membranes Placed Transcutaneously in Rats", *J. Clin. Periodontol.*, **18**, 1991, 581-586.
8. Gogolewski, S., "Resorbable Polymers for Internal Fixation", *Clin. Mater.*, **10**, 1992, 13-20.
9. Majola, A., Vainionpää, S., Vihtonen, K., Vasenius, J., Törmälä, P., and Rokkanen, P., "Intramedullary Fixation of Cortical Bone Osteotomies with Self-Reinforced Polylactic Rods in Rabbits", *Inter. Ortho.*, **16**, 1992, 101-108.
10. Vainionpää, S., "Biodegradation of Polyglycolic Acid in Bone Tissue: An Experimental Study on Rabbits", *Arch. Orthop. Trauma Surg.*, **104**, 1986, 333-338.
11. Mäkelä, E.A., Vainionpää, S., Vihtonen, K., Mero, M., Laiho, L., Törmälä, P., and Rokkanen, P., "Healing of Physeal Fracture after Fixation with Biodegradable Self-Reinforced Polyglycolic Acid Pins. An Experimental Study on Growing Rabbits", *Clin. Mater.*, **5**, 1990, 1-12.
12. Ruuskanen, M.M., Kallioinen, M.J., Kaarela, O.I., Laiho, J.A., Tormala, P.O., and Waris, T.J., "The Role of Polyglycolic Acid Rods in the Regeneration of Cartilage from Perichondrium in Rabbits", *Scand. J. Plast. Reconstr. Hand Surg.*, **25**, 1991, 15-18.
13. Böstman, O.M., "Intense Granulomatous Inflammatory Lesions Associated with Absorbable Internal Fixation Devices Made of Polyglycolide in Ankle Fractures", *Clin. Ortho. Rel. Res.*, **278**, 1992, 193-199.
14. Böstman, O., Hirvensalo, E., Makinen, J., and Rokkanen, P., "Foreign-Body Reactions to Fracture Fixation Implants of Biodegradable Synthetic Polymers", *J. Bone Jt. Surg.*, **72-B**, 1990, 592-596.
15. Matsusue, Y. and Yamamuro, T., "In-Vitro and In-Vivo Studies on Bioabsorbable Ultra-High-Strength Poly(L-lactic Acid) Rods", *J. Biomed. Mater. Res.*, **26**, 1992, 1553-1567.
16. Bos, R.R.M., Rozema, F.R., Boering, G., Nijenhuis, A.J., Pennings, A.J., Verwey, A.B., Nieuwenhuis, P., and Jansen, H.W.B., "Degradation of and Tissue Reaction to

- Biodegradable Poly(L-lactide) for use as Internal Fixation of Fractures: A study in Rats.”, *Biomaterials*, **12**, 1991, 32-36.
17. Lam, K.H., Schakenraad, J.M., Esselbrugge, H., Feijen, J., and Nieuwenhuis, P., “The Effect of Phagocytosis of Poly (L-lactic Acid) Fragments on Cellular Morphology and Viability”, *J. Biomed. Mater. Res.*, **27**, 1993, 1569-1576.
 18. Mikos, A.G., Sarakinos, G., Lyman, M.D., Ingber, D.E., Vacanti, J.P., and Langer, R., “Prevascularization of Porous biodegradable Polymers”, *Biotechnology and Bioengineering*, **42**, 1993, 716-723.
 19. Johnson, L.B., Aiken, J., Mooney, D., Schloo, B.L., Griffith, C.L., and Langer, R., “The Mesentery as a Laminated Vascular Bed for Hepatocyte”, *Transplantation, Cell transplant.*, **3**, 4, 1994, 273-281.
 20. Mooney, D.J., Park, S., Kaufmann, P.M., Sano, K., McNamara, K.M., Vacanti, J.P., and Langer, R., “Biodegradable Sponges For Hepatocyte Transplantation”, *J. Biomed. Mater. Res.*, **29**, 1995, 959-965.
 21. Mooney, D.J., Kaufmann, P.M., Sano, K., McNamara, K.M., Vacanti, J.P., and Langer, R., “Transplantation of Hepatocytes Using Porous Biodegradable Sponges”, *Transplantation Proceedings*, **26**, 6, 1994, 3425-3426.
 22. Vacanti, C.A., Langer, R., Schloo, B., and Vacanti, J.P., “Synthetic Polymers Seeded With Chondrocytes Provide a Template For New Cartilage Formation”, *Plastic and Reconstructive Surg.*, **88**, 5, 1991, 753-759.
 23. Park, J.B. and Lakes, R.S., Biomaterials: An Introduction, Plenum Press, New York, 1992.
 24. Lucas, L.C., Bearden, L.J., and Lemons, J.E., “Ultrastructure Examination of *In Vitro* and *In Vivo* Cells Exposed to Elements from Type 316L Stainless Steel”, Corrosion and Degradation of Implant Materials: Second Symposium, ASTM STP 859, A.C. Fraker and C.D. Griffin, Eds., American Society for Testing and Materials, Philadelphia, 1985, 208-222.
 25. Buchhorn, G.H., Willert, H.G., Semlitsch, M., Schoen, R., Steinemann, S., and Schmidt, M., “Preparation, Characterization, and Animal Testing of Iron-, Cobalt-, and Titanium-Based Implant Alloys.”, Particulate Debris from Metal Implants: Mechanism of Formation and Biological Consequences, ASTM STP 1144, K.R. St. John. Ed., American Society for Testing and Materials, Philadelphia, 1992, pp. 177-188.
 26. Agins, H.J., Alcock, N.W., Bansal, M., Salvati, E.A., Wilson, P.D., Pellicci, P.M., and Bullough, P.G., “Metallic Wear in Failed Titanium-Alloy Total Hip Replacements”, *J. Bone Jt. Surg.*, **70-A**, 3, 1988, 347-356.

27. Lombardi, A.V., Mallory, T.H., Vaughn, B.K., and Drouillard, P., "Aseptic Loosening in Total Hip Arthroplasty Secondary to Osteolysis Induced by Wear Debris from Titanium-Alloy Modular Femoral Heads", *J. Bone Jt. Surg.*, **71-A**, 9, 1989, 1337-1342.
28. Junqueira, L.C., Carneiro, J., and Kelley, R.O., Basic Histology, Appleton and Lange, Stanford, 1-19, 1995.
29. Personal Communication: Dr. C.D. Mackenzie
30. Matlaga, B.F., Yasenchak, L.P., Salthouse, T.N., "Tissue Response to Implanted Polymers: The Significance of Sample Shape", *J. Biomed. Mater. Res.*, **10**, 1976, 391-397.

APPENDIX 2

POROSITY DETERMINATION:

ID	Dia.	Length	Volume					Archimedes	Measured	Measured
Poly-Vol-Per-#	(mm)	(mm)	(mm ³)	D	S	M	V	Porosity	Density(gm/cc)	Porosity
75-25-50-1	1.7	7.07	16.03	0.023	0.01	0.037	0.027		1.43397283	49.14989964
								51.8518519		
75-25-50-2	1.62	7.18	14.79191	0.022	0.014	0.032	0.018	55.5555556	1.487299907	47.25886855
75-25-50-3	1.56	6.5	12.4174	0.015	0.006	0.024	0.018	50	1.207978067	57.16389833
75-25-50-4	1.85	6.65	17.86631	0.02	0.008	0.035	0.027	55.5555556	1.119425606	60.30405653
75-25-50-5	1.67	6.64	14.53686	0.016	0.01	0.025	0.015	60	1.100650168	60.9698522
75-25-50-6	1.6	6.42	12.90163	0.015	0.008	0.023	0.015	53.3333333	1.16264361	58.7715032
75-25-50-7	1.7	6.17	13.99757	0.017	0.007	0.029	0.022	54.5454545	1.214496473	56.93274919
75-25-50-8	1.65	6.35	13.57098	0.017	0.01	0.025	0.015	53.3333333	1.25267281	55.57897837
75-25-50-9	1.73	7.06	16.58695	0.02	0.01	0.031	0.021	52.3809524	1.205767105	57.24230123
75-25-50-10	1.85	7.26	19.50517	0.022	0.01	0.036	0.026	53.8461538	1.127906103	60.00332968
75-25-50-11	1.65	6.62	14.14802	0.02	0.013	0.029	0.016	56.25	1.413625794	49.87142574
50-25-50-1	1.93	7.37	21.55022	0.025	0.009	0.041	0.032	50	1.160080819	58.86238231
50-25-50-2	2.05	7.41	24.44531	0.028	0.009	0.049	0.04	52.5	1.145413888	59.38248625
50-25-50-3	1.65	4.55	9.724089	0.012	0.006	0.018	0.012	50	1.234048715	56.23940726
50-25-50-4	1.66	7.49	16.20196	0.026	0.012	0.043	0.031	54.8387097	1.604743767	43.09419267
50-25-50-5	1.61	6.08	12.37157	0.015	0.006	0.024	0.018	50	1.212456793	57.00507827
50-25-50-6	1.62	7.5	15.45116	0.021	0.015	0.03	0.015	60	1.359121697	51.80419515
50-25-50-7	1.67	4.5	9.851789	0.012	0.006	0.02	0.014	57.1428571	1.218052853	56.80663643
50-25-50-8	1.75	7.2	17.30925	0.02	0.01	0.03	0.02	50	1.155451565	59.02654025
50-25-50-9	1.75	5	12.02031	0.017	0.01	0.026	0.016	56.25	1.414272715	49.84848527
50-25-50-10	1.84	6.75	17.93945	0.027	0.019	0.04	0.021	61.9047619	1.505063032	46.6289705
50-25-50-11	1.62	6.61	13.61762	0.018	0.007	0.029	0.022	50	1.321817081	53.12705385
65-25-50-1	2.52	6.78	33.79873	0.038	0.012	0.059	0.047	44.6808511	1.124302469	60.13111812
65-25-50-2	1.9	6.18	17.51319	0.024	0.008	0.048	0.04	60	1.37039545	51.40441667
65-25-50-3	1.84	6.75	17.93945	0.025	0.02	0.034	0.014	64.2857143	1.393576882	50.58238009
65-25-50-4	2.28	7.42	30.27912	0.033	0.011	0.049	0.038	42.1052632	1.089859926	61.3524849
65-25-50-5	1.28	5.2	6.687949	0.011	0.004	0.03	0.026	73.0769231	1.644749433	41.675552
85-25-50-1	1.96	4.88	14.7164	0.017	0.007	0.027	0.02	50	1.155173719	59.03639294
85-25-50-2	1.94	5.32	15.71755	0.018	0.005	0.032	0.027	51.8518519	1.145216921	59.38947089
85-25-50-3	1.67	5.43	11.88783	0.014	0.01	0.024	0.014	71.4285714	1.17767541	58.23846064
85-25-50-4	1.87	6.03	16.55275	0.025	0.018	0.035	0.017	58.8235294	1.510322967	46.44244797
85-25-50-5	1.47	4.69	7.955677	0.013	0.003	0.027	0.024	58.3333333	1.634053168	42.05485219
85-25-50-6	1.76	6.93	16.8511	0.018	0.006	0.032	0.026	53.8461538	1.068179596	62.12129091
85-25-50-7	1.91	6.6	18.90081	0.023	0.007	0.038	0.031	48.3870968	1.216879316	56.8482512
65-25s-50-1	1.76	6.47	15.73256	0.019	0.006	0.033	0.027	51.8518519	1.207686823	57.17422612
65-25s-50-2	1.65	6.93	14.81054	0.016	0.009	0.026	0.017	58.8235294	1.080312007	61.6910636
65-25s-50-3	1.56	6.98	13.33442	0.015	0.009	0.025	0.016	62.5	1.124907942	60.10964745
65-25s-50-4	1.72	6.78	15.74549	0.017	0.011	0.031	0.02	70	1.079674084	61.71368496
65-25s-50-5	2.15	5.52	20.03022	0.02	0.008	0.035	0.027	55.5555556	0.998491429	64.59250251
65-25s-50-6	1.8	6.74	17.14252	0.021	0.012	0.03	0.018	50	1.225024378	56.55941922
85-25s-50-1	1.65	6.5	13.89156	0.02	0.007	0.039	0.032	59.375	1.439723501	48.94597514

85-25s-50-2	2.13	7.09	25.2508	0.028	0.018	0.042	0.024	58.3333333	1.108875869	60.67816068
85-25s-50-3	1.81	6.47	16.63915	0.02	0.012	0.028	0.016	50	1.201984614	57.37643213
85-25s-50-4	1.61	6.03	12.26983	0.015	0.007	0.024	0.017	52.9411765	1.222510332	56.6485698
85-25s-50-5	1.76	6.24	15.17328	0.019	0.009	0.029	0.02	50	1.252200921	55.59571202
85-25s-50-6	1.67	5.89	12.8949	0.017	0.013	0.023	0.01	60	1.318350923	53.24996727
85-25s-50-7	1.77	6.74	16.57586	0.021	0.012	0.031	0.019	52.6315789	1.266902545	55.07437782
65-40-50-1	1.47	6.5	11.02599	0.018	0.011	0.028	0.017	58.8235294	1.632506136	42.1097115
65-40-50-2	1.58	6.09	11.93441	0.025	0.019	0.035	0.016	62.5	2.094782251	25.71694147
65-40-50-3	1.65	4.33	9.253914	0.015	0.007	0.023	0.016	50	1.620935812	42.52000665
65-40-50-4	1.56	6.14	11.72971	0.021	0.014	0.029	0.015	53.3333333	1.7903258	36.51326952
65-40-50-5	1.9	6.88	19.49689	0.034	0.025	0.045	0.02	55	1.743868047	38.16070755
65-40-50-6	1.68	4.71	10.4354	0.017	0.012	0.025	0.013	61.5384615	1.62907018	42.2315539
65-30-50-1	2.43	6.23	28.87821	0.032	0.012	0.055	0.043	53.4883721	1.108101972	60.70560383
65-30-50-2	1.95	7.5	22.38722	0.025	0.017	0.033	0.016	50	1.116708613	60.40040379
65-30-50-3	1.54	6.32	11.76598	0.016	0.011	0.024	0.013	61.5384615	1.359852506	51.77827993
65-30-50-4	1.9	6.18	17.51319	0.023	0.008	0.039	0.031	51.6129032	1.313295639	53.42923264
65-30-50-5	2.5	6.42	31.49813	0.032	0.019	0.048	0.029	55.1724138	1.015933488	63.97398978
65-30-50-6	1.87	7.28	19.98408	0.024	0.013	0.037	0.024	54.1666667	1.200955713	57.41291797
65-20-50-1	1.75	5.88	14.13589	0.015	0.006	0.026	0.02	55	1.061128988	62.37131248
65-20-50-2	1.81	6.68	17.17921	0.019	0.012	0.027	0.015	53.3333333	1.105987789	60.78057486
65-20-50-3	1.61	6.75	13.73489	0.02	0.014	0.027	0.013	53.8461538	1.456145639	48.36362981
65-20-50-4	1.54	6.5	12.10109	0.014	0.004	0.026	0.022	54.5454545	1.156920671	58.97444431
65-20-50-5	1.24	6.78	8.183568	0.011	0.004	0.02	0.016	56.25	1.344156895	52.33486187
65-20-50-6	1.54	7.11	13.23673	0.018	0.009	0.028	0.019	52.6315789	1.359852506	51.77827993
65-20-50-7	1.67	6.36	13.92386	0.017	0.007	0.029	0.022	54.5454545	1.220925619	56.70476529
65-20-50-8	1.72	6.78	15.74549	0.019	0.01	0.031	0.021	57.1428571	1.206694565	57.2094126
65-10-50-1	1.72	6.55	15.21135	0.016	0.01	0.026	0.016	62.5	1.051845933	62.70049883
65-10-50-2	2.24	5.21	20.52123	0.022	0.009	0.034	0.025	48	1.072060424	61.9836729
65-10-50-3	2.08	5.61	19.05282	0.015	0.005	0.026	0.021	52.3809524	0.787285171	72.08208615
65-10-50-4	1.38	6.24	9.328513	0.008	0.0011	0.015	0.0139	50.3597122	0.857585773	69.58915698
65-10-50-5	1.6	6.62	13.30355	0.011	0.003	0.02	0.017	52.9411765	0.826846845	70.67918989
65-10-50-6	<u>1.94</u>	<u>7.18</u>	<u>21.21278</u>	<u>0.014</u>	<u>0.005</u>	<u>0.025</u>	<u>0.02</u>	<u>55</u>	<u>0.659979544</u>	<u>76.59647007</u>
Average								55.1201459		55.35424825
St.Dev.:								5.52197979		8.39915328

INITIAL POLYMER MAGNETIZATION:

50/50 P(dI)/PGA 25 Volume % Fe 50% porosity:		65/35 P(dI)/PGA 25 Volume % Fe 50% porosity:	
Pole Strength(emu/mm)	Volume Susceptibility(H/m)	Pole Strength(emu/mm)	Volume Susceptibility(H/m)
0.0002288	1.15114E-06	0.0001737	8.73919E-07
0.0002966	1.49225E-06	0.00007	3.52184E-07
0.000314	1.5798E-06	0.0003081	1.55011E-06
0.0001003	5.04629E-07	0.000169	8.50273E-07
<u>0.0001117</u>	<u>5.61985E-07</u>	<u>0.0001896</u>	<u>9.53916E-07</u>
Average: 0.00021028	1.05796E-06	0.00018208	9.16081E-07

St. Dev.:	0.000100456	5.05414E-07	8.47656E-05	4.26473E-07
-----------	-------------	-------------	-------------	-------------

	75/25 P(dI)/PGA		85/15 P(dI)/PGA	
	25 Volume % Fe		25 Volume % Fe	
	50% porosity:		50% porosity:	
	<u>Pole Strength(emu/mm)</u>	<u>Volume Susceptibility(H/m)</u>	<u>Pole Strength(emu/mm)</u>	<u>Volume Susceptibility(H/m)</u>
	0.0002031	1.02184E-06	0.0001218	6.128E-07
	0.0002373	1.1939E-06	0.0001184	5.95694E-07
	0.0000911	4.58342E-07	0.0001142	5.74563E-07
	0.0001408	7.08393E-07	0.00008161	4.10596E-07
	<u>0.0000866</u>	<u>4.35702E-07</u>	<u>0.0000678</u>	<u>3.41115E-07</u>
Average:	0.00015178	7.63638E-07	0.000100762	5.06954E-07
St. Dev.:	6.70792E-05	3.37489E-07	2.44314E-05	1.22919E-07

POROUS 65/35/FE INITIAL MAGNETIC DATA:

	65/35 P(dI)/PGA		65/35 P(dI)/PGA	
	10 Volume % Fe		20 Volume % Fe	
	50% porosity:		50% porosity:	
	<u>Pole Strength(emu/mm)</u>	<u>Volume Susceptibility(H/m)</u>	<u>Pole Strength(emu/mm)</u>	<u>Volume Susceptibility(H/m)</u>
	0.0001885	9.48381E-07	0.0001737	8.73919E-07
	0.00008107	4.07879E-07	0.00007006	3.52486E-07
	0.00002141	1.07718E-07	0.0003081	1.55011E-06
	0.0000775	3.89918E-07	0.000169	8.50273E-07
	<u>0.0001075</u>	<u>5.40854E-07</u>	<u>0.0001896</u>	<u>9.53916E-07</u>
Average:	0.000095196	4.7895E-07	0.000182092	9.16141E-07
St. Dev.:	6.08566E-05	3.06182E-07	8.47458E-05	4.26373E-07

	65/35 P(dI)/PGA		65/35 P(dI)/PGA	
	30 Volume % Fe		40 Volume % Fe	
	50% porosity:		50% porosity:	
	<u>Pole Strength(emu/mm)</u>	<u>Volume Susceptibility(H/m)</u>	<u>Pole Strength(emu/mm)</u>	<u>Volume Susceptibility(H/m)</u>
	0.00040011	2.01303E-06	0.0003397	1.7091E-06
	0.0003016	1.51741E-06	0.000585	2.94325E-06
	0.0002908	1.46307E-06	0.0003676	1.84947E-06
	0.0003375	1.69803E-06	0.0003622	1.8223E-06
	<u>0.0002675</u>	<u>1.34585E-06</u>	<u>0.0003547</u>	<u>1.78457E-06</u>
Average:	0.000319502	1.60748E-06	0.00040184	2.02174E-06
St. Dev.:	5.1648E-05	2.59852E-07	0.000102926	5.1784E-07

SOLID 65/35/FE INITIAL MAGNETIC DATA:

65/35 P(dl)/PGA 12.5 Volume % Fe 0% porosity:		65/35 P(dl)/PGA 25 Volume % Fe 0% porosity:	
<u>Pole Strength(emu/mm)</u>	<u>Volume Susceptibility(H/m)</u>	<u>Pole Strength(emu/mm)</u>	<u>Volume Susceptibility(H/m)</u>
0.00026	1.30811E-06	0.000503	2.53069E-06
0.000315	1.58483E-06	0.000506	2.54579E-06
0.000375	1.8867E-06	0.000492	2.47535E-06
0.000339	1.70558E-06	0.000503	2.53069E-06
<u>0.000324</u>	<u>1.63011E-06</u>	<u>0.000597</u>	<u>3.00363E-06</u>
Average: 0.0003226	1.62307E-06	0.0005202	2.61723E-06
St. Dev.: 4.18127E-05	2.10368E-07	4.32631E-05	2.17666E-07

65/35 P(dl)/PGA 30 Volume % Fe 0% porosity:		65/35 P(dl)/PGA 35 Volume % Fe 0% porosity:	
<u>Pole Strength(emu/mm)</u>	<u>Volume Susceptibility(H/m)</u>	<u>Pole Strength(emu/mm)</u>	<u>Volume Susceptibility(H/m)</u>
0.000754	3.79352E-06	0.000729	3.66774E-06
0.000482	2.42504E-06	0.000778	3.91427E-06
0.000739	3.71806E-06	0.000731	3.67781E-06
0.000568	2.85772E-06	0.000817	4.11049E-06
<u>0.000476</u>	<u>2.39485E-06</u>	<u>0.00043</u>	<u>2.16342E-06</u>
Average: 0.0006038	3.03784E-06	0.000697	3.50675E-06
St. Dev.: 0.00013536	6.81021E-07	0.000153647	7.7303E-07

65/35 P(dl)/PGA 40 Volume % Fe 0% porosity:		65/35 P(dl)/PGA 45 Volume % Fe 0% porosity:	
<u>Pole Strength(emu/mm)</u>	<u>Volume Susceptibility(H/m)</u>	<u>Pole Strength(emu/mm)</u>	<u>Volume Susceptibility(H/m)</u>
0.000829	4.17086E-06	0.000882	4.43752E-06
0.00071	3.57215E-06	0.000873	4.39224E-06
0.000559	2.81244E-06	0.001057	5.31798E-06
0.000722	3.63253E-06	0.000835	4.20105E-06
<u>0.001019</u>	<u>5.12679E-06</u>	<u>0.000675</u>	<u>3.39606E-06</u>
Average: 0.0007678	3.86296E-06	0.0008644	4.34897E-06
St. Dev.: 0.000170208	8.5635E-07	0.000136212	6.85311E-07

SmCo₅ INTITAL MAGNETIC DATA:

65/35 P(dI)/PGA		85/15 P(dI)/PGA	
25 Volume % SmCo₅		25 Volume % SmCo₅	
50% porosity:		50% porosity:	
<u>Pole Strength(emu/mm)</u>	<u>Volume Susceptibiliy(H/m)</u>	<u>Pole Strength(emu/mm)</u>	<u>Volume Susceptibiliy(H/m)</u>
0.02629	0.00013227	0.021166	0.00010649
0.037619	0.000189269	0.013707	6.89627E-05
0.039814	0.000200312	0.017083	8.5948E-05
0.027319	0.000137447	0.023078	0.00011611
<u>0.029056</u>	<u>0.000146187</u>	<u>0.029976</u>	<u>0.000150815</u>
Average	0.0320196	0.021002	0.000105665
St. Dev.	0.006241251	0.006193645	3.11615E-05

65/35 P(dI)/PGA		85/15 P(dI)/PGA	
50 Volume % SmCo₅		50 Volume % SmCo₅	
0% porosity:		0% porosity:	
<u>Pole Strength(emu/mm)</u>	<u>Volume Susceptibiliy(H/m)</u>	<u>Pole Strength(emu/mm)</u>	<u>Volume Susceptibiliy(H/m)</u>
0.159749	0.000803729	0.182766	0.000919532
0.182627	0.000918833	0.104476	0.00052564
0.154795	0.000778805	0.143092	0.000719924
0.175575	0.000883353	0.168229	0.000846394
<u>0.196047</u>	<u>0.000986352</u>	<u>0.177053</u>	<u>0.000890789</u>
Average	0.1737586	0.1551232	0.000780456
St. Dev.	0.016841969	0.032119664	0.0001616

COMPRESSIVE STRENGTH DATA:

Ultimate Yield Stress (MPa)		Elastic Modulus (MPa)	
50/50 P(dI)A/PGA		50/50 P(dI)A/PGA	
<u>0% porosity</u>		<u>0% porosity</u>	
	43.8		3637
	50.72		2899
	46.08		3987
	49.41		3594
	<u>50.35</u>		<u>3330</u>
Average:	48.072		3489.4
St. Dev.:	3.008715673		404.4481425

Ultimate Yield Stress (MPa)		Elastic Modulus (MPa)	
50/50 P(dI)A/PGA		50/50 P(dI)A/PGA	
<u>50% porosity</u>		<u>50% porosity</u>	
	10.02		133.56
	7.48		72.8
	6.84		84.08
	8.23		118.48
	<u>8.48</u>		<u>110.95</u>
Average:	8.21		103.974
St. Dev.:	1.199916664		25.01004558

ID	Dis.	Lth.	Initial Mag.	Pole Strength	Mag. 1 week	Pole Strength	% Mag remain.	Mag. 2 weeks	Pole Strength	% Mag remain.	Mag. 4 week	Pole Strength	% Mag remain.	Mag. 6 week	Pole Strength	% Mag remain.	Mag. 8 week	Pole Strength
75-25-50-1	1.65	6.35	0.00129	0.0002	0.00103	0.00018	0.80326	-0.001	0.00015	0.75548	-0.0007	0.00012	0.57305	-0.0008	9.4E-05	0.43085	-0.0005	8.2E-05
75-25-50-2	1.7	5.84	0.00139	0.00024	0.00103	0.00018	0.74212	0.00089	0.00015	0.64246	0.00072	0.00012	0.51896	0.0006	0.0001	0.43085	0.00052	8.9E-05
75-25-50-3	1.67	5.84	0.00053	9.1E-05	0.0005	8.6E-05	0.94742	0.00045	7.6E-05	0.83853	0.00032	5.4E-05	0.59412	0.00035	5.9E-05	0.65173	0.00031	5.3E-05
75-25-50-4	1.75	6.95	-0.001	0.00014	-0.0008	0.00014	0.78265	-0.0006	9.1E-05	0.64925	-0.0005	7.1E-05	0.50283	-0.0004	5.7E-05	0.40412	-0.0004	5.1E-05
75-25-50-5	1.79	6.17	-0.0005	8.7E-05	-0.0005	8.3E-05	0.95445	-0.0004	7.2E-05	0.83488	-0.0003	5.5E-05	0.57293	-0.0003	4.4E-05	0.51025	-0.0002	3.8E-05
Average:			0.00015	0.00012	0.00012	0.846	0.744		1E-04	0.744		8E-05	0.584		7E-05	0.492		6E-05
St. Dev.:			6.7E-05	4.3E-05	0.0963	4.1E-05	0.09567		3.5E-05	0.04018		3.5E-05	0.1067		3.3E-05	0.07226		2.2E-05
50-25-50-1	1.65	4.55	0.00104	0.00023	0.00069	0.00015	0.69572	0.00039	8.6E-05	0.37641	0.00024	5.2E-05	0.22713	0.0002	4.4E-05	0.191	0.00018	3.9E-05
50-25-50-2	1.66	7.49	0.00222	0.0003	0.00181	0.00024	0.81305	0.00143	0.00019	0.64393	0.00111	0.00015	0.50164	0.00078	0.0001	0.35285	0.00065	8.7E-05
50-25-50-3	1.62	7.5	0.00235	0.00031	0.00186	0.00025	0.79158	0.00146	0.00019	0.61816	0.00083	0.00011	0.35239	0.00044	5.9E-05	0.1881	0.00036	4.7E-05
50-25-50-4	1.87	4.5	0.00045	0.0001	0.00037	8.2E-05	0.81528	0.00017	3.8E-05	0.37815	0.00012	2.6E-05	0.25873	8.7E-05	1.9E-05	0.19171	6.1E-05	1.4E-05
50-25-50-5	1.75	5	0.00056	0.00011	0.00035	7E-05	0.62689	0.00025	5E-05	0.45091	0.00018	3.7E-05	0.33101	0.00015	3E-05	0.26718	0.00012	2.3E-05
Average:			0.00021	0.00016	0.00016	0.7425	0.49351		0.00011	0.49351		7.5E-05	0.33418		3.1E-05	0.23817		4.2E-05
St. Dev.:			0.0001	8.5E-05	0.08637	7.6E-05	0.12642		5.3E-05	0.1067		5.3E-05	0.1067		3.3E-05	0.07226		2.8E-05
85-25-50-1	1.93	5.1	-0.0006	0.00012	0.00058	0.00011	0.93893	0.0005	9.9E-05	0.80998	0.00038	7.4E-05	0.60528	0.00031	6E-05	0.49308	0.00028	5.4E-05
85-25-50-2	2.07	5.71	0.00068	0.00012	0.00062	0.00011	0.92248	0.00051	8.9E-05	0.75351	0.00031	5.4E-05	0.45747	0.00027	4.8E-05	0.40498	0.00025	4.4E-05
85-25-50-3	1.47	4.69	-0.0005	0.00011	-0.0005	9.9E-05	0.86806	-0.0004	7.7E-05	0.67134	-0.0002	5E-05	0.4405	-0.0002	4.9E-05	0.42993	-0.0002	4.7E-05
85-25-50-4	1.76	6.93	0.00057	8.2E-05	0.0004	6.2E-05	0.75393	-0.0003	5E-05	0.61073	-0.0003	4.3E-05	0.61131	-0.0003	2.9E-05	0.51894	-0.0003	3.9E-05
85-25-50-5	1.91	6.6	-0.0004	6.8E-05	-0.0004	5.3E-05	0.78172	-0.0003	4.3E-05	0.64066	-0.0003	4.3E-05	0.63992	-0.0002	2.9E-05	0.43191	-0.0001	1.6E-05
Average:			0.0001	8.7E-05	0.08303	7.2E-05	0.69724		5.4E-05	0.5507		5.4E-05	0.5507		4.6E-05	0.45576		4E-05
St. Dev.:			2.4E-05	2.8E-05	0.08266	2.4E-05	0.08251		1.2E-05	0.0939		1.2E-05	0.0939		1.1E-05	0.04796		1.4E-05
85-259-50-1	2.24	7.34	0.15536	0.02117	0.11681	0.01591	0.76187	0.10078	0.01373	0.64869	0.08229	0.01121	0.52965	-0.0619	0.00844	0.39855	-0.0647	0.00882
85-259-50-2	1.77	4.5	-0.0617	0.01371	-0.0606	0.01124	0.82018	-0.0477	0.0106	0.77323	-0.0438	0.00974	0.71046	0.0761	0.01691	1.23366	0.07034	0.01563
85-259-50-3	1.82	6.85	-0.117	0.01708	-0.0914	0.01335	0.78125	-0.0804	0.01173	0.68687	-0.0677	0.00889	0.57878	-0.0619	0.00904	0.52912	-0.0577	0.00842
85-259-50-4	1.98	6.17	-0.1424	0.02308	-0.0925	0.01499	0.64969	-0.0828	0.01341	0.58127	-0.0755	0.01224	0.5302	-0.1084	0.01767	0.76128	-0.1012	0.0164
85-259-50-5	1.8	6.74	-0.202	0.02998	-0.1584	0.0235	0.78385	-0.138	0.02048	0.68318	-0.1178	0.01748	0.58305	-0.0402	0.00596	0.19895	-0.0389	0.00547
Average:			0.021	0.021	0.1584	0.016	0.757		0.014	0.676		0.012	0.586		0.012	0.624		0.011
St. Dev.:			0.00619	0.00468	0.09489	0.00384	0.09652		0.00317	0.07369		0.00317	0.07369		0.0053	0.39719		0.00481
65-259-50-1	2.07	5.28	0.13884	0.0263	0.1121	0.02123	0.8074	0.10721	0.0203	0.77218	0.09805	0.01819	0.69177	0.0863	0.01672	0.63601	0.08664	0.01641
65-259-50-2	1.8	7.5	0.28214	0.03762	0.25985	0.03465	0.921	0.22128	0.0295	0.78429	0.16965	0.02089	0.55522	0.12951	0.01727	0.45903	0.11607	0.01548
65-259-50-3	1.77	6.66	-0.2652	0.03981	-0.1656	0.02487	0.82457	-0.1361	0.02044	0.51343	-0.1029	0.01545	0.38795	-0.0915	0.01374	0.34503	-0.0968	0.01454
65-259-50-4	1.77	6.26	0.17102	0.02732	0.11448	0.01829	0.6694	0.09231	0.01475	0.53976	0.07866	0.01225	0.44924	0.08731	0.01075	0.3936	0.06394	0.01021
65-259-50-5	1.73	6.93	0.20136	0.02906	0.12824	0.01851	0.63687	0.10779	0.01555	0.53531	0.08848	0.01277	0.4394	0.08241	0.01189	0.40927	0.07852	0.01133
Average:			0.032	0.032	0.12824	0.024	0.732		0.02	0.629		0.016	0.566		0.014	0.448		0.014
St. Dev.:			0.00624	0.00624	0.00677	0.00587	0.12637		0.00587	0.13667		0.00366	0.12107		0.00288	0.11239		0.00289
65-40-50-1	1.65	6.78	-0.0023	0.00034	-0.002	0.00029	0.84789	-0.0019	0.00028	0.82552	-0.0017	0.00025	0.74371	-0.0016	0.00023	0.68948	-0.0014	0.00021
65-40-50-2	1.75	7.42	-0.0043	0.00059	-0.0042	0.00056	0.95695	-0.0032	0.00043	0.74352	-0.0029	0.00039	0.67035	-0.0027	0.00038	0.61986	-0.0023	0.00031
65-40-50-3	1.67	5.1	0.00187	0.00037	0.00172	0.00034	0.91496	0.00149	0.00032	0.87817	0.00151	0.0003	0.80482	0.0014	0.00027	0.74504	0.00119	0.00023
65-40-50-4	1.67	4.57	-0.0017	0.00036	-0.0013	0.00028	0.77586	-0.0012	0.00025	0.70222	-0.0009	0.00019	0.51676	-0.0007	0.00016	0.44064	-0.0006	0.00014
65-40-50-5	2.38	5	0.00177	0.00035	0.00133	0.00027	0.75273	0.00121	0.00024	0.68073	0.00097	0.00019	0.54436	0.00084	0.00017	0.4745	0.00077	0.00015
Average:			0.00012	3E-04	0.00012	3E-04	0.766		7.8E-05	0.06362		3E-04	0.066		2E-04	0.594		2E-04
St. Dev.:			0.00012	0.00012	0.00012	0.00012	0.08749		7.8E-05	0.06362		8.4E-05	0.12434		8.3E-05	0.13266		6.8E-05

ID	Pole Strength	Max Attract. Distance	Mag. 1 week	Max Attract. Distance	Mag. 2 weeks	Max Attract. Distance	Mag. 4 weeks	Max Attract. Distance	Mag. 6 weeks	Max Attract. Distance	Mag. 8 weeks	Max Attract. Distance	Mag. 10 weeks				
65-30-50-1	1.95	7.5	-0.003	0.0004	-0.0025	0.00033	-0.0023	0.0003	0.75302	-0.0021	0.00027	0.68291	-0.0017	0.00022	0.55978	-0.0015	0.0002
65-30-50-2	1.54	6.32	0.00191	0.0003	0.00153	0.00024	0.80339	0.00118	0.82068	0.00092	0.00014	0.48036	0.00074	0.00012	0.38717	0.00062	9.8E-05
65-30-50-3	1.72	6.31	0.00189	0.0003	0.00153	0.00024	0.81032	0.00117	0.81684	0.00091	0.00014	0.48239	0.00072	0.00011	0.38717	0.00062	9.8E-05
65-30-50-4	2.5	6.42	0.00187	0.00029	0.00143	0.00022	0.76741	0.00124	0.86651	0.00105	0.00016	0.58191	0.00093	0.00013	0.49695	0.00085	0.00013
65-30-50-5	1.79	7.22	0.00244	0.00034	0.00187	0.00026	0.75847	-0.0013	0.54097	0.00127	0.00018	0.52332	0.00128	0.00018	0.52434	0.00117	0.00016
Average:			3E-04	5E-05	4.9E-05	0.03146	0.797	5.7E-05	0.84	0.84	5.8E-05	0.846	0.47	2E-04	0.47	4.1E-05	4.1E-05
St. Dev.:			5E-05	5E-05	5.7E-05	0.08859	0.08859	5.7E-05	0.08859	5.7E-05	5.8E-05	0.08714	0.08714	5.8E-05	0.08714	5.8E-05	5.8E-05
65-25-50-1	1.71	7.02	-0.0019	0.00027	-0.0016	0.00022	-0.0013	0.00014	0.70167	-0.0011	0.00015	0.57686	-0.0008	0.00013	0.49371	-0.0008	0.00012
65-25-50-2	1.87	7.28	-0.0012	0.00016	-0.0012	0.00016	-0.001	0.00014	0.85321	-0.0009	0.00012	0.72249	-0.0008	0.00011	0.8556	-0.0007	9.8E-05
65-25-50-3	1.72	6.56	0.00123	0.00019	0.00103	0.00016	0.8338	0.00082	0.86234	0.00084	9.8E-05	0.52192	0.00062	9.4E-05	0.50244	0.0006	9.1E-05
65-25-50-4	1.82	6.45	0.0016	0.00025	0.00138	0.00021	0.86699	0.00116	0.72772	0.00094	0.00015	0.58784	0.00087	0.00013	0.54492	0.00081	0.00013
65-25-50-5	1.9	6.18	-0.0007	0.00011	-0.0008	0.00011	-0.0005	8.2E-05	0.78821	-0.0004	6.1E-05	0.57507	-0.0003	5E-05	0.47197	-0.0003	4.5E-05
Average:			2E-04	5E-05	5.3E-05	0.05206	0.872	4.3E-05	0.743	0.743	3.8E-05	0.814	0.814	1E-04	0.814	1E-04	1E-04
St. Dev.:			6.5E-05	6.5E-05	5.3E-05	0.05206	0.872	4.3E-05	0.743	0.743	3.8E-05	0.814	0.814	1E-04	0.814	1E-04	1E-04
65-20-50-1	1.86	6.42	0.00112	0.00017	0.00089	0.00014	0.8014	0.00084	0.74957	0.00073	0.00011	0.65712	0.00084	0.0001	0.57825	0.00051	7.9E-05
65-20-50-2	1.44	6.99	-0.0005	7E-05	-0.0004	6E-05	0.85687	-0.0003	0.70166	-0.0003	3.8E-05	0.54164	-0.0002	2.5E-05	0.35987	-0.0001	1.8E-05
65-20-50-3	1.81	6.75	-0.0021	0.00031	-0.0019	0.00029	0.92883	-0.001	0.85615	-0.001	0.00024	0.78058	0.00144	0.00021	0.89418	-0.0014	0.00021
65-20-50-4	1.87	6.75	0.00114	0.00017	0.00089	0.00013	0.78348	0.00077	0.67772	0.00069	0.0001	0.60438	0.0006	8.8E-05	0.52359	0.00051	7.8E-05
65-20-50-5	1.67	6.36	0.00121	0.00019	0.00092	0.00014	0.78255	0.00075	0.62591	0.00059	9.2E-05	0.48778	0.0005	7.8E-05	0.41387	0.00044	6.9E-05
Average:			2E-04	5E-05	5.3E-05	0.05206	0.872	4.3E-05	0.743	0.743	3.8E-05	0.814	0.814	1E-04	0.814	1E-04	1E-04
St. Dev.:			6.5E-05	6.5E-05	5.3E-05	0.05206	0.872	4.3E-05	0.743	0.743	3.8E-05	0.814	0.814	1E-04	0.814	1E-04	1E-04
65-10-50-1	1.72	6.55	0.00123	0.00019	0.00093	0.00014	0.75297	0.00079	0.63984	0.00059	9E-05	0.47615	0.00048	7.3E-05	0.38752	0.00041	6.3E-05
65-10-50-2	1.47	5.96	-0.0005	8.1E-05	-0.0004	6.1E-05	0.74905	-0.0003	0.55946	-0.0002	3.3E-05	0.40893	-0.0002	2.8E-05	0.32051	-0.0001	2.3E-05
65-10-50-3	1.38	6.24	-0.0001	2.1E-05	-0.0001	1.7E-05	0.8166	-9E-05	0.70191	-8E-05	1E-05	0.48445	-9E-05	9.5E-06	0.44273	-8E-05	9.8E-06
65-10-50-4	1.6	6.62	0.00051	7.8E-05	0.00038	5.7E-05	0.74165	0.00032	0.63277	0.00024	3.6E-05	0.45899	0.00021	3.2E-05	0.41888	0.0002	3E-05
65-10-50-5	1.9	6.47	0.0007	0.00011	0.00051	9E-05	0.74034	0.00041	0.58487	0.00028	4.1E-05	0.37972	0.00021	3.2E-05	0.3009	0.00018	2.8E-05
Average:			1E-04	7E-06	7E-06	0.76	0.824	6E-06	0.824	0.824	4E-06	0.442	0.442	3E-06	0.374	3E-06	3E-06
St. Dev.:			6.1E-05	4.5E-05	4.5E-05	0.032	0.032	3.9E-05	0.05499	0.05499	2.9E-05	0.04535	0.04535	2.3E-05	0.08149	2E-05	2E-05
75-25-50-1	0.000203071	0.219502531	0.000163118	0.020404262	0.000153416	0.199915732	0.00011637	0.182321311	9.41165E-05	0.169868285	8.23055E-05	0.162442612	0.162442612	0.162442612	0.162442612	0.162442612	0.162442612
75-25-50-2	0.000237312	0.231204709	0.000176113	0.209324859	0.000152464	0.199501486	0.000123156	0.185798402	0.000102245	0.174624091	8.87329E-05	0.166565548	0.166565548	0.166565548	0.166565548	0.166565548	0.166565548
75-25-50-3	9.10859E-05	0.168031197	8.63065E-05	0.16503327	7.6387E-05	0.158451657	5.41216E-05	0.141258243	5.93699E-05	0.145684162	5.25342E-05	0.139863533	0.139863533	0.139863533	0.139863533	0.139863533	0.139863533
75-25-50-4	0.000140797	0.194277088	0.000110223	0.179052791	9.14128E-05	0.169225915	7.07971E-05	0.154488278	5.68993E-05	0.14363486	5.08892E-05	0.138388146	0.138388146	0.138388146	0.138388146	0.138388146	0.138388146
75-25-50-5	8.66013E-05	0.165220953	8.26564E-05	0.16267319	7.23015E-05	0.155574834	5.01688E-05	0.137731792	4.4188E-05	0.132025695	3.83339E-05	0.125817056	0.125817056	0.125817056	0.125817056	0.125817056	0.125817056
Average:			0.195647295	0.021891961	0.184025663	0.176333925	0.176333925	0.160319605	0.160319605	0.160319605	0.160319605	0.160319605	0.160319605	0.160319605	0.160319605	0.160319605	0.160319605
St. Dev.:			0.029680341	0.021891961	0.021891961	0.021891961	0.021891961	0.021891961	0.021891961	0.021891961	0.021891961	0.021891961	0.021891961	0.021891961	0.021891961	0.021891961	0.021891961
50-25-50-1	0.000228769	0.228396545	0.000162297	0.199428471	8.61121E-05	0.164909256	5.19604E-05	0.139352446	4.36945E-05	0.131532357	3.94889E-05	0.127179954	0.127179954	0.127179954	0.127179954	0.127179954	0.127179954
50-25-50-2	0.000296595	0.249045381	0.000241148	0.232443995	0.000190988	0.215059688	0.000148785	0.19788373	0.000104654	0.175985095	8.7235E-05	0.165622982	0.165622982	0.165622982	0.165622982	0.165622982	0.165622982
50-25-50-3	0.000313987	0.253820908	0.000248547	0.234797232	0.000194093	0.216219005	0.00010847	0.179281896	0.00005908	0.145430289	4.74867E-05	0.135232441	0.135232441	0.135232441	0.135232441	0.135232441	0.135232441
50-25-50-4	0.000100318	0.173520035	8.17867E-05	0.162100552	3.79356E-05	0.125479412	2.96558E-05	0.110569098	1.92318E-05	0.100053005	1.35464E-05	0.089022291	0.089022291	0.089022291	0.089022291	0.089022291	0.089022291
50-25-50-5	0.00011173	0.179865109	0.000070042	0.153937054	0.00005038	0.137925017	0.000036984	0.124421362	0.000029852	0.115848114	0.000023352	0.106741103	0.106741103	0.106741103	0.106741103	0.106741103	0.106741103
Average:			0.218929596	0.037654369	0.037654369	0.037654369	0.037654369	0.037654369	0.037654369	0.037654369	0.037654369	0.037654369	0.037654369	0.037654369	0.037654369	0.037654369	0.037654369
St. Dev.:			0.038019895	0.038019895	0.038019895	0.038019895	0.038019895	0.038019895	0.038019895	0.038019895	0.038019895	0.038019895	0.038019895	0.038019895	0.038019895	0.038019895	0.038019895

85-25-50-1	0.000121824	0.185125886	0.000114394	0.181278298	9.86745E-05	0.172587358	7.37373E-05	0.15597917	6.00898E-05	0.148253487	5.44078E-05	0.14150688
85-25-50-2	0.000118378	0.183384111	0.000109201	0.178497366	8.91988E-05	0.168857107	5.41541E-05	0.141286548	4.79387E-05	0.13586019	4.40105E-05	0.13184888
85-25-50-3	0.000114175	0.181167571	9.91109E-05	0.172821384	7.66503E-05	0.159833528	5.02842E-05	0.137846714	4.90874E-05	0.13873522	4.70832E-05	0.134848311
85-25-50-4	8.16075E-05	0.161982089	6.15287E-05	0.147427394	4.98398E-05	0.137430302	4.98874E-05	0.137474057	4.23482E-05	0.130168355	3.91703E-05	0.128826263
85-25-50-5	8.78727E-05	0.152331183	5.30578E-05	0.140326424	4.34833E-05	0.131320119	4.33652E-05	0.131201041	2.83152E-05	0.115147463	1.84348E-05	0.094946485
Average:	0.172784186			0.164070272		0.153361683		0.140881255		0.132782943		0.12599532
St.Dev.:	0.014744039			0.018852117		0.018155001		0.009509228		0.011436786		0.018151899
85-25a-50-1	0.021168213	1.033010437	0.015914189	0.93933026	0.013730245	0.894231073	0.011210827	0.835798001	0.008435895	0.760204808	0.008819074	0.771551015
85-25a-50-2	0.013707566	0.893738219	0.011242887	0.836591479	0.010599111	0.820314031	0.009738687	0.78748678	0.016910444	0.958536524	0.015831333	0.933732195
85-25a-50-3	0.017083212	0.961789788	0.013346277	0.865816381	0.011734015	0.848605548	0.009887445	0.801527368	0.009039124	0.777915529	0.008417664	0.759862797
85-25a-50-4	0.023077798	1.063216645	0.014993355	0.920852206	0.013414425	0.887321508	0.012235818	0.860533933	0.017588882	0.970819217	0.018403566	0.948862053
85-25a-50-5	0.028976281	1.160066308	0.023497033	1.059616268	0.020479228	1.021711282	0.017477745	0.999137829	0.00596365	0.87721677	0.005468548	0.857931907
Average:	1.022364281			0.930441318		0.894436686		0.852896342		0.87893857		0.814347983
St.Dev.:	0.101190459			0.087091629		0.077207759		0.069049593		0.129681531		0.124131648
85-25b-50-1	0.026295455	1.110496885	0.021231081	1.034064325	0.020304924	1.018804332	0.018190341	0.98213368	0.018724053	0.955001757	0.018409848	0.948863181
85-25b-50-2	0.037818667	1.251290435	0.034646867	1.217430406	0.028504	1.153941941	0.020886687	1.028442551	0.017268	0.965245247	0.015478	0.930628965
85-25b-50-3	0.039813814	1.275170486	0.024868366	1.090003187	0.020441441	1.021082495	0.015445946	0.930026154	0.013736937	0.894378323	0.014541742	0.911512162
85-25b-50-4	0.027319489	1.124728884	0.01828754	0.983879899	0.014748008	0.91576027	0.012245687	0.860765217	0.010752875	0.824261844	0.010213898	0.810253335
85-25b-50-5	0.029056277	1.148075144	0.018505051	0.987765265	0.015554113	0.93219207	0.01267244	0.872816022	0.011891775	0.852391712	0.011331025	0.838777396
Average:	1.181952303			1.062628616		1.008356222		0.934636725		0.898255377		0.888031008
St.Dev.:	0.075870795			0.096611027		0.094659008		0.071336089		0.061849333		0.060324959
65-40-50-1	0.000339861	0.260559825	0.000287894	0.246614262	0.000280398	0.244426758	0.000252611	0.236070032	0.000234189	0.230186064	0.000210805	0.222184125
65-40-50-2	0.00058504	0.312333778	0.000559852	0.307785393	0.000434987	0.28295384	0.000392183	0.273350593	0.000382842	0.266307152	0.000307507	0.252062873
65-40-50-3	0.000367808	0.267517328	0.000336353	0.259710038	0.000322824	0.256180097	0.000295784	0.248818139	0.000273882	0.242518575	0.000234178	0.230182027
65-40-50-4	0.000362188	0.266196138	0.000281007	0.244603395	0.000254337	0.236606586	0.000187164	0.213614725	0.000158595	0.202564617	0.000138083	0.193020701
65-40-50-5	0.00035468	0.264343859	0.00026688	0.240463908	0.00024144	0.232537714	0.000193074	0.21583983	0.000168298	0.206180817	0.000153076	0.199768048
Average:	0.274189945			0.259835399		0.250540999		0.237538684		0.229551445		0.219443515
St.Dev.:	0.021483336			0.027754661		0.020236488		0.024774341		0.02642918		0.023833407
65-30-50-1	0.000401107	0.275408254	0.000334147	0.259140944	0.00030204	0.250560042	0.00027392	0.242529687	0.000224533	0.228978088	0.000195173	0.216819302
65-30-50-2	0.00030163	0.250448547	0.000242328	0.232821795	0.000187215	0.213634154	0.000144891	0.196142008	0.000116782	0.182535997	9.80554E-05	0.172205878
65-30-50-3	0.0003	0.249894667	0.000243502	0.233187949	0.000186101	0.213209667	0.000144218	0.195836814	0.000114982	0.181598785	9.73851E-05	0.171812399
65-30-50-4	0.000290841	0.24742425	0.000223193	0.226525593	0.000193847	0.216127626	0.000163427	0.20417289	0.000144533	0.19598028	0.000132472	0.190369915
65-30-50-5	0.000337396	0.259978253	0.00025928	0.238129504	0.000182521	0.211833395	0.000176585	0.209503819	0.000178911	0.209640682	0.00016144	0.203342319
Average:	0.256650394			0.237963157		0.221072977		0.209637044		0.198346768		0.190869822
St.Dev.:	0.011519684			0.012534802		0.016556578		0.019263716		0.019224858		0.019560064

65-25-50-1	0.000287538	0.240630803	0.000223134	0.228505549	0.000187721	0.213828301	0.00015433	0.200312276	0.000132085	0.190184597	0.00011816	0.183251102
65-25-50-2	0.000164231	0.204507152	0.000158091	0.201926071	0.000140124	0.193966821	0.000118655	0.183506988	0.000107669	0.177658978	9.80398E-05	0.172780063
65-25-50-3	0.0001875	0.213742433	0.000157012	0.201465856	0.000125152	0.189797086	9.7561E-05	0.171915785	9.45122E-05	0.170105991	9.14634E-05	0.168256866
65-25-50-4	0.000247581	0.23449288	0.000214651	0.223598082	0.000180171	0.210820239	0.000145538	0.196433601	0.000134913	0.191532194	0.000125521	0.186980238
65-25-50-5	0.000106741	0.177147169	9.21861E-05	0.168698847	0.000082	0.162241372	6.13835E-05	0.147312928	5.03786E-05	0.137923777	4.48042E-05	0.132636562
Average:		0.214104047		0.2044338881		0.193550364		0.178986312		0.173481107		0.168780966
St.Dev.:		0.025384073		0.023165254		0.020849816		0.02138163		0.021783125		0.021582885
65-20-50-1	0.000173723	0.20837353	0.000139221	0.19354952	0.000130217	0.189283319	0.000114157	0.181158305	0.000100455	0.173599018	7.90312E-05	0.160259247
65-20-50-2	7.00844E-05	0.153953446	6.00358E-05	0.146226811	4.91617E-05	0.136804118	3.79499E-05	0.125495257	2.51302E-05	0.109384443	1.62389E-05	0.09456786
65-20-50-3	0.000308148	0.252237805	0.0002856	0.24592899	0.000263822	0.239512095	0.000240533	0.23224627	0.000213911	0.22334082	0.000208385	0.221400844
65-20-50-4	0.000168993	0.206464893	0.000132403	0.190336857	0.000114529	0.181354641	0.000102136	0.174582282	8.483E-05	0.168409028	7.59304E-05	0.158135302
65-20-50-5	0.00018956	0.214522281	0.000144549	0.195987528	0.000118648	0.183503163	9.24638E-05	0.168868104	7.84528E-05	0.159867382	6.94057E-05	0.153489457
Average:		0.207110387		0.194405941		0.186091467		0.17646604		0.166520138		0.157566502
St.Dev.:		0.035068121		0.035333994		0.038477154		0.038055306		0.040581583		0.044911128
65-10-50-1	0.000188458	0.214105848	0.000141902	0.194784081	0.000120583	0.184495566	8.97344E-05	0.167189847	7.30305E-05	0.158096016	6.32305E-05	0.148775908
65-10-50-2	8.10671E-05	0.161623789	6.07232E-05	0.146782777	4.5354E-05	0.133178913	3.3151E-05	0.11986537	2.58832E-05	0.110608369	2.34614E-05	0.108907545
65-10-50-3	2.14087E-05	0.103683956	1.74824E-05	0.096922314	1.50269E-05	0.092153892	1.03715E-05	0.081439886	9.47821E-06	0.079031282	9.84071E-06	0.080026237
65-10-50-4	7.75015E-05	0.159218568	5.74789E-05	0.144120687	4.90408E-05	0.136691906	3.5585E-05	0.12280925	3.24637E-05	0.119130568	2.99758E-05	0.116006078
65-10-50-5	0.000107487	0.177558767	7.95785E-05	0.160627025	6.28655E-05	0.149489083	4.08145E-05	0.128576595	3.23431E-05	0.118982833	2.77419E-05	0.113049588
Average:		0.163240182		0.148647379		0.139001472		0.12399619		0.116769813		0.112953071
St.Dev.:		0.039885013		0.035254635		0.03314243		0.030476907		0.027473537		0.02456283
65-12.5-0-1	1.85	4										
65-12.5-0-2	1.85	5.7										
65-12.5-0-3	1.72	6										
65-12.5-0-4	1.85	7.46										
65-12.5-0-5	2.18	8.665										
Average:												
St.Dev.:												
65-25-0-1	1.58	6.33										
65-25-0-2	1.81	5.98										
65-25-0-3	1.53	6.59										
65-25-0-4	1.8	6.01										
65-25-0-5	1.77	7.06										
Average:												
St.Dev.:												
65-30-0-1	1.71	6.83										

65-30-0-2	1.58	5.82	0.002807	0.000482	0.002074	0.000356	0.738805	0.002013	0.000346	0.717111	0.002038	0.000035	0.726159	0.001586	0.000269	0.557882	0.001379	0.000237
65-30-0-3	1.7	5.05	-0.00373	0.000739	-0.00281	0.000557	0.753696	0.002848	0.000564	0.762722	0.002422	0.00048	0.648677	0.002099	0.000416	0.562085	0.00179	0.000354
65-30-0-4	1.58	6.65	0.003776	0.000568	0.003017	0.000454	0.799025	-0.0027	0.000406	0.715198	-0.00251	0.000378	0.66498	-0.00168	0.000252	0.444324	-0.00155	0.000233
65-30-0-5	1.52	5.85	0.002783	0.000478	0.001944	0.000332	0.698428	0.001972	0.000337	0.70963	0.00174	0.000287	0.625027	0.00159	0.000272	0.57115	0.001386	0.000239
			Average:	0.000604		0.000476	0.778905		0.000454	0.743775		0.000413	0.681928		0.000321	0.53167		0.000283
			St.Dev.:	0.000136		0.000145	0.078926		0.000128	0.045348		0.000106	0.051333		7.78E-05	0.052146		6.49E-05
65-35-0-1	1.66	6.74	0.004911	0.000729	0.003467	0.000514	0.706044	0.002706	0.000401	0.551032	0.002312	0.000343	0.470778	0.002205	0.000327	0.448988	0.002115	0.000314
65-35-0-2	1.8	7.2	-0.0056	0.000778	-0.00437	0.000607	0.780273	-0.00335	0.000465	0.598485	-0.00288	0.0004	0.514388	-0.00293	0.000406	0.52248	-0.00275	0.000382
65-35-0-3	1.8	6.6	0.004821	0.000731	0.003558	0.000539	0.738043	0.003305	0.000501	0.685444	0.002406	0.000364	0.496942	0.002105	0.000319	0.436491	0.001946	0.000295
65-35-0-4	1.79	7.4	0.006048	0.000817	0.005143	0.000695	0.850333	0.004799	0.000648	0.79339	0.004442	0.0006	0.734363	0.004002	0.000541	0.661762	0.003785	0.000512
65-35-0-5	1.47	4	-0.00172	0.00043	-0.00134	0.000338	0.777978	-0.0013	0.000324	0.753238	-0.00092	0.000231	0.536227	-0.00085	0.000163	0.378088	-0.00063	0.000157
			Average:	0.000697		0.000538	0.7770894		0.000468	0.676318		0.000388	0.55094		0.000351	0.489562		0.000332
			St.Dev.:	0.000153		0.000133	0.054227		0.000121	0.101809		0.000135	0.105289		0.000138	0.109118		0.00013
65-40-0-1	1.75	6.6	-0.00547	0.000829	-0.00403	0.000611	0.737319	-0.00372	0.000563	0.679612	-0.00317	0.00048	0.579759	-0.00255	0.000386	0.466264	-0.0024	0.000363
65-40-0-2	1.6	6.62	-0.0047	0.00071	-0.00356	0.000538	0.758104	-0.00352	0.000532	0.749633	-0.00258	0.00039	0.549135	-0.00196	0.000296	0.417172	-0.00191	0.000288
65-40-0-3	1.68	4.49	0.002511	0.000559	0.001797	0.0004	0.715628	0.001295	0.000288	0.515812	0.001137	0.000253	0.452804	0.001103	0.000246	0.439238	0.001016	0.000226
65-40-0-4	1.8	5.61	0.004053	0.000722	0.003041	0.000542	0.750197	0.002432	0.000434	0.80002	0.002035	0.000363	0.502023	0.001901	0.000339	0.489111	0.001722	0.000307
65-40-0-5	1.7	3.98	-0.00406	0.001019	-0.00324	0.000815	0.79631	-0.00293	0.000736	0.722535	-0.00248	0.000622	0.610281	-0.00204	0.000513	0.503575	-0.00195	0.00049
			Average:	0.000768		0.000581	0.752112		0.000511	0.653522		0.000422	0.5388		0.000356	0.459072		0.000335
			St.Dev.:	0.00017		0.000151	0.030891		0.000165	0.095534		0.000138	0.062534		0.000102	0.032718		9.95E-05
65-45-0-1	1.66	5.13	0.004524	0.000882	0.003262	0.000636	0.721083	0.002472	0.000482	0.546379	0.00216	0.000421	0.477518	0.002093	0.000408	0.462751	0.002003	0.00039
65-45-0-2	1.67	6.05	0.005282	0.000873	0.00377	0.000823	0.713745	0.003076	0.000508	0.582261	0.002611	0.000432	0.494358	0.002215	0.000368	0.419368	0.002185	0.000361
65-45-0-3	1.78	7.92	-0.00637	0.001067	-0.00371	0.000577	0.69048	0.002748	0.000453	0.541862	0.002467	0.000406	0.496434	0.002243	0.000369	0.442245	0.002054	0.000338
65-45-0-4	1.7	6.07	0.005071	0.000835	0.003502	0.000577	0.69048	0.002748	0.000453	0.541862	0.002467	0.000406	0.496434	0.002243	0.000369	0.442245	0.002054	0.000338
65-45-0-5	1.57	4.57	-0.00309	0.000875	-0.00212	0.000484	0.687389	-0.00174	0.000381	0.584288	-0.00137	0.00039	0.444394	-0.00139	0.000303	0.449286	-0.00131	0.000287
			Average:	0.000816		0.000575	0.703169		0.000456	0.558697		0.00039	0.475876		0.000362	0.443412		0.000344
			St.Dev.:	9.61E-05		7.8E-05	0.016754		5.48E-05	0.016454		6.06E-05	0.02196		4.33E-05	0.018147		4.39E-05
65-50s-0-1	1.73	6.37	-1.0176	0.159749	-0.55423	0.087006	0.544644	-0.43896	0.088911	0.431368	-0.2952	0.046342	0.290094	-0.24034	0.03773	0.236183	-0.20938	0.03287
65-50s-0-2	1.87	6.32	1.1542	0.182627	0.65911	0.10429	0.571054	0.46669	0.073643	0.404341	0.34089	0.053907	0.295174	0.25928	0.041022	0.224823	0.22714	0.03594
65-50s-0-3	1.65	6.59	-1.0201	0.154795	-0.5763	0.087451	0.564945	-0.34916	0.052983	0.34228	-0.21716	0.032953	0.212881	-0.01898	0.002561	0.016548		
65-50s-0-4	1.82	6.87	-1.2062	0.175575	-0.5961	0.086769	0.494197	-0.32221	0.048901	0.267128	-0.19137	0.027856	0.158655	-0.16874	0.024562	0.138694		
65-50s-0-5	1.77	6.78	-1.3292	0.198047	-0.5958	0.087878	0.44824	-0.34301	0.050591	0.258057	-0.20815	0.030701	0.156598	-0.16796	0.024773	0.126362	-0.15405	0.022721
			Average:	0.173759		0.090678	0.524616		0.058646	0.340835		0.038352	0.222681		0.02613	0.148722		0.03051
			St.Dev.:	0.016942		0.007621	0.052304		0.01195	0.078288		0.011221	0.067753		0.015134	0.088683		0.008918
85-50s-0-1	1.57	6.29	1.1496	0.182766	0.6221	0.096903	0.541145	0.46979	0.074688	0.408655	0.33751	0.053958	0.293589	0.28978	0.04607	0.25207	0.26048	0.041412
85-50s-0-2	1.57	6.13	0.6404	0.104476	0.4467	0.072871	0.697489	0.3914	0.06395	0.611142	0.30755	0.050171	0.480217	0.26428	0.043113	0.412654	0.23897	0.038984
85-50s-0-3	1.75	6.83	0.97732	0.143092	-0.63935	0.093609	0.654187	-0.47161	0.06905	0.482554	-0.3081	0.048435	0.338487	-0.28499	0.041726	0.291604	-0.25905	0.037928
85-50s-0-4	1.79	5.02	0.84451	0.168229	0.50393	0.100384	0.596713	0.41596	0.082859	0.492534	0.32365	0.064472	0.3824	0.26102	0.051996	0.309079	0.22912	0.045841
85-50s-0-5	1.46	6.04	1.0894	0.177053	-0.56586	0.093685	0.529138	-0.44317	0.073373	0.41441	0.3269	0.054123	0.305685	-0.26943	0.044608	0.251945	-0.23001	0.038081
			Average:	0.155123		0.091891	0.603734		0.072764	0.481859		0.054172	0.360244		0.045502	0.30347		0.040409
			St.Dev.:	0.03212		0.011059	0.072227		0.007057	0.081757		0.006231	0.075523		0.003977	0.065836		0.00324

ID	Pole Strength	Max Attract. Distance	P.S. 1 week	Max Attract. Distance	P.S. 2 weeks	Max Attract. Distance	P.S. 4 weeks	Max Attract. Distance	P.S. 6 weeks	Max Attract. Distance	P.S. 8 weeks	Max Attract. Distance
65-12.5-0-1	0.00026	0.256844197	0.00024113	0.25039641	0.00022183	0.24351768	0.00018648	0.22982776	0.00016341	0.21993217	0.00014214	0.20894312
65-12.5-0-2	0.000315	0.273800465	0.00026158	0.25727323	0.0002304	0.24668172	0.00018201	0.22797923	0.00018754	0.23026429	0	0
65-12.5-0-3	0.000336	0.279689388	0.000294	0.26749116	0.00026817	0.25676859	0.0002085	0.23854062	0.00019583	0.2336088	0.00019233	0.23220872
65-12.5-0-4	0.000375	0.280082743	0.00034499	0.28213767	0.00031678	0.27422953	0.00028617	0.26509393	0.000251	0.25375802	0.00021917	0.2425438
65-12.5-0-5	0.000339	0.280539585	0.00031596	0.2739921	0.00027797	0.26253812	0.00026959	0.25987336	0.00020834	0.23848108	0.00019624	0.23377087
Average:		0.276191276		0.26625611		0.25713422		0.24426298		0.23520887		0.1836933
St. Dev.:		0.012289659		0.01270959		0.01245131		0.01720388		0.01240126		0.10338904
65-25-0-1	0.000503	0.318882878	0.00042651	0.30280959	0.00039052	0.29404147	0.00030433	0.27058762	0.0002532	0.25449604	0.00023397	0.2478815
65-25-0-2	0.000508	0.320622505	0.00045096	0.30848816	0.00042386	0.30220515	0.00033047	0.27812344	0.00029972	0.26921372	0.0002613	0.25718185
65-25-0-3	0.000482	0.317610047	0.00039392	0.29489077	0.00039366	0.29482638	0.0003003	0.26938937	0.00025915	0.2564745	0.00024225	0.25077203
65-26-0-4	0.000503	0.319992043	0.00044101	0.30620441	0.00036861	0.28791219	0.00031248	0.27298201	0.00028403	0.2580732	0.00023642	0.24874633
65-25-0-5	0.000597	0.338757456	0.00052608	0.32474561	0.00050894	0.32118003	0.00040636	0.29796407	0.00030759	0.27155223	0.00027386	0.26123804
Average:		0.323372986		0.30742771		0.30003304		0.2778093		0.26196194		0.25316395
St. Dev.:		0.008675687		0.01096623		0.01286309		0.0117544		0.00783479		0.00579818
65-30-0-1	0.000754	0.386208539	0.00068824	0.35416604	0.00061499	0.34209782	0.00056187	0.3319505	0.00039448	0.29503174	0.00035321	0.28436089
65-30-0-2	0.000482	0.315480095	0.00035634	0.2851994	0.00034598	0.28238	0.00035024	0.28356272	0.00028908	0.25970842	0.00023688	0.24890593
65-30-0-3	0.000739	0.363752343	0.00055723	0.33103296	0.0005639	0.33234918	0.00047958	0.31488256	0.00041556	0.30019705	0.00035442	0.28488508
65-30-0-4	0.000568	0.333105477	0.00045365	0.3091021	0.00040606	0.29789082	0.00037755	0.29074888	0.00025227	0.25418411	0.00023305	0.24755931
65-30-0-5	0.000478	0.314051049	0.00033231	0.27863807	0.00033716	0.2799894	0.00029738	0.26851373	0.00027175	0.2605656	0.00023866	0.24952966
Average:		0.338519101	0.00047639	0.31162771	0.0004536	0.30694124	0.00041333	0.297937168	0.00032063	0.27393738	0.00028324	0.26300817
St. Dev.:		0.025308593	0.00014549	0.03154054	0.0001281	0.02869307	0.00010625	0.02533815	7.776E-05	0.02182889	6.4452E-05	0.01965348
65-35-0-1	0.000729	0.361980535	0.00051441	0.32232636	0.00040147	0.29676381	0.000343	0.28159425	0.00032712	0.27718098	0.00031386	0.27338281
65-35-0-2	0.000778	0.369914689	0.00060669	0.34055218	0.00046535	0.31173534	0.00039996	0.29639116	0.00040625	0.29793724	0.00038199	0.29188348
65-35-0-3	0.000731	0.36230145	0.00053915	0.32741402	0.00050073	0.31944352	0.00036448	0.28735592	0.00031886	0.27482864	0.00029479	0.2677299
65-35-0-4	0.000817	0.37611681	0.00069499	0.35633005	0.00064845	0.34819157	0.0006002	0.33933317	0.00054086	0.32776048	0.00051151	0.32172097
65-35-0-5	0.00043	0.303745352	0.00033568	0.27957607	0.00032425	0.27636751	0.00023083	0.24677016	0.00016276	0.21963793	0.00015684	0.2169443
Average:		0.354811763		0.32523974		0.31050035		0.29028893		0.27946905		0.27433229
St. Dev.:		0.029143043		0.02872048		0.0267202		0.03324401		0.03962218		0.0383784
65-40-0-1	0.000829	0.377846142	0.00061097	0.34135025	0.00056315	0.33220188	0.00048041	0.315063	0.00038636	0.29299424	0.00036324	0.28702905
65-40-0-2	0.00071	0.358829314	0.00053804	0.32718811	0.00053202	0.32596486	0.00038973	0.29384225	0.00029607	0.26811824	0.00028835	0.26576781
65-40-0-3	0.000559	0.331422704	0.00040018	0.29644545	0.00028844	0.2657945	0.00025321	0.25449874	0.00024562	0.25193145	0.00022631	0.24514618
65-40-0-4	0.000722	0.360970785	0.00054201	0.32799249	0.00043351	0.30445789	0.00036271	0.2868886	0.00033893	0.28047697	0.0003069	0.27134711
65-40-0-5	0.001019	0.404823101	0.00081457	0.37569635	0.00073633	0.36326048	0.00062193	0.3433802	0.00051319	0.32207226	0.00048997	0.31714042
Average:		0.366776409		0.33373453		0.31833592		0.29873456		0.28311863		0.27728607
St. Dev.:		0.027003869		0.02865788		0.0361313		0.03309428		0.02654969		0.02685244

65-45-0-1	0.00082	0.385758887	0.00063583	0.34591839	0.00048179	0.31536532	0.00042107	0.30151748	0.00040805	0.29837679	0.00039037	0.29400358
65-45-0-2	0.000873	0.384480812	0.00062314	0.34360198	0.00050835	0.32105575	0.0004316	0.3040105	0.00036613	0.2877982	0.00036114	0.28647434
65-45-0-3	0.001057	0.409810043	0	0	0	0	0	0	0	0	0	0
65-45-0-4	0.000835	0.378884397	0.00057689	0.33488093	0.00045272	0.3088894	0.00040641	0.297978	0.00038949	0.2886851	0.00033837	0.28032201
65-45-0-5	0.000875	0.352962947	0.00046431	0.31150372	0.00038116	0.29167285	0.00030018	0.26935098	0.00030348	0.27033564	0.00028656	0.26521687
Average:		0.382379417		0.33397625		0.30924583		0.29321373		0.28629143		0.2815042
St. Dev.:		0.018142876		0.01571732		0.01272608		0.01610004		0.0116693		0.0122149
65-50a-0-1	0.159749	2.182761164	0.08700628	1.78255879	0.06891052	1.64925889	0.04634223	1.44494939	0.03772988	1.34923989	0.0328697	1.28862213
65-50a-0-2	0.182827	2.282346928	0.10428956	1.89353762	0.07384335	1.68770862	0.05390865	1.51964134	0.04102215	1.38739399	0.03593987	1.32755496
65-50a-0-3	0.154795	2.159961982	0.08745068	1.78558857	0.05298331	1.51081495	0.03285298	1.28970921	0.00258131	0.55040298	0	0
65-50a-0-4	0.175575	2.252585021	0.08676856	1.78093386	0.04690102	1.45073389	0.02785559	1.21945572	0.02456186	1.16935784	0	0
65-50a-0-5	0.196047	2.3369381	0.08787611	1.78847935	0.05059145	1.48782788	0.03070059	1.25962877	0.02477286	1.17269675	0.02272124	1.13938632
Average:		2.242918639		1.80621964		1.55728885		1.34667689		1.12581831		1.25185447
St. Dev.:		0.064789531		0.04373556		0.09359181		0.1153988		0.30117609		0.09932651
85-50a-0-1	0.182766	2.282928786	0.09890302	1.86035938	0.07468839	1.69412208	0.05365819	1.51730304	0.04606985	1.44211397	0.04141176	1.39177247
85-50a-0-2	0.104476	1.894687422	0.07287113	1.68028903	0.06384992	1.60785586	0.05017129	1.48389787	0.04311256	1.41057098	0.03898369	1.36402176
85-50a-0-3	0.143092	2.104096677	0.09360908	1.82655597	0.06904978	1.65036915	0.04843485	1.46637924	0.04172621	1.39528621	0.03792826	1.35159931
85-50a-0-4	0.168229	2.220721119	0.10038446	1.86960199	0.08285857	1.75377086	0.06447211	1.61306163	0.05199602	1.50147124	0.04584143	1.43762878
85-50a-0-5	0.177053	2.258888234	0.093688543	1.82705245	0.07337252	1.68411393	0.05412252	1.52166712	0.04460762	1.42669126	0.03808113	1.35341273
Average:		2.152260449		1.81276776		1.67804634		1.52042174		1.43522673		1.37968701
St. Dev.:		0.158534073		0.07655908		0.05413444		0.05670687		0.04086272		0.03615233

ID	B(Long)	B(Lat.)	F		B(Long)	B(Lat.)	F
50/25/50/1	0.0037115	0.0008699	0.810124	85/25/50/1	0.002823	0.0007118	0.798631
50/25/50/2	0.0002044	0.00004487	0.819994	85/25/50/2	0.001821	0.0007577	0.70617
50/25/50/3	0.002386	0.0005597	0.809994	85/25/50/3	0.0013215	0.0005825	0.694065
50/25/50/4	0.01049	0.002048	0.836657	85/25/50/4	0.002047	0.0008035	0.71812
50/25/50/5	0.0012817	0.0006072	0.678543	85/25/50/5	0.0006306	0.000286	0.687977
50/25/50/6	0.0013936	0.00026166	0.841922	85/25/50/6	0.0008035	0.000265	0.751989
50/25/50/7	0.002154	0.000362	0.856121	85/25/50/7	0.0004321	0.000187	0.697949
50/25/50/8	0.001947	0.0006405	0.752464	85/25/50/8	0.000865	0.000225	0.793578
50/25/50/9	0.0020448	0.00046519	0.814665	85/25/50/9	0.000746	0.000278	0.728516
50/25/50/10	0.0018543	0.0004606	0.801028	85/25/50/10	0.0007964	0.000293	0.731045
Average	0.00274673	0.000631962	0.802151	Average	0.00122861	0.00043895	0.730804
Std. Dev.	0.003017759	0.000575208	0.05481	Std. Dev.	0.000797537	0.000253967	0.041872

MICHIGAN STATE UNIVERSITY LIBRARIES



3 1293 02088 0864